MODELING, OPTIMIZATION, MONITORING, AND CONTROL OF POLYMER DIELECTRIC CURING BY VARIABLE FREQUENCY MICROWAVE PROCESSING

A Thesis
Presented to
The Academic Faculty

by

Cleon E. Davis

In Partial Fulfillment
of the Requirements for the Degree of
Doctor of Philosophy

School of Electrical and Computer Engineering
Georgia Institute of Technology

May 2007

MODELING, OPTIMIZATION, MONITORING, AND CONTROL OF POLYMER DIELECTRIC CURING BY VARIABLE FREQUENCY MICROWAVE PROCESSING

Approved by:

Dr. Gary S. May, Advisor
School of Electrical and Computer Engineering
Georgia Institute of Technology

Dr. Russell Dupuis
School of Electrical and Computer Engineering
Georgia Institute of Technology

Dr. Ayanna Howard
School of Electrical and Computer Engineering
Georgia Institute of Technology

Dr. William Hunt
School of Electrical and Computer Engineering
Georgia Institute of Technology

Dr. Paul H. Kohl
School of Biomolecular and Chemical Engineering
Georgia Institute of Technology

Date Approved: April 2, 2007

In memory of Lenard Bradford Davis

ACKNOWLEDGEMENTS

I give honor to God, the creator and sustainer of life, for blessing me to be able to pursue and complete this milestone. I thank God for endowing me with the knowledge, wisdom, and understanding to accomplish this goal.

Without the love and support of my family this would not have been possible. My wife, Dr. Angela Davis, has helped me to become a better person and offered me encouragement and support throughout my graduate school years. I would like to thank my parents, Lindsey and Betty Davis, Jr., for bringing me into the world and for raising me to be the man that I am today. I am gratified that I had a number of siblings to learn from and grow with: Timothy Jackson, Lindsey Davis, III, Sennieal Crutchfield, Lisa Quince, Samuel Davis, Lenard Davis, Kermit Davis, Randell Davis, and numerous nieces and nephews. Their support and encouragement has been invaluable.

I would like to express my sincerest gratitude to my advisor, Dr. Gary S. May, for his guidance and support throughout the latter half of the PhD process. He has been an extremely positive role-model for me. Having an opportunity to work with him and for him has contributed significantly to my professional and personal development.

I would like to thank Dr. William Hunt, Dr. Ayanna Howard, Dr. Russell Dupuis, and Dr. Paul Kohl for serving on my dissertation defense committee. I would like to especially thank Dr. Hunt and Dr. Howard for serving on my reading committee.

I am especially grateful to Dr. Kohl for his support of my work and his invaluable advice regarding professional success. I would also like to thank one of his former graduate students, Dr. Ravindra Tanikella, for his assistance and training me on the variable frequency microwave (VFM) furnace.

I am appreciative for the assistance given to me by a number of employees at Lambda Technologies, Inc. for their help with maintenance of the VFM furnace and for altering their software so that I could test my sensor and control algorithm.

I am truly thankful to Dr. Hunt and Dr. F. Levent Degertekin who were both instrumental in helping me to gain an understanding of acoustic devices. I am very appreciative to one of Dr. Hunt's graduate student, Anthony Dickherber, for his help in depositing the zinc oxide thin film that allowed me to fabricate the acoustic sensor.

I would like to thank the Microelectronics Research Center staff for all of their support. I especially like to thank the cleanroom staff (Gary Spinner, Charlie Suh, Brandon Harrington, and Tran-Vinh Nguyen) for their help with processing and with maintenance of the cleanroom equipment.

I am grateful to the current and former members of the Intelligent Semiconductor Manufacturing Group (ISMG): Dr. Frances Williams, Dr. Gregory Triplett, Dr. Rana Pratap, Dr. Sang Jeen Hong, Dr. Terrence Brown, Dr. Ronald Sertia, Mr. Bryan Morris, and Mr. Benjamin Ku for all of their assistance, discussions, and feedback during my time as a part of the group.

Throughout the PhD process, I have found that having the support of friends a valuable resource. Thus, I would like to thank the many members of the Black Graduate Student Association at Georgia Tech. This organization has provided a strong support system for me throughout my time at Georgia Tech. There are several friends in this organization in which I have had the opportunity to work and study with that I would like to thank: Dr. Cameron Coates, Dr. Paul D. Smith, Dr. Amos Johnson, Jr., Dr. Raymond Mooring, Mr. Cornelius Ejimofor, and Mr. Russell Marzette, Jr.

There are a few friends that have encouraged me and provided moral support throughout my graduate career that I would like to thank: Torrance Lawery, Earl McBride, Devon Grant, and Charles Spencer.

Finally, I would also like to thank School of Electrical and Computer Engineering, Packaging Research Center, Interconnect Focus Center, National Aeronautics and Space Administration (NASA), Graduate Education for Minority Engineers (GEM), Facilitating Academic Careers in Engineering and Sciences (FACES), the National Science Foundation, the Ford Motor Company, Texas Instruments, United Technologies Research Center, and the Office of Naval Research for financial and other tangible support for graduate school and this work. I am also appreciative of Dr. George Davis at the Ford Motor Company, Scientific Research Laboratory for his support.

TABLE OF CONTENTS

LIST OF TABLES

LIST OF FIGURES

SUMMARY

Several statistically designed experiments were performed to verify that VFM curing results in comparable material properties to conventionally cured films. These experiments were on samples of the polymer benzocyclobutene (BCB) and the polyimide PI 2611 cured on silicon wafers. Curing was performed in the Lambda Technologies MircoCure™ 2100 system, as well as a conventional thermal furnace. All samples were heated to an appropriate temperature and held at temperature for a specific amount of time for both processing methods. After the BCB samples cooled, through-plane and in-plane indices of refraction were measured via ellipsometry. Upon cooling of the PI 2611 samples, the indices of refraction were measured using a Metricon prism coupler. The percent imidization was measured using attenuated total reflection Fourier transform infrared (ATR-FTIR) spectroscopy.

Neural networks were then trained using the data from the designed experiments to model the variation of the responses as a function of the process conditions. The back-propagation algorithm was utilized to train the neural networks. The network inputs were temperature and time-at-temperature. The outputs for cured BCB were the in-plane and through-plane indices of refraction. The indices of refraction were then used as metrics to determine the extent of cure of the BCB. The output variables of the cured polyimide were the in-plane and through-plane indices of refraction, the birefringence, and percent of imidization. To validate the neural network models, the root-mean-square (RMS) error was used as a performance metric. The neural network models were then used for process optimization via genetic algorithms. Using this approach, the appropriate input conditions to achieve desirable film properties were determined.

To enhance process monitoring for the VFM system, an acoustic temperature sensor was developed by depositing a ZnO transducer onto a sapphire buffer rod or sapphire wafer. The acoustic temperature sensor operates on the principle that the velocity of an acoustic wave in silicon is a function of temperature. Thus, an estimate of the temperature of a silicon wafer can be determined by measuring the time it takes for an acoustic wave to travel through silicon. For this research, the time-of-flight of a longitudinal wave is measured by generating a high voltage pulse, which produces the acoustic wave in the transducer. The acoustic wave travels through the sapphire into the silicon wafer and reflects off of either the silicon/air interface (or polymer/air interface if the silicon is coated with a polymer) and returns back to the transducer which then converts the mechanical signal back to an electrical signal, where it is read on an oscilloscope.

A sensor holder was developed to house the acoustic sensor for use in the VFM furnace. Once the sensor was mounted in the holder and placed inside the VFM furnace, a GUI developed in MATLAB was used to monitor both the time-of-flight of the returned pulses and a thermocouple attached to a polymer-coated wafer. The time-of-flight data had a strong correspondence to the temperature profile from the thermocouple that was attached to the polymer-coated wafer.

Based on the capability of neural networks to model nonlinear processes, a neural network indirect adaptive control scheme was developed for VFM curing of polymer dielectrics. This adaptive control scheme was used along with the ATS to monitor and control the temperature during curing of a polymer on a silicon wafer in the VFM furnace.

CHAPTER 1

INTRODUCTION

1.1 Research Objectives

The development of advanced materials plays a vital role in the manufacture of thinner, smaller, and faster electronic devices. The Interconnect Committee of the International Technology Roadmap for Semiconductors (ITRS) states: "In the near term, the most difficult challenge for interconnect is the introduction of new materials that meet the wire conductive requirements and reduce the dielectric permittivity [1]." Thus, one of the limiting factors in the forefront of improving electronic device performance is the interconnections (or wires) within integrated circuits. Since the interconnect delay depends on the dielectric constant of the insulator between interconnects, lower dielectric constant materials are needed. As such, a number of research studies have been conducted to develop low-k and ultra low-k dielectrics for use in the semiconductor manufacturing industry [2, 3].

Dielectric materials are not only used as inter-level insulation in the semiconductor industry, but they are also used as passivation layers, underfill materials (which are used to reduce stress) and encapsulants (see Figure 1). In the past, dielectrics were mainly inorganic materials such as silicon dioxide, silicon nitride, and poly-crystalline silicon. These inorganic layers were deposited by chemical vapor deposition (CVD), sputtering, or evaporation, and they were patterned using wet or dry etching techniques [4]. However, these inorganic materials were prone to cracking, had high dielectric constants (approximately 3.5-4.0), and tended to reproduce the topography upon which they were

deposited (i.e., poor planarization). Planarization is essential for fabricating multilayer interconnected packages.

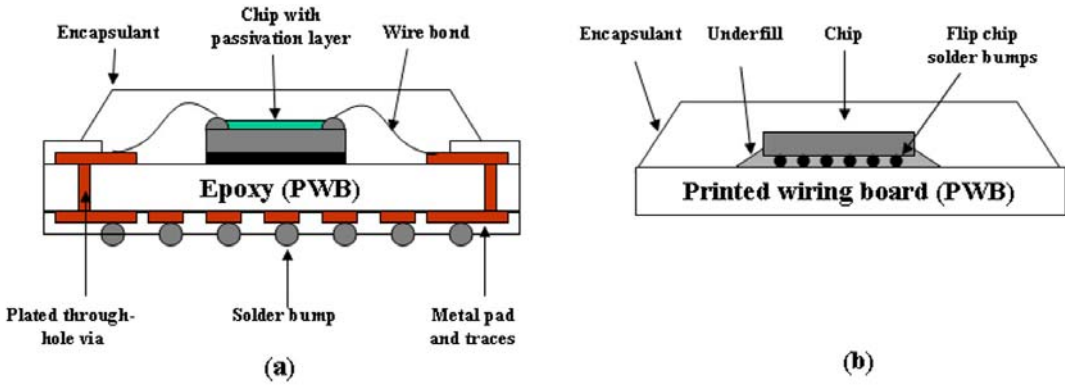

Figure 1 – Conceptual sketch of (a) a ball grid array with polymer dielectrics serving as the encapsulant, passivation layer, and the inter-level dielectric (epoxy printed wiring board) and (b) flip chip device with the polymer dielectric serving as the underfill.

As passivation layers, dielectrics are deposited as the last layer before an integrated circuit is packaged. This layer is patterned to expose the underlying metal contacts so that the chip can be attached to metal wires or leads, and it protects the chip from moisture and ionic contaminants that can gain access to the circuit metallization via bond pad openings or defects and pinhole in the material, leading to corrosion of the internal metallization [4]. It also serves to protect the semiconductor device from mechanical damage during the subsequent assembly steps. Thus, for a dielectric to server as a successful passivation layer, it should possess some of the following attributes: low defect density, low dielectric constant, low deposition and processing temperatures, high chemical stability, high thermal stability, good adhesion, good planarization, low moisture absorption, low stress, low coefficient of thermal expansion, high elongation to break, low modulus, and low cost.

The limitations of the traditional inorganic dielectrics have driven the microelectronics industry to develop new organic, inorganic, and porous dielectric materials that have superior performance over traditional inorganic dielectrics. A considerable number of these novel dielectrics are polymers, polyimides, spin-on glasses and porous materials. With increasing demand for novel dielectrics, there is a corresponding demand for new processing techniques that lead to comparable or better properties than conventional methods.

Presently, conventional thermal curing steps can take several hours, and there is a need to shorten the processing time for cost reasons [5]. A new thermal processing technique known as variable frequency microwave (VFM) curing can perform the same processing steps in minutes without compromising the intrinsic material properties [6-8]. In the future, VFM processing could be a viable alternative to conventional thermal processing techniques because of advantages like rapid heating, selective heating of materials though differential absorption, penetrating radiation, controllable electric field distribution, and self-limiting reactions. However, current limitations in VFM processing include uncertain process characterization methods, lack of reliable temperature measuring techniques, and the lack of control over the various processes occurring in the VFM chamber. The current research addresses these challenges by: (1) development of accurate empirical process models using statistical experimental design and neural networks; (2) recipe synthesis using genetic algorithms; (3) implementation of an acoustic temperature sensor for VFM processing monitoring; and (4) implementation of an intelligent control strategy for VFM processing.

1.2 Summary of Work

In this research, several statically designed experiments were performed to verify that VFM curing results in comparable material properties. These experiments were on samples of the polymer benzocyclobutene (BCB), Cyclotene 3022, and the polyimide, PI 2611, cured on silicon wafers. The curing was performed in the Lambda Technologies MircoCure™ 2100 system, as well as a conventional thermal furnace. All samples were heated to an appropriate temperature and held at temperature for a specific amount of time for both processing methods. After the BCB samples cooled, the through-plane and in-plane indices of refraction were measured via ellipsometry. After the PI 2611 samples cooled, through-plane and in-plane indices of refraction were subsequently measured using a Metricon prism coupler. The percent of imidization was measured using attenuated total reflection Fourier transform infrared (ATR-FTIR) spectroscopy.

Neural networks were then trained using the data from the designed experiment to model the variation of the output as a function of input variables. To train the neural networks, the back-propagation algorithm was utilized. The inputs to the neural networks were temperature and time-at-temperature. The outputs of the networks for cured BCB were the in-plane and through-plane indices of refraction. The indices of refraction were then used as metrics to determine the extent of cure of the BCB. The output variables of the cured polyimide were the in-plane and through-plane indices of refraction, the birefringence, and the percent of imidization of polyimide. To validate the neural network models, the root-mean-square (RMS) error was used as a performance metric. The neural network models were then used for process optimization via genetic algorithms. Using this

approach, the appropriate input conditions to achieve desirable film properties were determined.

In order to achieve the desired film properties, the VFM curing process must be monitored and controlled. For polymer curing, one of the important process parameters to monitor and control is the cure temperature. Although a few methods exist to monitor the temperature in the VFM furnace (thermocouple, IR pyrometer, and fiber optic probe), they each have limitations. Hence, an acoustic temperature measure device has been developed. Several groups have exploited the concept of measuring temperature in a gas by measuring the speed of sound in that gas [9]. Where, this technique has been in use for a number of years, a variation on the same idea is to measure the temperature by sending ultrasonic pulses down a crystalline rod of known expansion and propagation properties [10]. By placing slots in the rod at known and calculable distances from the excitation position, the temperature of the medium can be calculated by measuring the reflection times of the pulses from the notches. Similarly, the current technology exploits the temperature dependence on the acoustic velocity in silicon to monitor the temperature of the wafer while curing a polymer dielectric deposited on it a VFM furnace.

For process control, it is important to reduce process variability so that good electrical and mechanical properties are produced as a result of the cure. Improved processing monitoring and control of the VFM system can be accomplished by utilizing the acoustic temperature measuring device in addition to an intelligent control scheme. Intelligent control techniques are methodologies that combine symbolic and numeric manipulations in addressing problems of identification, modeling, and control of complex large-scale systems. One such intelligent control scheme is a neural network feedback

controller. This technique has been implemented to control the VFM system using the acoustic temperature sensor as the monitoring device.

1.3 Outline of Thesis

While the first chapter provided the motivation and the objectives of this research, the remainder of this thesis will provide additional information on microwave processing, artificial intelligence techniques used for microwave curing, and an acoustic temperature sensor used in-situ during microwave curing. Including the current chapter, this thesis is divided into eight chapters. The second chapter provides background information on microwave processing in general and specific information on microwave curing of polymer dielectrics. In Chapter 3, a review of the current literature on artificial intelligence used for modeling and optimization in the semiconductor industry is provided. In Chapter 4, neural networks are used to model VFM curing of benzocyclobutene. These neural networks model the variation of the in-plane and through-plane indices of refraction, as well as the percent cure of the BCB as a function of VFM temperature and time-at-temperature. In Chapter 5, neural networks are used to model VFM curing of polyimide, and these process models are used for process optimization using genetic algorithms. Process monitoring using the acoustic temperature sensor is discussed in Chapter 6, and the neural controller is discussed in Chapter 7. Finally, conclusions and recommendations for future work are given in Chapter 8.

CHAPTER 2

BACKGROUND AND MOTIVATION

Polymers are very large molecules composed of many repeating units called monomers. When these monomers are bonded together or cured, they form long chains. For microelectronics, the usefulness of a given polymer is governed by several major factors [4]. First, the intrinsic chemical activity of the repeating units is important because in certain applications, inertness to heat, radiation, and moisture is desirable; while in others, sensitivity to these parameter may be desirable. Size and architecture are also important molecular parameters. The size of a polymer is measured by its molecular weight, which is directly proportional to the degree of polymerization, or the number of monomers contained in the molecule. The molecular architecture can be thought of as the chain geometry, which can be very complex and have infinite variations of the basic linear connection structure. Polymer chain geometries consist of linear, branched, and crosslinked network structures (see Figure 2). Branched polymers consist of tree-like structure with side branches. When a branched polymer grows very large, a three-dimensional network called a crosslinked network is formed, where all of the monomers are connected by crosslinks to other monomers. A crosslinked network polymer structure no longer dissolves in any solvent unless chemical bonds are broken by some external agent, which causes molecular degradation. Thus, crosslinked networks can absorb large quantities of strong solvents, which can lead to significant swelling.

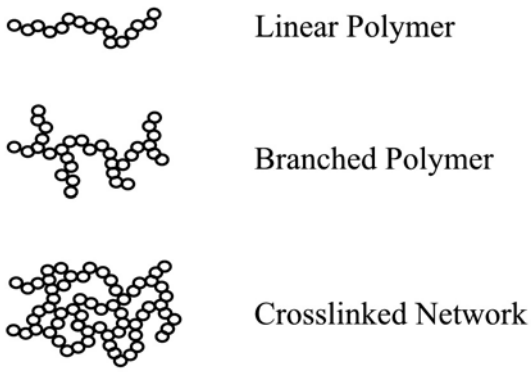

Figure 2 – Major network chain architectures: linear, branched, and crosslinked structures.

The chemical composition of a polymer is also a key component in determining its usefulness in the microelectronics industry. A polymer may consist of all identical monomers (called "homopolymers"), or may be composed of several different monomeric units (called "copolymers"). The spatial arrangement of the monomers along the backbone of a polymer can be random or block-like for the linear architecture. Branched polymers may have homopolymers backbones with different grafted copolymer side branches.

Starting with one or two monomers, an infinite number of different polymer systems can be constructed. These polymers can differ in primary sequencing along the backbone, chain length, side branching, composition, spatial arrangements, and the type of intermolecular bonding or interactions between the monomer units [4]. However, most of the physical and chemical characteristics of a polymer are a function of its basic building blocks, the chemical nature of its monomers, and how it is cured.

Curing affects mechanical and electrical properties as well as the long-term reliability of polymers. Curing drives polymeric reactions to completion. Thus, the degree of cure is very important. If a polymer is not fully cured, it can have a tremendous adverse impact on the properties of the film. For example, curing removes solvent and water,

which if not done properly, can cause the loss of adhesion. The degree-of-cure also affects the amount of moisture intake. Moisture intake can cause adhesion loss, change the electrical properties, and cause the metal interconnects to rust, which could lead to short circuits. High stress, which can be caused by a coefficient of thermal expansion (CTE) mismatch, can cause wafer warpage and fracturing of different layers

Over the past decade, much research has focused on finding alternatives to thermal processing techniques for curing polymer dielectrics [11, 12]. Considerable effort has focused on the use of electromagnetic radiation. However, it has been determined that traditional radiation sources--such as gamma rays, ultraviolet (UV) light, and electron beam accelerators--have limitations. For instance, gamma radiation is dangerous, which creates liability problems. Electron beam radiation has high startup cost and limited throughput. UV light has poor penetration for thick resist and low intensity at wavelengths that are useful for processing photoresist. Due to these limitations and the time required to cure polymers for a conventional curing cycle, a number of researchers have recently investigated the use of microwave radiation to cure polymeric dielectrics [8, 13-15]. Microwave processing has advantages over conventional thermal processing techniques, including rapid heating, selective heating of materials though differential absorption, penetrating radiation, controllable electric field distribution, and self-limiting reactions.

Although microwave ovens are found in almost every home in the United States, there are two primary limitations of home microwave ovens being applied to semiconductor manufacturing and packaging - thermal runaway (hot and cold spots in food) and arcing of metals (such as utensils and aluminum foil). These problems are largely related to the fixed-frequency (2.45 GHz) operation of such appliances in the home.

However, a relatively new process called variable frequency microwave (VFM) does not suffer from the limitations of fixed-frequency microwaves. VFM operates by sweeping 4096 frequencies over a 1 GHz bandwidth about a center frequency every 100 milliseconds. The center frequency can be selected from a variety of bands. With this frequency stepping, VFM technology eliminates hot and cold spots and allows the use of metals in the microwave chamber. Figure 3a) is a schematic representation of an electric field established in a cavity by a fixed-frequency microwave, while Figure 3(b) is a schematic representation of an electric field established in a cavity by a variable frequency microwave [16].

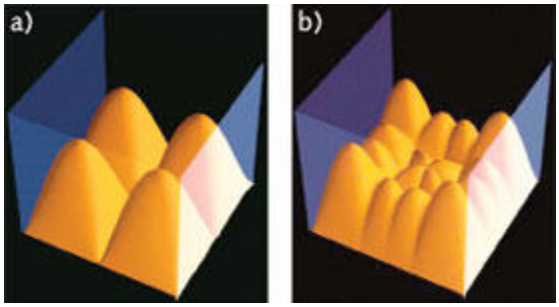

Figure 3 – Schematic representations of microwave energy distribution in cavities for (a) fixed frequency microwave and (b) variable frequency microwave [16].

2.1 Microwave Fundamentals

The electromagnetic (EM) spectrum consists of a range of frequencies going from kilohertz range to the 10^{22} gigahertz range. The microwave region of the EM spectrum corresponds to frequencies of 3–300 GHz [11, 17]. Figure 4 illustrates the electromagnetic spectrum and shows the range of frequencies and wavelengths of various electromagnetic waves within the spectrum [18].

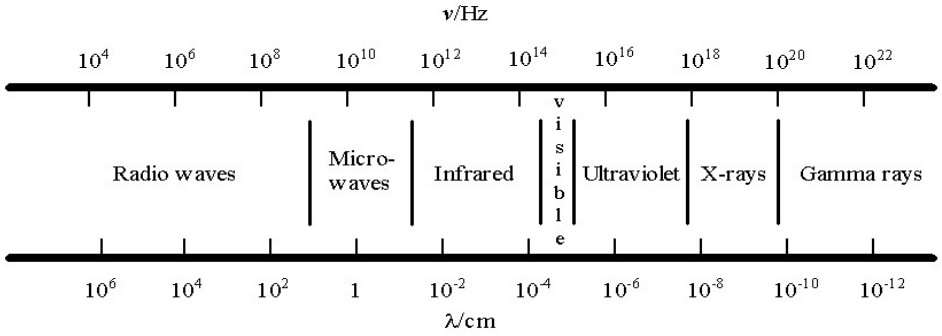

Figure 4 – Electromagnetic spectrum.

2.2 Fixed Frequency Microwave Systems

Microwaves are commonly generated by electronic devices such as klystrons or magnetrons whose power outputs range from microwatts to megawatts. These systems can produce continuous or pulsed wave oscillation of a single tunable frequency. In the literature, an experimental setup in which microwaves are generated is referred to as a microwave circuit. These microwave circuits consist of a waveguide that directs the propagating microwave along some path. The material is exposed to the microwave radiation in the part of the circuit called the applicator, which can be a waveguide or a cavity resonator that can be cylindrical or rectangular. These cavity applicators can be design to operate in either single or multiple resonate modes, where the most common frequency used is 2.45 GHz [11, 18]. In a single-mode format, a standing wave is generated, and in this location the microwave energy intensity is the highest. In a multi-mode format, there are several energy intensity peaks (see Figure 3).

Heat is generated within the material by microwave absorption. The heating properties of materials depend critically on their dielectric properties and how these properties change with temperature and the microwave field distribution in the chamber.

Microwave radiation can be applied to materials in the form of continuous waves or pulsed waves. In the continuous wave mode, energy is supplied continuously at a constant power level during material processing. In the pulsed mode, the microwave energy is pulsed in an on-off manner at preset values of pulse length, pulse period, and pulse peak in order to give a desired average power level [18].

There are limitations to processing materials using single frequency microwave applicators. For instance, there is not an efficient way to tune or control the modes during processing. There is also uncontrolled coupling efficiency, and they are limited ways to couple microwave energy into the material because of the lack of control of the modes. Furthermore, because of the standing wave patterns that are formed, there is uneven heating of the sample, and at the location(s) of peak energy intensity, the temperature of the material can increase more rapidly than their surrounding areas, producing what is termed "thermal runaway". Finally, metals cannot be processed in fixed-frequency microwave applicators. Thus, an alternative approach to fixed-frequency microwave processing is needed for polymer dielectric curing.

2.3 Variable Frequency Microwave Systems

VFM is a patented microwave technology developed at Oak Ridge National Laboratory that does not have the limitations of a fixed-frequency operation [19]. A VFM furnace has the capability to step through several thousand frequencies over a gigahertz frequency range in fractions of a second. This frequency stepping provides a time-averaged uniformity in energy distribution throughout the cavity, and thus eliminates the uniformity issues involved in the temperature distribution that occurs in fixed-frequency microwave ovens. Like fixed-frequency microwave systems, in VFM processing, heat is generated

within the material by microwave absorption. The heating properties of a material depend critically on the dielectric properties of that material and how those properties change with temperature and the microwave field distribution in the furnace. Contrary to fixed-frequency microwave systems, metals may be processed in a VFM cavity because cycling through thousand of frequencies in less than a second eliminates charge buildup, and hence, arcing [13-15].

There are several limitations for processing materials with VFM furnaces. The limitations include uncertain process characterization methods, a lack of understanding of the interactions between microwaves and materials, a lack of reliable temperature measurement techniques, and the lack of control over the various processes occurring [15]. With the lack of reliable temperature measuring devices, VFM processing has a limited capacity to effectively monitor and control the temperature of a polymer being cured. In addition, given the lack of understanding of the process and control over the various processes of VFM, there is a need to develop models that can predict the output response of a VFM process for a given application.

2.4 Polymer Dielectric Curing by Microwave Radiation

Microwave heating of polymers is a volumetric heating process in which strong dipole groups couple to the microwave field. This coupling of microwave energy to dipole groups in the polymer resin leads to rotation and vibrations of these groups resulting in heating and faster curing. Figure 5 illustrates this process.

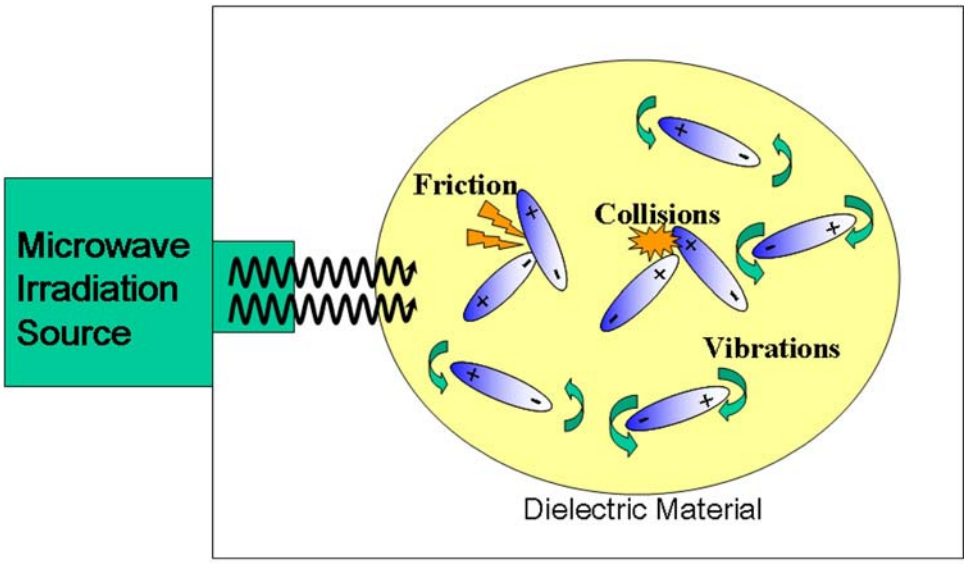

Figure 5 – Microwave irradiation of polymer dielectric dipoles leading to vibrations and rotations of the dipoles and ultimately heating.

The absorption energy of a microwave is proportional to dielectric loss [20]. There are four polarization mechanisms in polymers: 1) electronic, 2) ionic or atomic, 3) dipolar or orientational, and 4) interfacial. Electronic polarization consists of the displacements of electrons with respect to their atomic nucleus under an electric field. Ionic or atomic displacement is due to the asymmetrical distribution of atoms and ions in a molecule. An applied electric filed can displace these atoms or ions relative to one another and induce atomic polarization. Dipolar polarization occurs when a molecule having a permanent dipole moment is placed in an electric field. The dipole moment will try to orient in the direction of the electric field, which causes polarization. Interfacial polarization occurs when charge accumulates at the interface between components [5, 21].

With an applied electric field, polarization may be in-phase or lag behind the electric field, depending on the field strength and the properties of the material. One such property is the complex dielectric constant, which has the form

$$\varepsilon = \varepsilon' + j\varepsilon'' \tag{1}$$

where ε' is the real part or relative permittivity and ε'' is the relative loss factor. The ratio of the imaginary and real parts of the dielectric constant is known as the dielectric loss tangent, $\tan\delta$, where δ is the loss angle. Both the relative permittivity and the relative loss factor are functions of frequency, temperature, and material properties [21].

At lower frequencies, the polarization is in-phase with the electric field. The phase shift (or loss angle) is zero. Therefore, the charged particles have the ability to follow the alternating electric field, and the dielectric stores energy. At higher frequencies, the polarization lags behind the electric field. With a phase shift present in this case, the dielectric dissipates energy, which produces heat. When the relaxation time of the polarization is equal to the period of the applied field, a resonant condition is obtained at which the loss tangent is a maximum.

One of the main mechanisms of coupling microwave radiation to polymer dielectrics is through dipole orientation. The amount of microwave energy absorbed by a material is given by [5, 20]:

$$P_{absorbed} = 2\pi f E_{rms}^2 \varepsilon_o \varepsilon'' \tag{2}$$

where $P_{absorbed}$ is the power absorbed, f is the frequency, E_{rms} is root-mean squared applied electric field, ε_o is the dielectric constant of free space, and ε'' is the relative loss factor. The conversion of electric field into heat is proportional to the frequency, the dielectric loss, and to the square of the electric field strength. Therefore, materials with high dielectric loss values are easily heated by microwave radiation, and materials with low dielectric loss are "transparent" to microwave radiation [18].

2.5 Applications of Polymers Cured by Microwave Radiation

For a number of years, polymers have been cured using microwaves in various industries [18]. They have been cured using both fixed and variable frequency methods utilizing a number of applicators. Polymers in the microelectronics industry are mainly used as dielectric layers and stress buffer passivation layers [6], and microwave radiation has been used to cure some of them [5]. VFM technology was first introduced to the microelectronics packaging industry for curing glob top, dam and fill, flip chip, and a number of other encapsulation and adhesive applications. More recently, VFM technology has been used for curing adhesives in the fiber optics and optoelectronics industry. In these industries, VFM offers the advantages of faster cure and selective heating. Selective heating allows for a polymer to heat faster than the substrate, which reduces the thermal budget that a device may undergo. Curing has been reported to be 2 to 10 times faster with VFM technology than conventional heating methods [16].

2.5.1 *Epoxy Resins*

Epoxy resins are used in a number of diverse applications including surface coatings, printed circuit boards, the potting of electrical components, rigid frames,

adhesives, and fiber reinforced composites. However, conventional thermal processing of epoxy can require long cure times and large temperature gradients. Therefore, a number of researchers have investigated curing epoxy resins with microwave energy [11, 18, 22-25]. Several of these studies compare the difference between curing epoxy using a conventional thermal furnace and microwave radiation and the influences that these methods have on final film properties. However, there is disagreement on whether resins cured by microwave heating follow the same reaction path, develop the same cross-linking network, or other properties compared to those cured by conventional thermal heating [26]. Furthermore, there is still not a consensus on the appropriate process conditions.

2.5.2 *Polyimide*

Polyimides are an important class of high-temperature, dimensionally stable, high-performance polymers with a wide range of applications in aerospace and microelectronics [13]. Prior research has been conducted on curing polyimides using microwave irradiation. Lewis, et al. [14] used a single mode microwave operating at 2.45 GHz for polyimide curing. Farnsworth, et al. [8] characterized photosensitive polyimide that was cured in a variable frequency microwave furnace (VFM). In that study, it was determined that there was no significant difference in polyimide cured using microwave curing as those cured using conventional thermal processing.

The ability to selectively heat polyimide on an epoxy substrate using a VFM furnace was demonstrated by Tanikella, et. al. [20]. The polyimide with a cure temperature of approximately 350^{o}C was cured while not significantly heating the FR-4 epoxy substrate, which has a degradation temperature of below 250^{o}C. It was shown that the

temperatures used to cure the polyimide in the VFM furnace could not be used in the conventional furnace for the same degree of conversion without destroying the substrate.

2.5.3 *Benzocyclobutene*

Benzocyclobutene is a low-k polymer dielectric. It has a dielectric constant of 2.7. In [15], benzocyclobutene (BCB) was cured in the VFM furnace. It was determined that there were no significant differences in chemical structure between VFM and thermally cured films. In addition, it was discovered that BCB could be cured at a lower temperature or for shorter processing times using VFM curing. With the microelectronics industry moving to lower processing temperatures, curing in a VFM system is an advantage over conventional thermal curing.

In [27], Sung conducted a study to evaluate VFM heating characteristics of polyimide and benzocyclobutene on copper clad bismaleimide triazine (BT)/epoxy substrates. It was determined that VFM heating rates are affected by the copper cladding, that degradation occurs at the end of copper lines due to the fringing effect of the microwave fields inside of the VFM chamber, and that the electric field focuses at sharp edges of copper lines. The results of this study imply that it may be difficult to process organic laminates with patterned sharp metal edges.

2.5.4 *Conductive adhesives*

Conductive adhesives are used in the microelectronic packaging industry as a composite consisting of metal particles in a polymeric resin. The packed structure of contacting metal particles provides the electrical conductive path between the chip and substrate connection pads. Conductive adhesives need to be raised to a minimum

temperature to initiate cross-linking of the resin polymers. Traditionally, this has been done in a conventional furnace to avoid arcing of the metal particle in the polymer resin that occurs the conductive adhesives are placed in a single-frequency microwave oven. However, this is not a problem with variable frequency systems. Therefore, research is now being performed on curing and modeling VFM curing of conductive adhesives [28, 29]. One of the goals of the aforementioned research is to reduce the amount of time it takes to cure these adhesives.

2.5.5 *PMMA*

Polymethyl methacrylate (PMMA) is a widely used industrial and commercial polymeric material because it is well characterized. PMMA was used in a study to compare the heating of a polymer with different power settings for a microwave applicator [11]. The microwave applicator was a single frequency of 2.45 GHz. The study concluded that microwave curing produces a slight rate enhancement over thermal curing, but a decrease in the percentage conversion as the power is increased.

2.6 Summary

Polymers are widely used in the semiconductor industry as dielectrics, underfills, encapsulants, and passivation layers. The physical and chemical characteristics of a polymer are functions of properties such as the chemical composition, molecular weight, and the molecular architecture. Curing or the extent-of-curing can also affect polymer properties. To reduce curing times, microwave furnaces, more specifically VFM furnaces, have been used instead of conventional thermal furnaces, and it has been shown that microwave curing produces films with comparable material properties. The next chapter

will provide a review of artificial intelligence techniques used for modeling, optimization, and control in semiconductor manufacturing and research.

CHAPTER 3

LITERATURE REVIEW

3.1 Introduction

The emergence of neural networks in semiconductor manufacturing has been directed at minimizing process variation. To this end, neural networks have been used for process modeling, optimization, control, and diagnosis. Neural networks are capable of performing highly complex mappings on noisy and/or nonlinear data, thereby inferring very subtle relationships between diverse sets of input and output parameters. As a result, neural networks can illuminate I/O relationships from limited data. This capability is extremely useful in semiconductor manufacturing, where highly nonlinear fabrication processes are numerous and experimental data for process modeling is expensive to obtain [30-36]. A natural extension of neural network based process modeling is using the models derived to optimize processes via automated recipe synthesis [37-41]. Furthermore, neural networks are also well-suited to process control, since they can be used to build predictive models from multivariate sensor data generated by process monitors [42, 43]. Finally, neural network can be used for *in-situ* diagnostic schemes by working in tandem with expert systems to facilitate fault detection and identification.

3.2 Neural Networks

Artificial neural networks can be used to model microelectronic manufacturing processes because they have the capability of learning arbitrary nonlinear mappings between input and output patterns. Figure 6 illustrates a neuron, which consists of a summation and a nonlinear transfer function. The activation level on the neuron is

determined by the transfer function, which generally used has a sigmoidal shape such as that represented by the following equation:

$$f(x) = \frac{1}{1 + e^{-x}} \tag{3}$$

where x is the weighted sum of the neural inputs and $f(x)$ is the output of an individual neuron. This activation function enables a neural network with the capability to generalize with an added degree of freedom not available in statistical regression techniques [35, 44].

Beyond semiconductor manufacturing, neural networks are used in various fields, including biology, finance, and medicine for such diverse applications as pattern recognition, modeling, prediction, and data clustering. As a consequence of such demand, there are a number of commercially available neural network software packages. A notable general-purpose package is the MATLAB Neural Network Toolbox from Mathworks™ [45].

For semiconductor manufacturing applications, the Object-Oriented Neural Network Simulator (ObOrNNS) software tool was developed by the Intelligent Semiconductor Manufacturing Group at Georgia Tech. The original version of ObOrNNS, which was developed in object C in the early 1990s [35], consisted of a collection of classes used for direct neuromorphic simulation. The next revision added an interface to run the program with a DOS command line interface. The current version, which has been used for this research, is a Java implementation of ObOrNNS. This version of ObOrNNS has been shown to be faster than a neural network implemented with the Neural Network Toolbox in MATLAB in terms of number of epochs needed to converge and the actual

computational time required for convergence. In addition, ObOrNNS now includes a genetic algorithm-based feature that uses a trained neural network for process optimization and recipe synthesis.

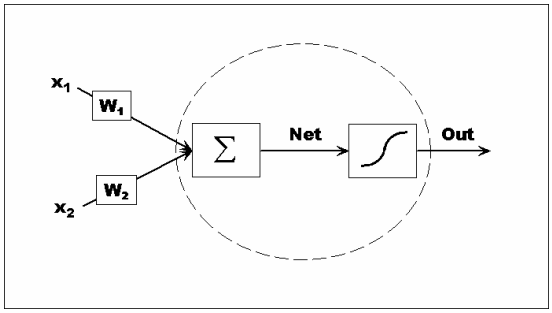

Figure 6 – Functional diagram of a neuron (enclosed in dotted circle).

3.2.1 *Neural Network Structure*

Neural network learning is designed to determine an appropriate set of interconnection strengths (or weights) that facilitate the activation of the neurons to achieve a desired state related to a given set of sampled patterns. A neural network consists of several layers of neurons, which are interconnected in such a way that information is stored in the weights assigned to the connections. Figure 7 is an illustration of a neural network. The first layer is the input layer where data is introduced to the network. The next layers are the hidden layers, where there may be one or several hidden layers. The last layer is the output layer.

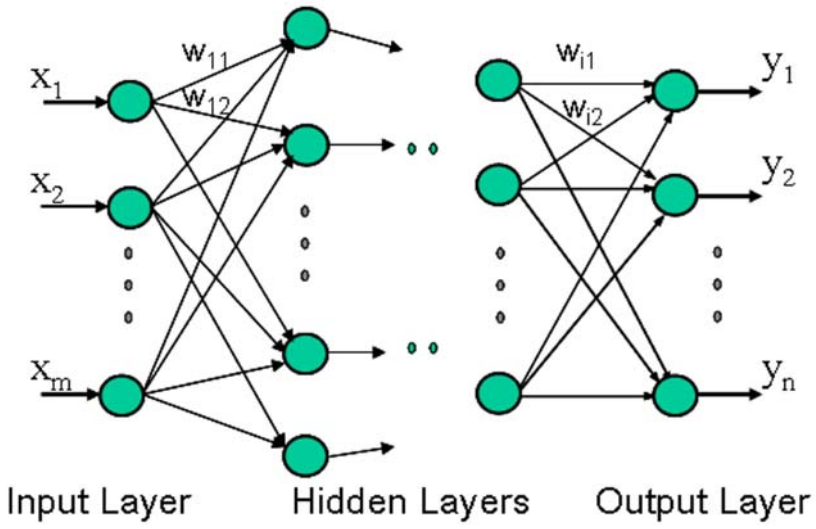

Figure 7 – Feed forward neural network with two input layer neurons, three hidden layer neurons, and two output layer neurons

3.2.2 *Neural Network Training*

Training of a neural network can either be supervised or unsupervised. Supervised training occurs when input-output data is available, and the error between the output of the network and the target data is used to generate feedback (or supervision) to the network for learning. Unsupervised training occurs when there is no output data for the corresponding input data. Typically for microelectronic processing, supervised training is used to model the process data that occurs during fabrication. Therefore, supervised training is emphasized in the remainder of this chapter.

Supervised training of a neural network involves updating the weights in such a manner that the error between the outputs of the neural network and the actual output data is minimized. A network can be trained using this approach via the error back-propagation (BP) algorithm [46], which is an iterative algorithm that starts with a vector of values being input into the network. The output is calculated by summing the weighted input

connections of each layer and filtering this sum with the activation function. The calculated result of the output layer is compared to target data, and the squared difference between these two vectors determines the error. This error is minimized using the gradient descent approach.

The weight update equation for BP training at the $(n+1)^{th}$ iteration is given by:

$$w_{ijk}\left(n+1\right) = w_{ijk}\left(n\right) + \alpha \Delta w_{ijk}\left(n-1\right) + \eta w_{ijk}\left(n\right) \tag{4}$$

where w_{ijk} is the connection strength between j^{th} neuron in layer (k-1) and i^{th} neuron in layer k, and Δw_{ijk} is the calculated change in the weight that reduces the error function of the network. The parameter η (a constant between zero and one) is the learning rate, and α is the momentum constant. The learning rate determines the speed of convergence by setting the step size. The momentum term prevents the training algorithm from settling in local minima and increases the speed of convergence.

The performance of the model is generally evaluated in terms of network training error and prediction error. Each measure of learning capability is quantified by root-mean-square-error (RMSE) given by:

$$RMSE = \sqrt{\frac{1}{n-1}\sum_{i=1}^{n}\left(y_i - \hat{y}_i\right)^2} \tag{5}$$

where n is the number of trials and y_i is the measured values of each response, and $\hat{y}_i$ is the neural model output. The training error is the RMSE of the data used for network training, and the prediction error is the RMSE of the data reserved for network testing.

3.3 Genetic Algorithms

While neural networks can model the relationships between process set points and responses, search techniques must be used to generate optimal recipes for desired target responses. To achieve (potentially conflicting) process objectives, genetic algorithms (GAs) have recently been used successfully to determine optimal set points in electronic packaging and semiconductor manufacturing processes [37-41]. GAs are guided stochastic search techniques based on the mechanics of genetics [47, 48]. They simulate basic genetic operations found in natural selection and evolution to guide their search through the solution space. Some benefits of GAs include: the obviated need derivative information to search the solution space, resulting in a low probability of GAs getting "trapped" in local minima (or maxima); the implementation of a parallel search as opposed to a point-by-point search; and the manipulation of potential solutions, rather than the solutions themselves. GAs, consequently, do not require a complete model of the problem or the search space to be regularly shaped and differentiable. The only problem-specific requirement of GAs is the ability to evaluate the trial solutions on their relative fitness [48].

The beginning step to implementing a GA is the creation of a population of trial solutions (often called "individuals"). Those possible solutions are commonly represented as binary strings (called "chromosomes"), which are manipulated by a set of genetic operators. The number of digits assigned to a given parameter determines the numerical accuracy achieved in the search. Multiple parameters are encoded and concatenated in a

single chromosome, where individual sections of the string represent the encoded parameters of the proposed solution. If $\alpha \in [0, 2^l]$ is the parameter of interest (where l is the number of bits in the string), the decoded unsigned integer α is mapped linearly from $[0, 2^l]$ to a specified interval $[U_{min}, U_{max}]$. The multi-parameter code is constructed by concatenating as many single parameters as required. Each bit string may have its own range. Figure 8 shows a 3-parameter coding where the first, second, and third parameter ranges are 1-8, 0-31, and 1-14, respectively. The actual parameters encoded are 8, 20, and 14, respectively.

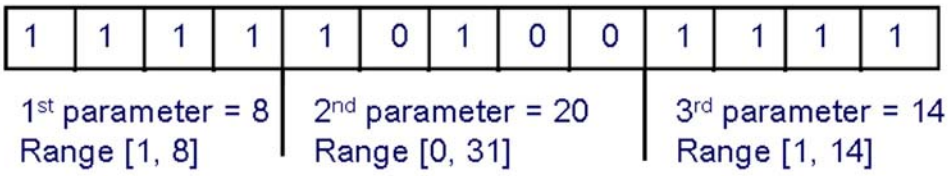

Figure 8 – Example of multi-parameter coding

These strings are then decoded and evaluated on how well they solve the problem. This fitness measure is used to allocate reproductive opportunities in such a way that the chromosomes representing a better solution to the problem are given a greater opportunity to generate offspring. In the reproduction process, individuals with high fitness values (i.e., good solutions to the optimization problem under consideration) receive larger number of copies in the new population. In the *elitist roulette wheel* selection method, those strings with large fitness values (F_i) are assigned a proportionately higher probability of survival into the next generation. This probability distribution is determined by the following formula [47]:

$$P_{select\_i} = \frac{F_i}{\sum F} \tag{6}$$

An individual whose fitness in *n* times better than another will potentially produce *n* times the number of offspring in the subsequent generation. This scenario allows GAs to take advantage of a "survival-of-the-fittest" strategy. The fitness of each individual of the population is evaluated with respect to the constraints imposed by considering the desired set points of each parameter. An example of a fitness formula is:

$$F = \frac{1}{1 + \sum_n \left| K_n (y_d - y_o) \right|} \tag{7}$$

where n is the number of responses, K_n is the weight of the process responses, y_d is the desired process response, and y_o is the process output resulting from the current input parameters. Values of F near unity indicate high degrees of fitness.

Once the individuals have reproduced, they are stored in a "mating pool" awaiting the genetic manipulation process. As the population evolves through reproduction and genetic manipulation, each generation is increasingly capable of solving the problem. In general, the GAs operate through a cycle of four stages: (1) creation of a "population" of strings; (2) evaluation of each string; (3) selection of "best" strings; and (4) genetic manipulation to create a new population of strings.

The genetic reproduction process combines chromosomes from one generation and produces new chromosomes that maintain many of the features of the previous generation. The most common methods for recombination are crossover and mutation (see Figure 9). The crossover operator takes two randomly selected chromosomes and interchanges part of their genetic information to produce two new chromosomes. The crossover point is randomly chosen, and portions of the parent strings are swapped to produce new offspring based upon a specified crossover probability. Mutation is motivated by the possibility that the initially defined population may not contain all the information necessary to solve the problem. This operation is implemented by randomly changing a fixed number of bits every generation based upon a specified mutation probability. Typical values of the probabilities of crossover and mutation range from 0.6 to 0.9 and 0.001 to 0.03, respectively.

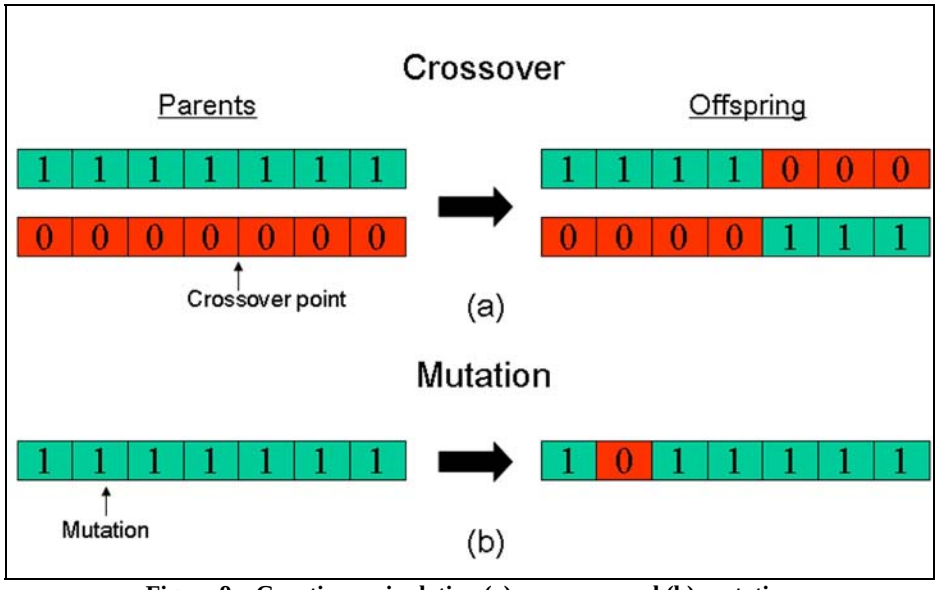

Figure 9 – Genetic manipulation (a) crossover and (b) mutation

3.4 Neuro-Genetic Algorithms

When GAs and neural networks are combined for process optimization, GAs produce the proposed process inputs for the neural network models. The neural networks then calculate predicted responses, and their output is fed back into the GA until a suitable stopping criterion, such as a maximum number of generations or a user defined minimum error, is achieved. The weighting coefficients for the desired responses (see Equation (7)) must also be determined. Figure 10 illustrates the process optimization procedure for a combined GA and neural network implementation.

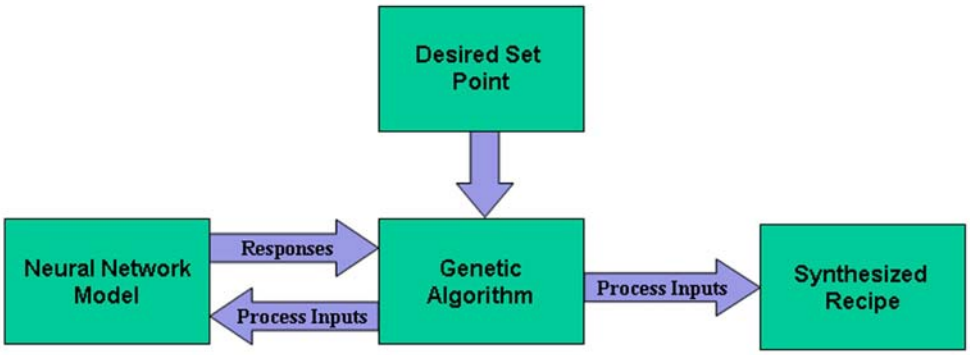

Figure 10 – Process optimization procedure

3.5 Neural Control

Semiconductor processes and equipment are often highly nonlinear dynamical systems, and controlling these types of systems with traditional time-domain and frequency techniques can be challenging [49]. Nevertheless, neural networks are good candidates for controlling nonlinear systems because they are universal approximators [50], and they do not require prior knowledge of the system dynamics [49, 51]. It has been proven that a multi-layer neural network with one hidden layer and sigmoid activation functions can approximate any continuous relationship [52]. In addition, neural networks are easily

trained and can interpolate relationships from partial data, which makes them well-suited to model plant dynamics and the inverse of a plant.

In general, neural networks have been shown to be effective tools in the identification and control of nonlinear dynamical systems [49, 53-60] and, more specifically, semiconductor processes [42, 43, 61-64].

While neural network control ("neurocontrol") was still in it infancy, Werbos [65] has identified five basic types of neurocontrol techniques: supervised, direct inverse control, adaptive control, back-propagation, and adaptive critic (also know as reinforcement learning). The supervised control technique is where a neural network is trained to map input to desired outputs. Direct inverse control is used to track desired trajectories by training neural networks to model the inverse dynamics of a system. An adaptive neural controller uses neural network models in place of one or more subsystems in a model-reference adaptive control system [63]. Back-propagation, as defined earlier, deals with training the network by propagating the error signal backwards to update the weights based on a gradient descent algorithm [54]. The adaptive critic is characterized by neural systems that learn from autonomous interaction with their environments, where the network is reward or punished based on a critic (which could be another network) [53]. It should be noted that the boundaries of each category have not been rigid over time and that back-propagation has been used in each group.

It has been shown that neural networks can provide better performance than linear [43, 51] and other nonlinear [66] controllers. In [51] a neural network was trained offline to learn the inverse dynamic model of a temperature control for a water bath system. When this neural network controller was compared with a proportional-plus integral PI controller,

it provided better tracking performance and load disturbance rejection. In [66], the same authors as [51] compared a neural network controller with three other control schemes (a fuzzy logic controller, a generalized predictive controller (GPC), and a conventional feedback controller) in the regulation of temperature in a water bath. While the neural controller and the fuzzy logic controller are capable of regulating nonlinear systems as well as linear, the GPC is a linear control technique. In this study as well, the neural controller showed the best tracking performance. It performed as well as the GPC and better than the others with load disturbances, but it did not do as well as the GPC in dead time test.

For semiconductor processing, neural networks have been used to control a reactive ion etching process in real-time using a model-based, feedback neural controller [42, 43, 61, 63, 67]. Stokes et al. [43] showed that a neural feedback controller performed batter than the linear quadratic Gaussian with loop-transfer recovery method (LGQ/LTR). In this study, the neural network showed improved set-point tracking, disturbance rejection, response to changes in system dynamics, and response to variable dead time.

In [64], a two-multilayer neural network scheme was proposed for use as an adaptive tracking controller of a reactive ion etcher. One of the proposed networks would be trained off-line to approximately invert the plant dynamics, and the other network would be trained on-line to dynamically cancel the inversion error. A Lyapunov method was derived for on-line training that guaranteed closed-loop stability. A dual-time-scale control strategy was used, where the RIE plant dynamics were split into two separate plants with an inner feedback control loop and outer control loop. Because of an assumption that the feedback coupling from wafer surface reactions to plasma states was negligible, one of the plants represented the bulk plasma dynamics, which could be controlled in the faster inner

loop. The other plant represented the etching dynamics, which could be controlled in the slower outer loop. The inputs to the plasma plant were direct controllable variable such as gas flows and RF power, and the outputs of this plant were the plasma state parameters responsible for etching that included the mechanical energy of impinging ions (DC bias). The etching plant parameters were the etch depth and the etch rate. These parameters are not available in real-time, and thus the outer loop controller was designed to operate on a slower time scale than the inner loop.

For direct adaptive neural control, which is based on a nonlinear difference equation of the process [57], it is required that the input-output dynamics of the process be invertible [67]. If a given system cost function is invertible or approximately invertible, the computation of the control signal is minimized. This means that the control input at any time can be exactly or approximately determined. However, the assumption that a cost function be invertible is very limiting, and control algorithms based on this assumption do not yield good tracking performance. By using a 1-step ahead predictive model, exact or approximate invertibility is often achievable [67]. To generate the control input, a forward neural network process model is generated to emulate the plant. The output of the model is compared to the measured value of the output, and the resulting difference signal is used to tune an inverted neural model, which becomes the neural controller and then is capable of generating the control signals to be applied to the process. In this scheme both the neural emulator and the neural controller are trained continuously on-line [67].

3.5.1 *Reinforcement feedback control*

A challenge to supervised control is that learning requires training data or a teacher of the subject domain for adaptation to take place. In most real-world applications, training

data is often hard to obtain or may not be available at all. Furthermore, the control structures may be prefixed or may only be appropriate for a limited set of problems [68].

An approach to solve this problem is based on a neural network training paradigm known as reinforcement learning. Interest in this paradigm stems from the desire to make systems that learn from autonomous interaction with their environments. In reinforcement learning, it is assumed that the equations describing the system are not known to the controller and that the only information available are the states of the system and a feedback evaluating the performance via a failure or success signal [53]. Due to a limited amount of information, the controller or "agent" has to learn an appropriate policy that transfers an unknown system from its current state to a target state, which is expected to be better [68]. The agent learns what to do by trial-and-error exploration through the state space and receiving a scalar reward (or punishment) for a given action. In other words, the agent maps situations to actions, so as to maximize the scalar reward signal. Not being told what actions to take, the agent must discover which actions yield the most reward by trying them [69]. If an action is tried that produces a favorable response, a reward is given to that action to increase the probability of the system repeating that action should the system find itself in the same or similar state. On the other hand, if the system reaches a non-favorable state, a penalty or punishment is associated with the action that produces the unfavorable response from that state. Furthermore, because of this rewards system, if an action is followed by a satisfactory state of affairs (as defined by some clearly defined goal), then the tendency to reproduce the action is strengthened or reinforced. Reinforcements received by the agent can only be used to learn how to predict the outcome of the selected actions in the future [70]. Reinforcement learning techniques assume that, during the learning

process, no supervisor is present to directly judge the quality of the selected control actions, and therefore, the final evaluation of a process is only known after a long sequence of actions.

In the past ten years, much work has been done in the development of reinforcement learning as a tool of artificial intelligence, computer learning, and intelligent controls [53, 71-75]. Franklin [74] developed a reinforcement learning controller for a system that consisted of a ball rolling on a track. The controller had to evolve to be able to predict the behavior of the system, and then, it had to be able to control it. Tesauro [75] applied reinforcement learning to the game of backgammon. The backgammon game learned to play on an expert level starting from scratch through the use of self-play.

3.5.2 *Different types of neural networks*

There are a few drawbacks to using neural networks. For instance, offline training times for neural networks can be very long, which has discouraged the use them for some practical control applications [57]. To overcome this, Tanomaru et. al. [57] proposed a few algorithms where neural networks are trained completely online. There is also potential for overtraining the network [57, 76]. To overcome the overtraining and long training times, neural networks have been combined with other control schemes to achieve performance objectives that may not have been capable with a single technique. For example, neural networks have been combined with fuzzy logic (some times called neuro-fuzzy logic) [76] and model-based predictive controllers [67]. Numerous training algorithms and new network structures have been developed to cope with some of these issues [49]. Neuro-fuzzy controllers consisted of two neural networks where one represents a traditional back-propagation network and the other approximates a fuzzy logic controller. Lin et al. used a

neuro-fuzzy network [76, 77] to regulate the water bath temperature. This network reduced training time and the problem of over training when compared with a basic neural network.

3.6 Temperature sensing

A limitation of VFM processing is the lack of reliable temperature measuring devices. This limitation reduces the capacity to effectively monitor and control temperature while processing in a VFM furnace. One novel approach to temperature measurement is acoustic temperature sensing. An acoustic temperature sensor (ATS) can be developed based on two phenomena: (1) the change in acoustic velocity as a function of temperature [78], and/or (2) the phase-shift of acoustic wave as it is reflected from an interface as a function of temperature [79].

For many years, researchers have exploited the concept of measuring the temperature of a gas by measuring the speed of sound in that gas; this is a technique known as acoustic pyrometry [80, 81]. These sensors have been developed for real-time temperature profile measurements inside automobile catalytic converters and industrial furnaces and boilers. Another example of change in acoustic velocity being used to measure the temperature is that of the slotted acoustic rod [10]. Where, ultrasonic pulses are excited in an acoustic rod with known expansion and propagation properties. With the rod having notches at known distances from the excitation position, the temperature of the medium can be calculated by measuring the reflection times of the pulses from the notches.

In the 1990s, several acoustic sensors were developed in the Edward L. Ginzton Laboratory at Stanford University [78, 82-85]. One of these sensors was used to measure the temperature in a wafer by exploiting the inter-dependence of the Lamb wave acoustic velocity and temperature of silicon [78, 82-84]. This sensor was used to measure the

temperature in a rapid thermal processing system. In addition to measuring temperature, this technique was used to determine the film thickness on the same substrate that temperature was being measured by using two sets of transducers operating at different frequencies [84]. In [85], Lee and others developed a non-invasive technique to measure temperature using a laser to excite acoustic waves in a substrate and then exploited the change in the dispersion relations of the plate modes through the wafer as a function of temperature. In the late 1990s, the group out of Stanford developed an ultrasonic sensor that was used to monitor pre-bake photoresist processing [79, 86].

Temperature sensors have been developed based on other acoustic wave phenomena as well. Surface acoustic waves (SAW) and surface skimming bulk waves (SSBW) have also been used to measure temperature of films [87, 88].

3.7 Summary

This chapter discusses neural networks use as a tool for modeling, optimization, control and diagnostic in semiconductor manufacturing. It also discusses how using neural networks with genetic algorithms can be used to synthesis recipes for semiconductor processing. In addition, this chapter discusses temperature sensing methods that may be used in a VFM furnace. The next chapter will discuss using neural networks to model curing of benzocyclobutene in the VFM furnace.

CHAPTER 4

NEURAL MODELING OF BENZOCYCLOBUTENE

With VFM curing, heat is generated within the material by microwave absorption. The heating properties depend on the dielectric properties of the material, how these properties change with temperature, and the microwave field distribution in the chamber. However, there is a lack of process characterization methods, a limited understanding of the interactions between microwaves and materials, and limited control over the various processes occurring in the VFM chamber [15]. Given the limited understanding of VFM processes, there is a need to develop models that can predict the output responses of a VFM process for a given application.

To this end, this chapter discusses the modeling of variable frequency microwave curing of Dow Chemical Cyclotene™ 3022 benzocyclobutene (BCB) using neural networks. The response under consideration is the extent-of-cure. The extent-of-cure in polymer dielectrics can be determined by several methods, such as infrared spectroscopy and differential scanning calorimetry. Alternatively, the properties of the cured films can be correlated to the extent-of-cure as an indirect method. For example, for Dow Cyclotene 3022 BCB, the index of refraction is known to be a function of the degree of cure achieved in the films [15, 89]. Thus, the index of refraction is used as the output response in these experiments. The input variables of the experiments are temperature and time-at-temperature. The neural network models developed are able to accurately predict indices of refraction given the temperature and time as inputs.

4.1 Experimental Apparatus

VFM curing was performed in a MircoCure™ 2100 (see Figure 11), which was manufactured by Lambda Technologies, Inc., Research Triangle Park, NC. The controllable parameters for the MicroCure™ 2100 are center frequency, bandwidth, sweep rate, power level, and ramp rate. Samples may be processed at a fixed frequency, with variable frequencies at specific center frequency and bandwidth, with a varying bandwidth, and/or a varying sweep rate. However, the unique feature of this system is the capability of frequency stepping. The system can step through 4096 frequencies over a 1.15 GHz bandwidth every 0.1 s. This frequency stepping provides a time-averaged uniform energy distribution throughout the cavity, which eliminates the non-uniform temperature distribution that occurs in single-frequency microwave furnaces.

Figure 11 – MicroCure™ 2100, Manufactured by Lambda Technologies, Inc.

This VFM furnace also has a feedback control system that regulates the temperature of the sample being processed. The control system can automatically adjust the power levels to maintain the sample at the desired temperature, which allows good control of

ramp rates and final hold temperatures of the samples to be processed. The VFM furnace has provisions to maintain an inert atmosphere during processing of samples. The processing cavity can be pumped down using a mechanical pump and back-filled using nitrogen gas for processing in an oxygen-free environment [15], [8]. Another important characteristic of a VFM furnace is the ability to place metal inside the microwave cavity because charge build up and arcing due to the presence of the field is eliminated [8].

Three temperature measuring devices can be used in the VFM furnace: an infrared pyrometer, a fiber optic probe, and a thermocouple. The pyrometer is a non-contacting device, whereas the thermocouple and fiber optic probe need to be held in contact with the substrate with high-temperature Kapton™ tape and a metal clip insulated with the tape [15]. When processing in the VFM furnace, a sample is placed on a quartz substrate, which is supported by quartz mounts. The fiber optic probe and thermocouple are attached to the sample. Figure 12 is an illustration of the three sensors inside the microwave oven with the thermocouple and fiber optic probes being taped on the silicon wafer. The experimental data is most often taken with the infrared pyrometer as the temperature measuring device, with the fiber optic probe acting as the temperature verification sensor [8, 15].

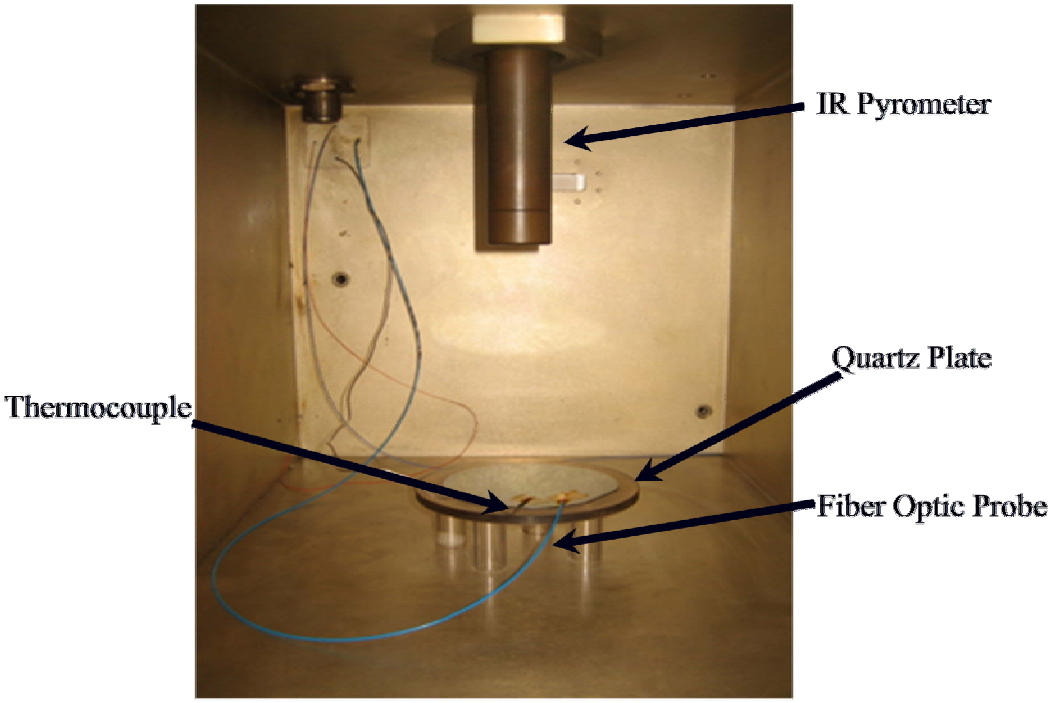

Figure 12 – Illustration of the three sensors (thermocouple, IR pyrometer, and fiber optic probe) inside of the MicroCure™ 2100.

In a high volume semiconductor manufacturing setting, it would be impractical to have fiber optic probes and/or thermocouples contact samples using tape [85]. This would cause contamination. In addition, the tape often peels during processing, and it can be difficult to removal without damaging the polymer after the polymer is cured. Furthermore, the fiber optic probe is limited in its high temperature range, and the thermocouple temperature readings may be unreliable because the way thermocouples measure temperature. Thermocouples measure temperature based on a voltage difference that may be altered by the presence of alternating electromagnetic fields in a VFM furnace. All of these things limit the ability of thermocouples and fiber optic probes to accurately measure and monitor temperature during processing.

To set up the pyrometer for processing, a calibration must be done to determine the emissivity of the sample. The emissivity of the pyrometer is set to the final cure emissivity

of the polymer. The IR pyrometer measures the temperature by sending an IR signal toward the sample and detecting the reflection of the IR signal from the sample. The infrared pyrometer measures radiance received from the target, which provides one variable to Planck's radiation law governing the relationship between the radiance and temperature. The integration of Plank's radiation law requires knowledge of a second variable, which is the target's surface emissivity. The solutions to this problem has been a combination of operator estimates based on experience and/or the use of multi-wavelength pyrometers [90], which attempt to sidestep the mathematical problem by taking the ratio of the different wavelengths and ratioing-out the emissivity using two or more simultaneous measurements of the radiance. For a number of applications, operator experience and multi-wavelength technology are not valid. Without determining a target's emissivity value, true target temperature cannot be determined. Since the current IR pyrometer installed on the VFM does not have a way to automatically change the emissivity during processing, the standard approach is to calibrate the emissivity of the sample for the highest temperature that the polymer will reach and then set the emissivity of the IR pyrometer to that value. This means that the initial temperature readings of the sample are inaccurate, and since the sample's surface changes during curing, subsequent temperature readings are inaccurate [91]. Finally, the IR pyrometer only measures the temperature of the top surface of the polymer. Multi-wavelength pyrometers are limited to low temperature ranges.

4.1.1 *Experimental Technique*

An investigation of the effects of VFM processing on the physical and chemical properties of BCB is outlined in [15]. In that study, the properties of BCB cured using a VFM furnace were characterized under various process conditions and compared to that of

a standard thermal cure. The investigation also attempted to determine if VFM processing led to any enhancement in the reaction kinetics of curing.

Experimental data was taken from samples of BCB spun cast onto 4-inch diameter silicon wafers of <100> orientation. The coated wafers were pre-baked for two minutes at 120ºC to remove solvent, and then they were processed individually in a VFM furnace and in bulk in a conventional thermal furnace.

In order to determine the emissivity of the sample to set up the pyrometer, trial runs were performed on a BCB sample. The emissivity of the pyrometer was set to the final cure emissivity of BCB, which was experimentally found to be 0.52 at a temperature of 250 °C. The process parameters were set in the VFM control interface, and the system was ramped to the cure temperature and held at that temperature for a specified amount of time. Samples were allowed to cool naturally to room temperature.

The BCB samples were taken to an appropriate temperature level in both the thermal and VFM furnaces and held at that temperature for a specific amount of time. For VFM processing, the curing temperature was varied from 175-250 °C and the cure time was varied from 10-30 minutes. For conventional thermal processing, the curing temperature was the same as VFM processing, but the processing times were 20-60 minutes. After processing, the samples were allowed to cool to room temperature naturally. The through-plane and in-plane indices of refraction were then measured with a Metricon™ thin film prism coupler at a wavelength of 632.8 nm. In order to obtain the through-plane and in-plane indices of refraction of the cured films, the refraction measurements were taken in both the transverse electric (TE) and transverse magnetic (TM) modes. The process parameters are illustrated in Table 1.

Table 1 – VFM and conventional thermal processing parameters

Furnace	Parameter	Range
VFM	Temperature	175-250 ºC
	Time	10-30 min
	Index of Refraction	1.551- 1.596
Conventional thermal	Temperature	175-250 ºC
	Time	20-60 min
	Index of Refraction	1.551- 1.596

4.1.2 *Process Characterization*

A number of experimental techniques were used to characterize the mechanical, electrical, optical, and chemical properties of BCB films cured by both VFM and convention thermal methods [15]. Results of that study suggest that chemical changes in VFM cured films are identical to the changes that occur in conventional thermally cured films.

Fourier transform infrared spectroscopy (FTIR) is used as a non-destructive test to determine the chemical changes that occur during a film cure and hence to measure the extent of cure by monitoring the growth of a band in the infrared spectrum [15, 89, 92]. Thus, the extent of cure for BCB was measured using the following equation:

$$Extent\ of\ cure = \frac{\left(A_{1500} / A_{1253}\right)}{\left(A_{1500} / A_{1253}\right)_{hardcure}} * 0.95 \tag{8}$$

where A is the absorbance and the subscripts represents the wavenumber corresponding to the peak. The reference absorbance is determined from a film that has been fully cured with a standard thermal cure. The equation is multiplied by the value 0.95, which is the degree

of conversion of the standard thermal cure [8, 15, 89, 92]. Differences in film thickness or polymer orientation, as well as uncertainty in determining the baseline, may result in slight changes in peak heights. These changes can significantly influence the calculation of the extent of cure, and thus this method is considered only semi-quantitative [8].

As shown in [93], the index of refraction measurement can be used as an indirect method for determining the extent of cure because the index of refraction value decreases when either the curing time or temperature is increased. The following equation can be used as an indicator of the extent of cure:

$$Cure\ index = \left[n - \max(n)\right] / \left[\min(n) - \max(n)\right] \tag{9}$$

where n is the index of refraction, max(n) corresponds to the index of refraction of the uncured sample, and min(n) corresponds to the index of refraction of the fully cured sample. Therefore, a cure index of 0 is for uncured samples, and a fully cured sample has a cure index of 1.

In-plane and through-plane refractive indices of the film were evaluated with the Metricon prism coupler [15]. This data was used to develop a neural network model that predicts the index of refraction given a cure temperature and time-at-temperature. The extent of cure is then determined by calculating the cure index using Equation (9).

4.1.3 *Neural Network Modeling*

In order to model and compare a complex manufacturing process such as VFM processing, two neural network models were developed: a neural network model for VFM curing and a neural network model for thermal curing. Both networks are modeled using the feed-forward, error back-propagation algorithm implemented with the *MATLAB* Neural Network Toolbox. Each network has three layers: input, hidden, and output layers. There

are two inputs, one hidden, and two output neurons. The activation function from the input layer to the hidden layer is the standard sigmoid function (see Equation (3)). The output activation function is purely linear.

4.1.4 *Discussion*

The objective of this study was to use neural networks to model the effects of temperature and time-at-temperature on the curing of BCB on silicon in a VFM system. The inputs to the networks were temperature and time-at-temperature, and the outputs were the indices of refraction. The parameter ranges for the networks are shown in Table 1. Since indices of refraction at five points per wafer were measured, each input pair is associated with the average of the five data points. To train and test the networks, the original data sets were split into training and test sets. The training data consisted of approximately 60 percent of the data. The remaining data were used for testing. In the VFM network, there were 24 data points used for training and 20 data points used for testing. The network was trained for 26 epochs using the mean-square error as the performance metric. The output of the network was used in Equation (9) to produce the cure index.

The response surfaces for the outputs of the VFM and thermally cured neural network are shown in Figure 13(a) and (c). In these graphs, it is seen that as the time and temperature increase, the index of refraction decreases, which signifies that the degree of cure increases. The response surfaces for the cure index are shown in Figure 13(b) and (d). These plots corroborate the above statement, in that as the time and temperature increase so does the cure index or degree of cure.

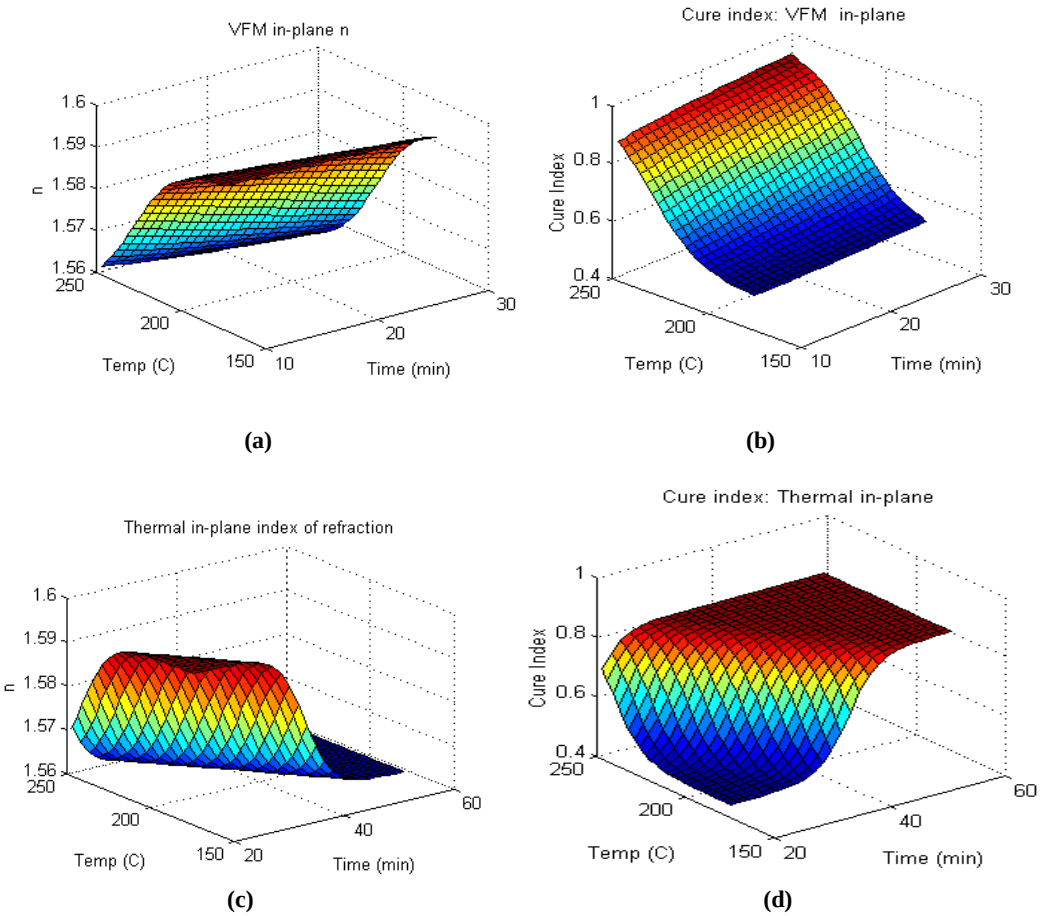

Figure 13 – VFM cured response surfaces of neural network (a) in-plane n, (b) cure index for in-plane n. Thermally cured response surfaces of neural network (c) in-plane n, (d) cure index for in-plane n.

4.1.5 *Predictive Capability*

Both neural network models predict the degree of cure of BCB on silicon with an experimental error, σ, which is the square root of the residual sum-of-squares, S_R, for each response. S_R is calculated as follows [35]:

$$S_R = \sigma^2 = \frac{1}{(n-1)} \sum_{1}^{n} (y_i - \hat{y}_i)^2 \tag{10}$$

where n is the number of experiments, y_i is the measured value of each response, and $\hat{y}_i$ is the corresponding model prediction. As illustrated in Table 2, the S_R for the outputs of the test data is on the order of 1e-2 for VFM and 1e-3 for the conventional thermal furnace.

Table 2 – Neural network experimental error

Furnace	CURE INDEX Model	σ_{NN}
VFM	In-plane	0.020
	Through-plane	0.021
Conventional thermal	In-plane	0.0034
	Through-plane	0.0040

4.2 Summary

Curing was performed with samples of benzocyclobutene (BCB) cured on silicon wafers. The curing was performed in the Lambda Technologies MircoCure™ 2100 system, as well as a conventional thermal furnace. The BCB samples were heated to an appropriate temperature and held at temperature for a specific amount of time for both processing methods. Neural networks were then implemented to model the VFM curing and the conventional curing processes. The error back-propagation algorithm was utilized to train the networks. The inputs to the neural networks were temperature and time-at-temperature, and the outputs of the networks were the in-plane. The next chapter will explore modeling and recipe optimization of a polyimide dielectric using neural networks and genetic algorithms.

CHAPTER 5

PROCESS MODELING AND OPTIMIZATION OF POLYIMIDE

5.1 Introduction

Polyimides are an important class of high-temperature, dimensionally stable, high-performance polymers with a wide range of applications in the microelectronics industry [13]. Prior research has been conducted on curing polyimides using microwave irradiation. Lewis, et al. [14] used a single mode microwave operating at 2.45 GHz for polyimide curing. Farnsworth, et al. [7] characterized photosensitive polyimide that was cured in a variable frequency microwave furnace (VFM). In that study, it was determined that there was no significant difference in polyimide cured using microwave curing as those cured using conventional thermal processing. Thus, VFM curing can achieve the same results as conventional thermal curing in minutes, without compromising the intrinsic material properties.

The remainder of this chapter presents a method to determine an optimal VFM curing recipe for polyimide. The recipe was determined using genetic algorithms to explore the response surface defined by a neural network process model. A central composite inscribed (CCI) experiment was used to characterize the VFM curing of the polyimide. The data from the CCI was used to train a neural network process model. The neural networks model the variation of the in-plane and through-plane indices of refraction, birefringence, and percent of imidization of the polyimide as a function of VFM ramp rate, temperature, and time-at-temperature. The neural network models were then used for process optimization using genetic algorithms.

5.2 Experimental Technique

Curing polyimide involves the removal of solvent or other volatiles from the film and the imidization (or hardening) of the polymer into an intractable polyimide film [94]. The curing process is performed in several steps. Hot plates are commonly used for a soft bake after the polymer is applied. Post bakes range from 50-150°C on one or more in-line hot plates. Typically, a furnace or programmable oven is then used for the final cure. Final curing is usually done at temperatures between 280-400°C, depending on the application.

The polyimide used in this experiment was 3,3',4,4'- Biphenyltetracarboxylic acid dianhydride / P-Phenylenediamine (BPDA/PPD), which is manufactured by HD MicroSystems™ and sold under the name PI 2611. At high temperatures, PI 2611 undergoes a conversion from a soluble polyamic acid to an insoluble, fully imidized polymer. Many of the unique properties of this polymer are a result of its rigid backbone and high degree of orientation, which occurs during a traditional thermal cure. In [7], the mechanical, electrical, and chemical properties of PI 2611 films cured with VFM processing were compared with films cured using a conventional thermal furnace and a rapid hotplate. It was shown that films cured by VFM processing have similar properties to films cured by conventional methods.

For the current experiment, PI 2611 was spun-cast onto silicon wafers and subsequently soft baked at 120 °C for 2 minutes on a hotplate. The spun-on film thicknesses were in the range of 18-22 μm. The coated wafers were then cured in the VFM furnace under a nitrogen atmosphere. During VFM processing, the temperature of the polyimide samples was ramped to an appropriate level and held there for a specific amount of time. After curing, the wafers were allowed to cool to room temperature. Through-

plane and in-plane indices of refraction were subsequently measured using a Metricon prism coupler. The cured film thicknesses were in the range of 10-12 μm. Birefringence, which is the division of light into two components because a material has two different indices of refraction, is calculated by taking the defense between the two indices of refraction:

$$Birefringence = \Delta n = n_{\square} - n_{\perp} \tag{11}$$

where $n_{\square}$ is the in-plane refractive and $n_{\perp}$ the through-plane refractive index. Birefringence is also an indication of the degree of orientation in the film. It has been established that rigid rod polyimides undergo significant orientation during cure, which results in very different properties in and through the plane of the films [7].

The percent imidization is measured using attenuated total reflection Fourier transform infrared (ATR-FTIR) spectroscopy. FTIR is a non-destructive test to determine the chemical changes that occur during a film cure, and hence, to measure the extent of cure by monitoring the growth of a band in the infrared spectrum [14, 15]. The extent of cure for polyimide was measured using the following equation:

$$Percent\ imidization = \frac{\left(A_{1357} / A_{1516}\right)}{\left(A_{1357} / A_{1516}\right)_{hardcure}} * 100 \tag{12}$$

where A is the absorbance and the subscripts represent the wavenumber corresponding to the peak. The reference absorbance is determined from a film that has been fully cured with a standard thermal cure, which is defined as a ramp rate of 3 °C/min and a hold temperature

of 350 °C for one hour. Differences in film thickness or polyimide orientation, as well as uncertainty in determining the baseline, may result in slight changes in peak heights. These changes can significantly influence the calculation of the extent of cure, and thus this method is considered only semi-quantitative [15].

5.3 Statistical Modeling

The order of the experimental trials was determined by a implementing a CCI design, which consisted of 15 runs plus 2 replicates, for a total of 17 runs. The input factors were time, temperature, and ramp rate. Table 3 illustrates the input factors and their ranges. The responses were percent imidization, the in-plane and through-plane indices of refraction, and the birefringence. Table 4 is the analysis of variance (ANOVA) for the CCI design of experiment where the values in the Significance column below 0.05 represent a factor that has significant effects on the variability of the process. The temperature, hold time, and higher level factors involving these inputs are significant effects.

Table 3 – Ranges of input factors

Parameter	Range	Units
Time	0 to 30	Seconds
Temperature	20 to 350	°C
Ramp rate	15 to 45	°C /min

Table 4 – ANOVA for CCI experimental design

Source	Df	Sum Sq.	Mean Sq.	F-Ratio	Significance
Constant	1	134992			
Ramp	1	0.043	0.043	0.00	0.9578
Temperature (Temp)	1	1430.039	1430.039	100.5	0.0000
Hold Time (HT)	1	209.033	209.033	14.70	0.0064
Ramp*Temp	1	6.734	6.734	0.47	0.5135
Ramp*HT	1	0.000	0.000	0.00	0.9971
Temp*HT	1	204.829	204.829	14.40	0.0068
Ramp**2	1	4.850	4.850	0.34	0.5776
Temp**2	1	198.356	198.356	13.94	0.0073
HT**2	1	11.406	11.406	0.80	0.4003
Residual	1	99.567	14.224		

5.4 Neural Network Modeling

The data from the CCI experiment were used to train the neural network model. The network was trained using the mean-square error performance metric. Six data points from a separate experiment were used for testing. The neural network model predicts the degree of cure of polyimide with an experimental error, σ (see Equation (10)). As illustrated in Table 5, σ_{NN} for the test data is on the order of 3e-2 for the in-plane and through plane refractive indices, 5e-2 for birefringence, and 13.58 for percent imidization. The percent imidization prediction error is considerably higher than that of the other three parameters. This is likely due to the semi-quantitative way that percent imidization is calculated using Equation (12).

Table 5 – Neural network experimental error

Parameter	σ_{NN}
In-plane	0.033
Through-plane	0.038
Birefringence	0.059
Percent Imidization	13.53

The neural network model was used to generate response surfaces spanning the input space of two of the input parameters while setting the third parameter to its mid-point. Figure 14 shows response surfaces for the in-plane and through-plane indices of refraction, birefringence, and percent imidization plotted over hold time and temperature with the ramp rate set at its midpoint of 30^{o}C/minute. In these graphs, it is seen that as the time and temperature increase, the percent imidization increases, which signifies that the degree of cure increases. At temperatures greater than 200 °C, PI 2611 undergoes a conversion from a soluble polyamic acid to an insoluble, fully imidized polymer. This rapid increase in percent imidization is illustrated in Figure 14(d). The orientation in the cured PI 2611 films leads to differences in the in-plane and through-plane indices of refraction [7]. Soft-baked films have an in-plane index of 1.6260 and a through-plane index of 1.6106, which results in a birefringence of 0.0153. During cure, the in-plane index increase significantly resulting in a birefringence of 0.1709 as illustrated in Figure 14(c). The conditions that produce the birefringence of 0.1709 are ramp rate of 30 °C/minute, temperature of 350 °C, and hold time of 30 minutes.

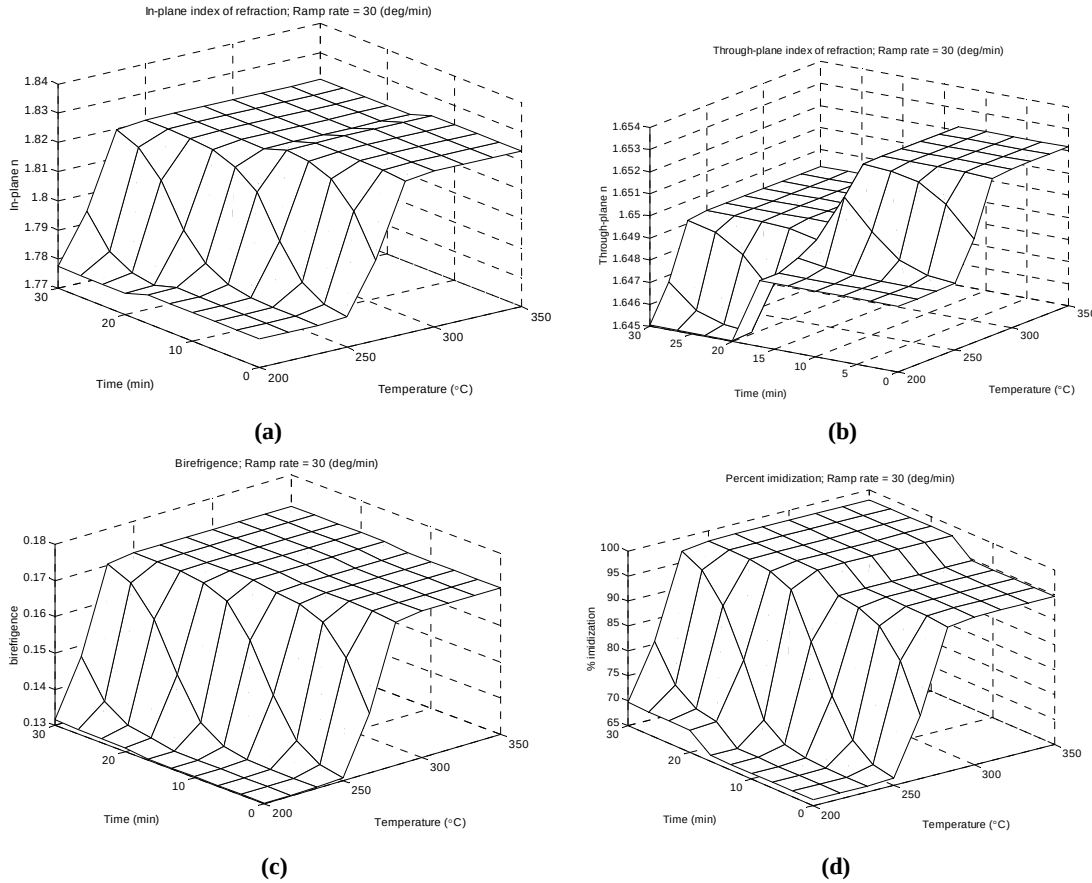

Figure 14 – VFM cured PI 2611 response surfaces: (a) in-plane refractive index; (b) through-plane refractive index; (c) birefringence, and (d) percent imidization

5.5 Sensitivity Analysis

One of the goals of developing a process model is to quantify the variation in an output parameter for an incremental change in a particular input variable. This quantification process is called sensitivity analysis. The sensitivity of an input to an incremental change in one of the outputs is performed by obtaining the partial derivative of the response with respect to the input of interest while holding the other outputs constant [95]. This is expressed with the following equation:

$$\frac{df}{dx_i} = \frac{f(x + \Delta x_i) - f(x)}{\Delta x_i}\bigg|_{\Delta x_i \to 0} \tag{13}$$

where f is the functional relationship modeled by the network model, x is the vector of input parameters, and Δx_i is an incremental change in one of the elements of x. Sensitivity analysis for VFM curing of PI2611 was performed by examining the mean of the input parameters and making incremental changes in the input of interest. Sensitivity has been calculated by varying the input parameters by 10% of their full range of deviation. The values of the outputs were normalized, and the results are shown in Figure 15.

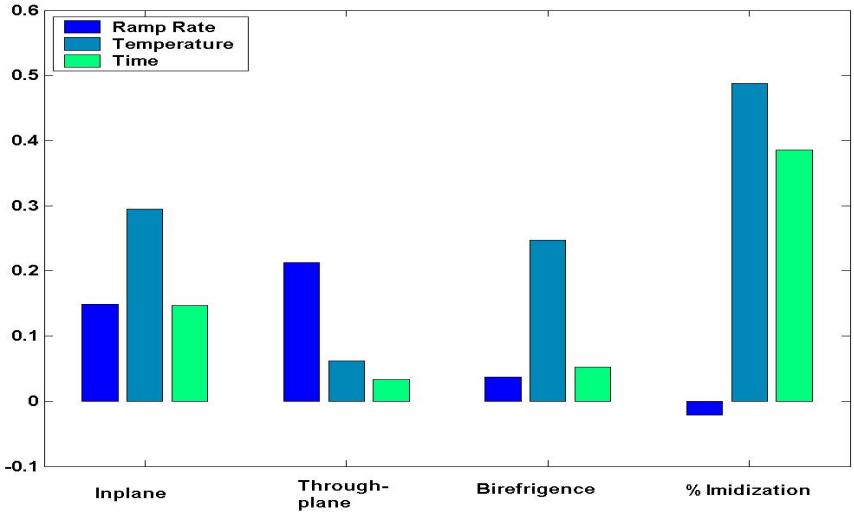

Figure 15 – Sensitivity analysis of output parameters

5.6 Process Optimization using Genetic Algorithms

When appropriate process conditions need to be identified to produce favorable responses, process optimization (or recipe synthesis) is required. Genetic algorithms have

been demonstrated as a suitable tool for this application [38, 40-42]. For this experiment, a typically genetic algorithm, which cycled through four stages--"population" creation, evaluation chromosomes, selection, and genetic manipulation--was used. The selection method was *elitist roulette wheel* approach [41], where chromosomes with large fitness values are assigned a proportionately higher probability of survival into the next generation. The probability distribution function was of the form in Equation (13).

Figure 16 illustrates a flow diagram for the genetic algorithm based optimization scheme implemented in MATLAB. The desired set points are input into the genetic algorithm. Based on the constraints imposed by the problem, the desired set points were used to calculate the fitness of each string based of the following equation:

$$F = \frac{1}{1 + \sum_{n} \left| K_n \left(y_d - y_o \right) \right|} \tag{14}$$

where n is the number of response variables, K_n are the weights of the process responses, y_d represent the desired process response, and y_o are the process outputs that result from the current input parameters.

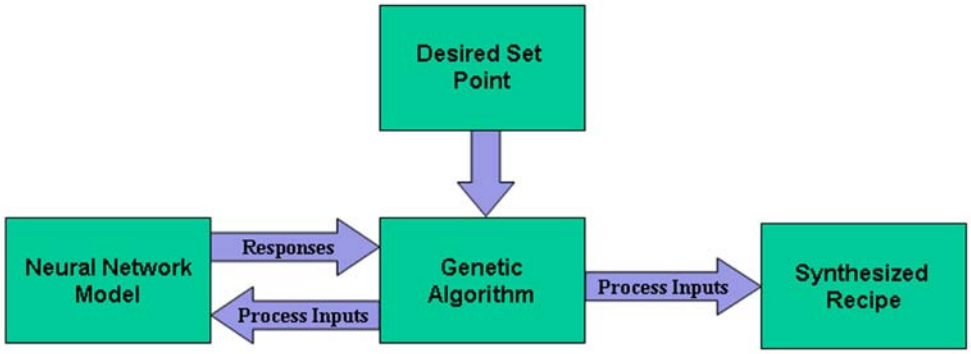

Figure 16 – Process optimization procedure

The genetic algorithm produces inputs for the neural network model, which calculates the predicted responses. The output is fed back into the genetic algorithm until a suitable stopping criterion is met (such as a maximum number of generations). The crossover rate, mutation rate, population size, and chromosome length used are listed in Table 6.

Table 6 – Genetic Algorithm Parameters

Genetic algorithm parameters	Value
Crossover	0.65
Mutation	0.01
Population size	50
Chromosome Length (each parameter)	100

The weighting coefficients for the desired responses (i.e., the K_n's in Equation (10)) must also be set. These coefficients should be determined by an expert in the domain. In this simulation, it was determined that having a high birefringence was desirable. Therefore, the weight for the birefringence was higher than the other responses. The simulated results are shown in Table 7. The recipe used to produce the simulated results called for a ramp rate of 19 °C/minute, a temperature of 294 °C, and hold time of 23 minutes. This temperature and hold time is less than the values required by a conventional thermal cure, while the ramp rate is higher than a conventional cure. The recipe resulted in a simulated in-plane refractive index of 1.828, a through-plane a refractive index of 1.637, a birefringence of 0.190, and a percent imidization of 95.55%. These results correspond to a cured film that is almost fully cured. The high birefringence value indicates that the polymer is almost fully oriented, which yield low residual stress levels in the polymer. It

should be noted that choosing different weights and/or targeted responses will produce different optimal recipes.

Table 7 – Recipe synthesis results

	In-plane	Through-plane	Birefringence	Percent Imidization
Target	1.809	1.600	0.20	100%
Weight	1	1	10000	1
Simulated Results	1.828	1.637	0.190	95.55%
Actual Results	1.823	1.659	0.174	99.97%
% Error	0.3%	1.32%	9.19%	4.42%
Recipe:	**Ramp Rate = 19 °C/min, Temp = 294 °C, Time = 23 min**			

5.7 Summary

In this chapter, the modeling and optimization of PI 2611 cured using VFM processing have been discussed. Curing was performed with samples cured on silicon wafers in the Lambda Technologies MircoCure™ 2100 system. The samples were heated to an appropriate temperature and held at temperature for a specific amount of time. Neural networks were then implemented to model VFM curing process. The inputs to the neural networks were temperature, time-at-temperature, and ramp rate. The outputs of the networks were the in-plane and through-plane indices of refraction, birefringence, and the percent imidization. These models yielded RMS errors are on the order of 5e-2 for the birefringence, and the in-plane and through-plane indices of refraction. The RMS error for the percent of imidization was on the order of 13.53. The neural network model was used for process optimization using a genetic algorithm. The optimal recipe indicated that an in-plane refractive index of 1.828, a through-plane refractive index of 1.637, a birefringence of 0.190, and a percent imidization of 95.6 could be achieved by using a ramp rate of 19

°C/minute, temperature of 294 °C, and a hold time of 23 minutes. These results suggest that using a VFM to cure polyimide can produce similar properties in less time and at lower temperatures than a conventional cure.

In this study, only a few properties of PI 2611 were considered as response for the process model. However, there are a number of other properties that are important to the characterization of a polymer. These properties include dielectric constant, residual stress, modulus, solvent resistance, tensile strength, and coefficient of thermal expansion. In future work, the neural network model will be expanded to include several of these responses. The next chapter will discuss the implementation of an acoustic temperature sensor that was used for real-time monitoring of PI2611 curing in the VFM system.

CHAPTER 6

IN-SITU TEMPERATURE MONITORING

6.1 Introduction

The objective of curing is to remove residual solvents and to complete the chemical reactions that convert monomers into polymers. Because curing conditions play a major role in the final properties of a polymer, it is important to reduce variability when curing polymers so that acceptable electrical and mechanical properties result. Some of the parameters that must be controlled to ensure a proper cure include the polymer composition and molecular weight; the glass transition temperature; the time, temperature, and heating rate; and environmental conditions such as the atmosphere, relative humidity, exhaust flow rate [96]. For a given polymer with constant molecular weight and composition, the primary factors that control the curing process are time, temperature, and heating rate [96].

In microelectronic applications, minimizing stress is a very important issue. A ramped cure cycle is typically used to facilitate solvent removal and to minimize the development of thermal stresses arising from the coefficient of thermal (CTE) mismatch between the polymer and the substrate [96]. To further reduce the potential for stress, polymers should not be cured above their glass transition temperatures. However, if a polymer is not fully cured, any subsequent processing of the film that exceeds the final cure temperature may result in the release of volatiles. Consequently, the final cure temperature should be at least as high as the maximum temperature of any subsequent processing [96].

A standard curing process is typically done in either a laminar flow forced air convection oven or in a diffusion furnace [96]. The primary requirements of the curing

equipment are uniform temperature distribution, the capability to adequately control the heating rate, the capability to maintain a dry inert atmosphere (exclude moisture and oxygen), and the provision of adequate ventilation to remove volatiles that are released during the cure [96].

The VFM furnace used in this research, the MicroCure™ 2100, has the capability of sweeping 4096 frequency over a 1.15 GHz bandwidth about a center frequency every 100 millisecond, which allows for a uniform temperature distribution. It also has the capability to maintain a dry inert atmosphere and an adequate ventilation system. However, there is a need to improve the monitoring and control of the heating rate and temperature because of the limitations with the current temperature measuring devices. Current temperature measuring devices are an infrared pyrometer, thermocouple, and a fiber optic probe. See section 4.1 for a discussion of their limitations.

To improve process monitoring for the VFM system (with the goal of better control of the heating rate and temperature), an acoustic temperature sensor was developed and implemented in the VFM furnace to monitor polymer dielectric curing on a silicon wafer. This chapter discusses the development and implementation of an acoustic temperature sensor in the VFM furnace.

6.2 Acoustic Temperature Sensor

The acoustic temperature sensor developed in this research measures the temperature of a polymer-coated silicon wafer in a variable frequency microwave furnace. The time-of-flight of an acoustic wave in silicon is related to the temperature through the dependence of the elastic constants [82, 83, 97]. In the seminal paper by McSkimm [97], acoustic velocity was characterized as a function of temperature in silicon. This data

showed that the acoustic velocity decreases as temperature increases, which corresponds to a negative velocity coefficient of temperature (-31e-6 [dimensionless quantity]). Thus, there is an increase in the time-of-flight of the acoustic wave when the silicon temperature increases. For this research, the ATS relied on this monotonic relationship between temperature and time-of-flight of acoustic waves to monitor the temperature of silicon in the VFM furnace.

6.2.1 *Sensor Design*

6.2.1.1 ***Piezoelectricity***

A piezoelectric transducer may be used to fabricate an acoustic sensor [98]. A piezoelectric transducer converts electrical signals into mechanical signals and vice versa. One of the more widely used piezoelectric materials for acoustic applications is zinc oxide (ZnO). Zinc oxide has been widely used because of its relatively high coupling coefficient (0.28 [99]), the fact that it adheres well to a number of substances, and because its methods of deposition coincides with IC fabrication techniques [100].

Zinc oxide has been used for acoustic devices such as surface acoustic wave devices (SAW) [101, 102], surface skimming balk wave [87], flexural plate wave devices [103], Lamb wave devices [82, 83], bulk acoustic wave devices [101, 104], longitudinal wave devices [79], and acoustic-optic devices.

6.2.1.2 ***Zinc Oxide Deposition***

The deposition of ZnO is very important because the thickness of a transducer determines the fundamental operating frequency for the device [105] and because the film quality (crystalline structure, lack of voids, etc.) determines if a device will be piezoelectrically active or not. Lee, et. al., reported that polycrystalline ZnO thin films must meet two requirements to be properly suited for acoustic wave devices: (1) the basal

plane of ZnO crystallites must be oriented parallel to the plane of the substrate, which is sometimes referred to "c-axis orientation;" and (2) the ZnO film must have a columnar structure with void free boundaries [106].

Zinc oxide can be deposited in a number of ways: RF magnetron sputtering [101, 102, 106-108], DC magnetron sputtering [109, 110], DC triode sputtering [101, 102], molecular beam epitaxy [111], metal organic chemical vapor deposition (MOCVD) [112], and pulsed laser [113]. ZnO can be deposited by sputtering a zinc target in an oxygen atmosphere [107, 109] or sputtering a ceramic ZnO target [99]. From the literature, it appears that RF sputtering of a ceramic ZnO target is the most common method of deposition. Because of the number of methods and system configurations in a particular method, there has been a considerable amount of research conducted on processing, characterizing, and optimizing (trying to produce highly c-axis oriented) ZnO films [99, 100, 104, 106, 108-110, 114].

Although the techniques used to deposit ZnO come from the IC domain, ZnO is highly reactive. After it is deposited, subsequent processing can contaminate processing chambers as well as other device fabricated on silicon [100]. However, a passivation layer of silicon nitride can help reduce device contamination [115].

6.2.1.3 ***Sensor Modeling***

To help with the design of acoustic devices and to gain a better understanding of the affects of changing a transducer's parameters, a model was developed of the acoustic device. There are two major approaches for modeling acoustic devices: Mason's lumped-element circuit model [98, 116, 117] and the Krimholt-Leedom-Matthaei (KLM) model [118]. These modeling techniques can be use to determine the resonant frequency and insertion loss of devices. They may also be used to optimize transducer parameters: film

thickness, transducer area, type of transducer material, type of contact, and contact thicknesses. Mason's model is a one-dimensional, lumped-element equivalent circuit model of a piezoelectric device. It consists of an equivalent circuit that separates the piezoelectric material into an electrical port and two acoustic ports through the use of an ideal electromechanical transformer, where network theory can be used to analyze the circuit [119]. One of the drawbacks of the Mason's model is that it contains a (non-realizable) negative capacitance [116]. The KLM model is also a three-port network, but the equivalent circuit models an acoustic device using transmission line theory.

For this research, KLM modeling was used in the design of the acoustic temperature sensor. The KLM modeling program was developed in the Ginzton Laboratory by Gokhan Percin (copyright 1997 [120]). Figure 17 illustrates the input impedance of the acoustic device parameters listed in Table 8. This figure shows that the device should have a bandwidth of 200 MHz to 1.6 GHz with a center frequency of 700 MHz. The insertion loss, the loss resulting from a device being inserted into a transmission line, is plotted in Figure 19. One of the design goals is to have a low insertion loss.

Table 8 – The acoustic device parameters used in the KLM modeling

Acoustic Device Parameters	
Buffer rod length	4.7 mm
Active transducer area	1 mm^2
ZnO Thickness	3 μm
Contact Thicknesses (Au)	1500 Å

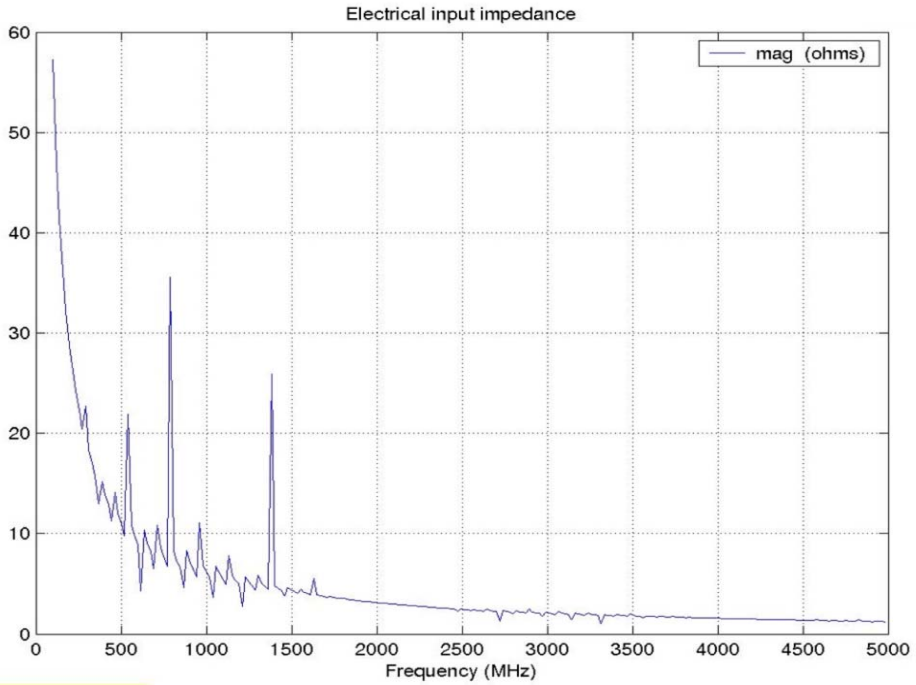

Figure 17 – Input impedance from KLM model showing that the sensor should resonate around 200 MHz to 1.6GHz.

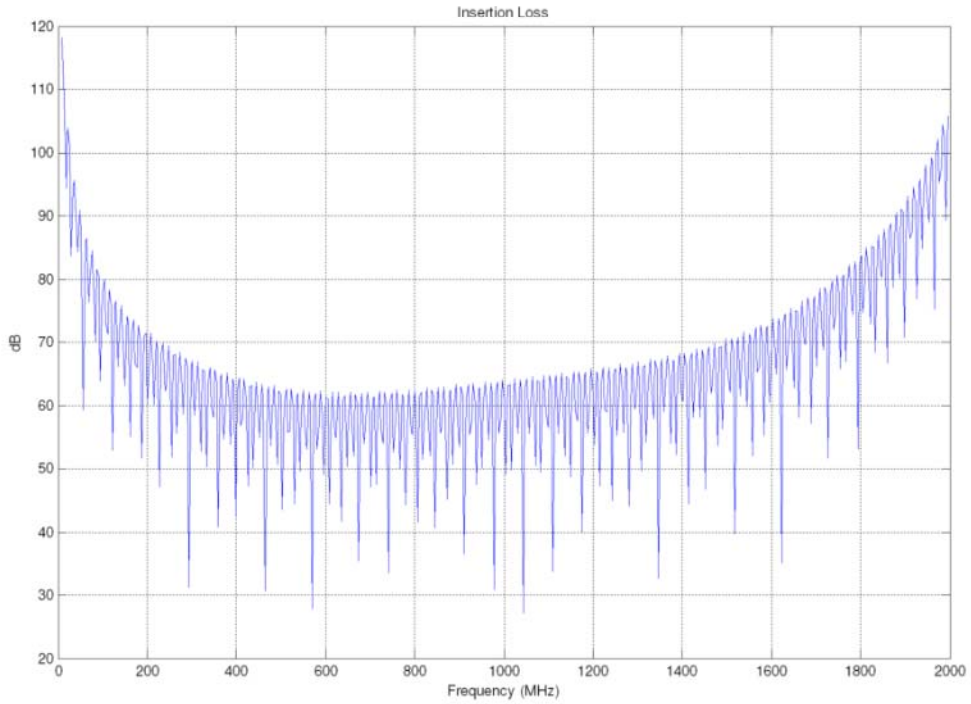

Figure 18 – Insertion loss of transducer from KLM model

6.2.2 *Sensor Fabrication*

To fabricate the acoustic temperature sensor, a ZnO piezoelectric transducer was deposited onto a sapphire acoustic buffer rod. In this research, sapphire was used as the acoustic buffer rod because it was inert to microwave radiation [6], and it has a low acoustic attenuation [116]. First, the sapphire buffer rod was ultrasonically cleaned with acetone, methanol, and isopropanol. Then, the piezoelectric transducer was fabricated by depositing a bottom contact of Ti/Au, a ZnO layer, and a top contact of Cr/Au onto the flat polished surface of the sapphire buffer rod. The bottom contact was deposited by electron-beam evaporation with the titanium layer, approximately 100 Å thick, serving as an adhesion layer. The gold layer was 1500 Å thick. The ZnO layer was deposited by RF sputtering at a temperature of 325 °C. The top contact consisted of 100 Å of chromium,

which serves as an adhesion layer, and 1500 Å of gold, both deposited by electron-beam evaporation. Figure 19 illustrates a fabricated transducer on a sapphire buffer rod.

Applying a voltage pulse between the two metal layers of the transducer generates a longitudinal wave in the transducer that is transmitted to the buffer rod. The longitudinal wave travels through the buffer rod, the wafer, and the polymer. The wave reflected from the wafer/air interface and/or polymer air interface back to the transducer, where the phase difference of the original signal and reflected signal is measured. Temperature is subsequently calculated from the time-of-flight measurement. Figure 19(b) shows a wave traveling through a buffer rod and wafer being reflected at the polymer/air interface.

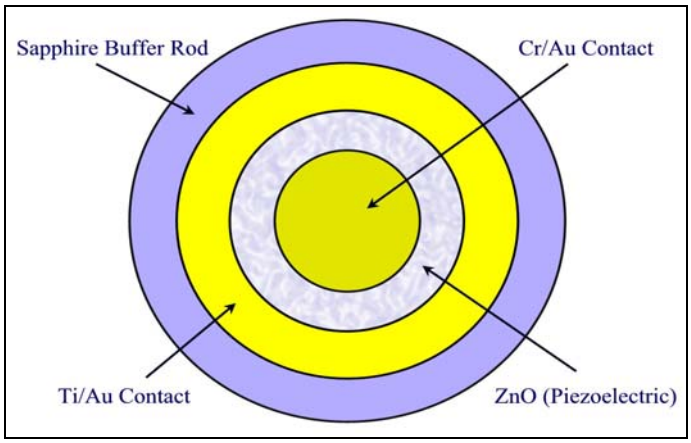

(a)

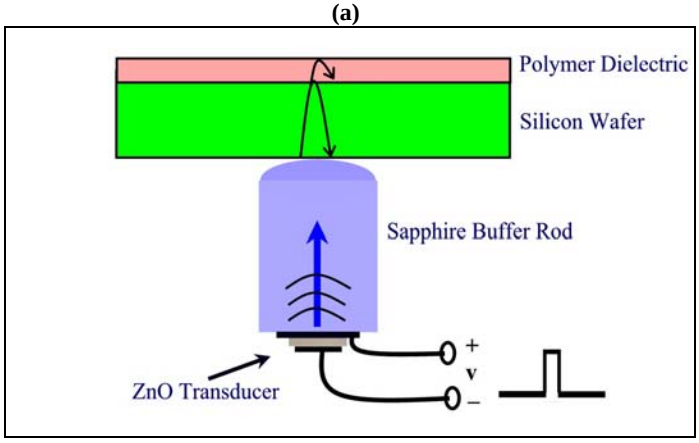

(b)

Figure 19 – (a) Illustration of a zinc oxide transducer fabricated on a sapphire buffer rod; and (b) an ultrasonic wave traveling through acoustic temperature sensor

6.2.3 *Sensor Measurements*

6.2.3.1 ***X-Ray Diffraction***

In order for the transducer to resonate properly, it must have the correct zinc oxide crystal orientation (c-axis oriented). To determine the crystalline structure of the ZnO, x-ray diffraction (XRD) measurements were performed using a Phillips X'PERT Pro X-ray Diffractometer using Cu-Kα radiation. XRD (Ω-2θ scan) measurements were taken of ZnO films that were deposited on the titanium/gold bottom contact, which had been deposited on 430 μm, double-sided double-polished, 2 inch, c-axis oriented, sapphire wafers. It should be noted, that these films were deposited using the same recipe that was used for the buffer rod (see Table 9). The thicknesses of the films were approximately

3μm. The XRD measurement shown in Figure 20 was taken from a film deposited by the Acoustic Electronics Group at the Georgia Institute of Technology using an RF sputterer, while the XRD plot shown in Figure 21 was of a film that was deposited by the author. Table 1 lists the typical RF sputterer parameters for films deposited by the Acoustic Electronics Group [104]. Figure 21 illustrates a ZnO with the proper (002) orientation, which has a peak around 34.1 (2θ degrees). The XRD plot in Figure 21 illustrated a polycrystalline ZnO film with the (001), (002), and (101) orientations. The films with this type of XRD scan can be thought of a poor quality, and these types of films were not piezoelectrically active when a top electrode was deposited and a voltage was subsequently applied to the contacts. Thus, these films did not produce transduction and were not used for the acoustic temperature sensor.

Table 9 – Typical sputtering parameters deposited by the Microelectronic Acoustic Group at the Georgia Institute of Technology[104]

Sputtering parameters	
RF Power	125 W
Argon Partial Pressure	2 mTorr
% Oxygen	3%
Deposition Pressure	5 mTorr
Temperature	325ºC

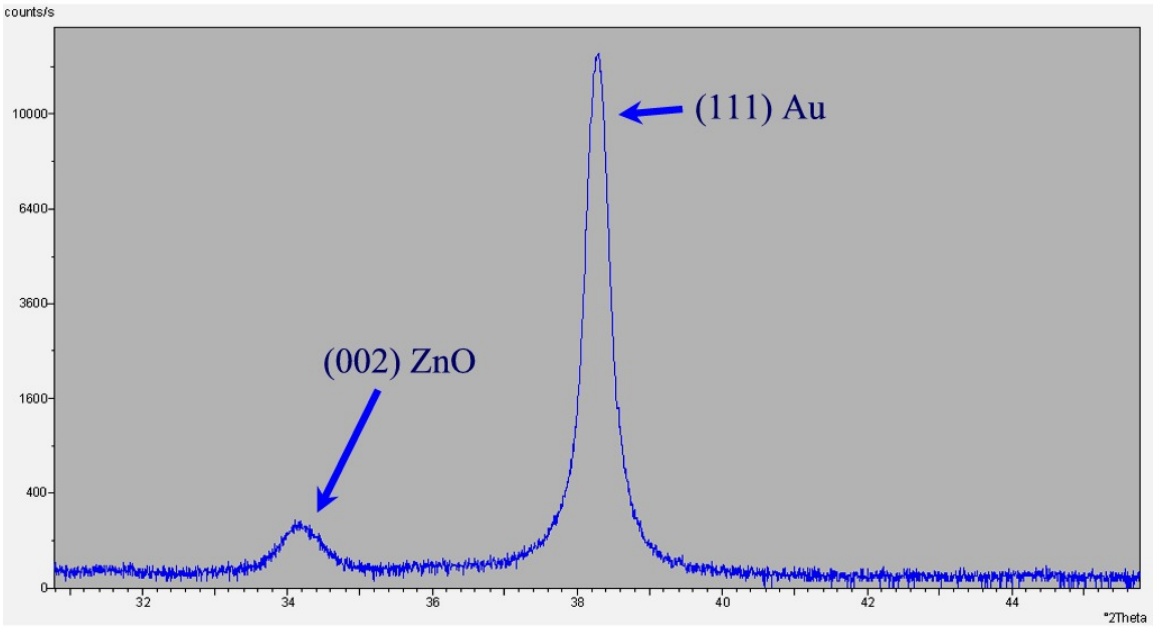

Figure 20 – XRD plot of ZnO/Au/sapphire wafer

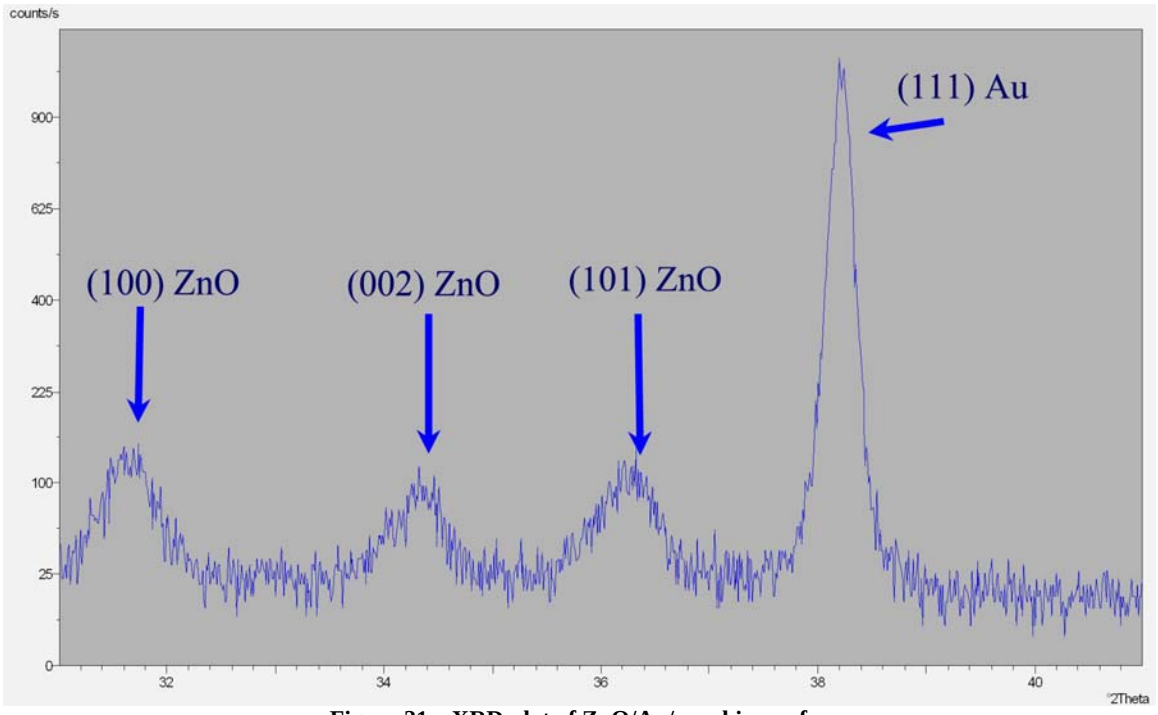

Figure 21 – XRD plot of ZnO/Au/sapphire wafer

6.2.3.2 ***Network Analyzer Measurements***

To validate the operating frequency range of the ATS, scattering parameter (s-parameter) measurements were taken with an Agilent 85107B vector network analyzer. Scattering parameters are a parameter set that relates to the traveling waves that are scattered or reflected when an n-port network is inserted into a transmission line. Figure 22 is a plot of the one-way s-parameter data for the ATS measured from 100 MHz to 2 GHz. From this measurement, it can be seen that the sensor has a bandwidth from 200 MHz to 900 MHz with a center frequency of approximately 600 MHz. Figure 23 consist of four plots: (Top left) Real part of the input impedance measurements, (top right) imaginary part of the input impedance measurements, (bottom left) input impedance measurements, and (bottom right) s-parameter measurements plotted on a Smith chart from 100 MHz to 5 GHz. From Figure 23 (bottom left), the input impedance of this device is approximately 40 ohms, while the KLM model predicts that the input impedance will be around 10 ohms (see Figure 17).

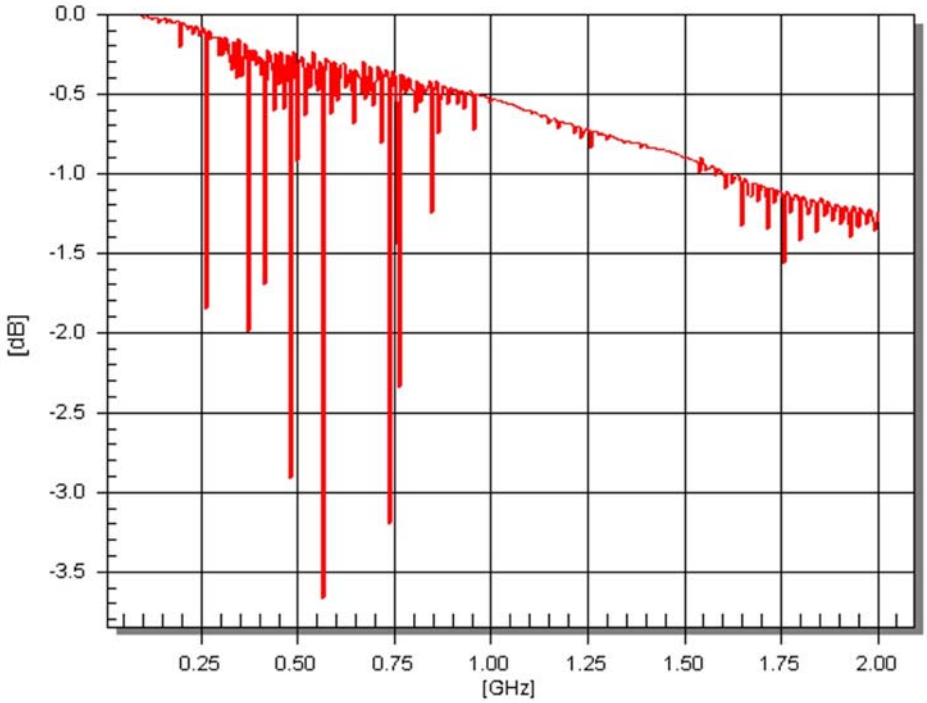

Figure 22 – ATS s-parameter measurement from 100 MHz to 2 GHz

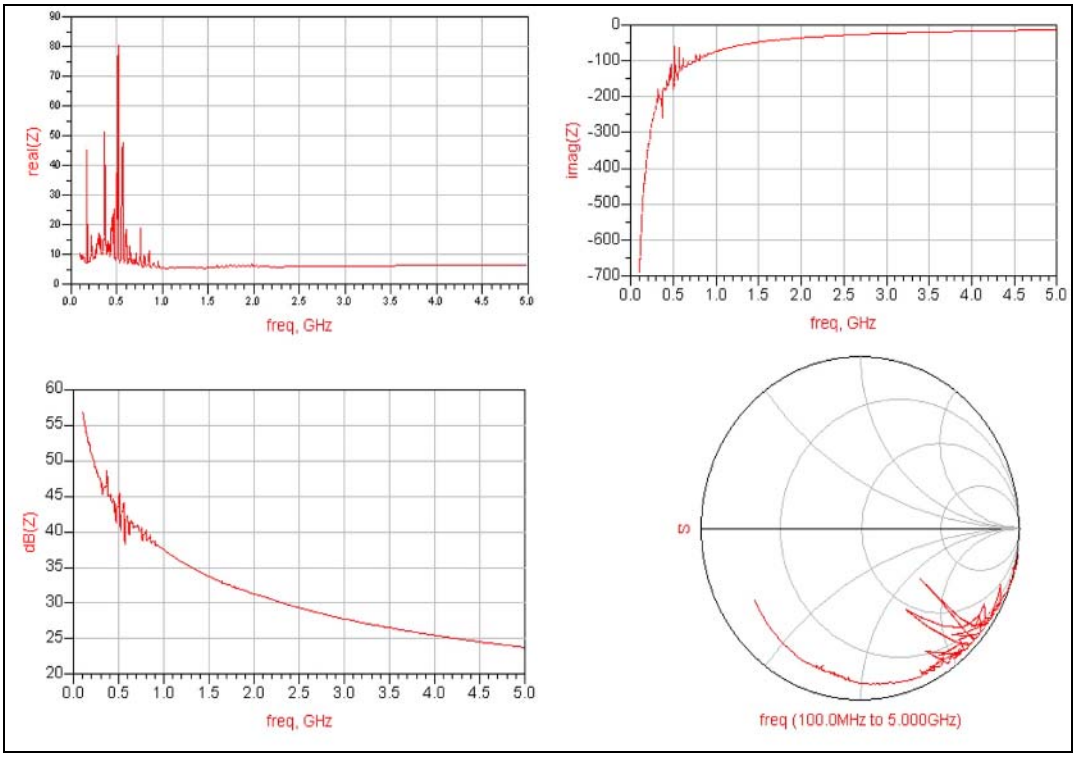

Figure 23 – (Top left) Real part of the input impedance measurements, (top right) imaginary part of the input impedance measurements, (bottom left) input impedance measurements and (bottom right) s-parameter measurements plotted on a Smith chart from 100 MHz to 5 GHz

6.2.4 *Sensor Calibration*

Before the acoustic temperature sensor was used in the VFM system, it was calibrated to determine the temperature sensitivity. Figure 24 illustrates the ATS calibration process. For calibration, the silicon wafer was heated on a hotplate. The ATS was placed in contact with the silicon wafer, and a high-voltage pulsing circuit is used to generate a 100V, 90ns pulse that produces a longitudinal wave in the sapphire rod. Time-of-flight measurements were made by monitoring the returned pulses of the sensor using a computer-controlled oscilloscope (Tektronix TDS 5054 digital oscilloscope). A thermocouple is placed in contact with the wafer, and its readings are monitored with an Omega TAC80B-K thermocouple-to-analog converter connected to an Agilent 34401A digital multimeter, which was linked to the oscilloscope via an RS 232 serial connection.

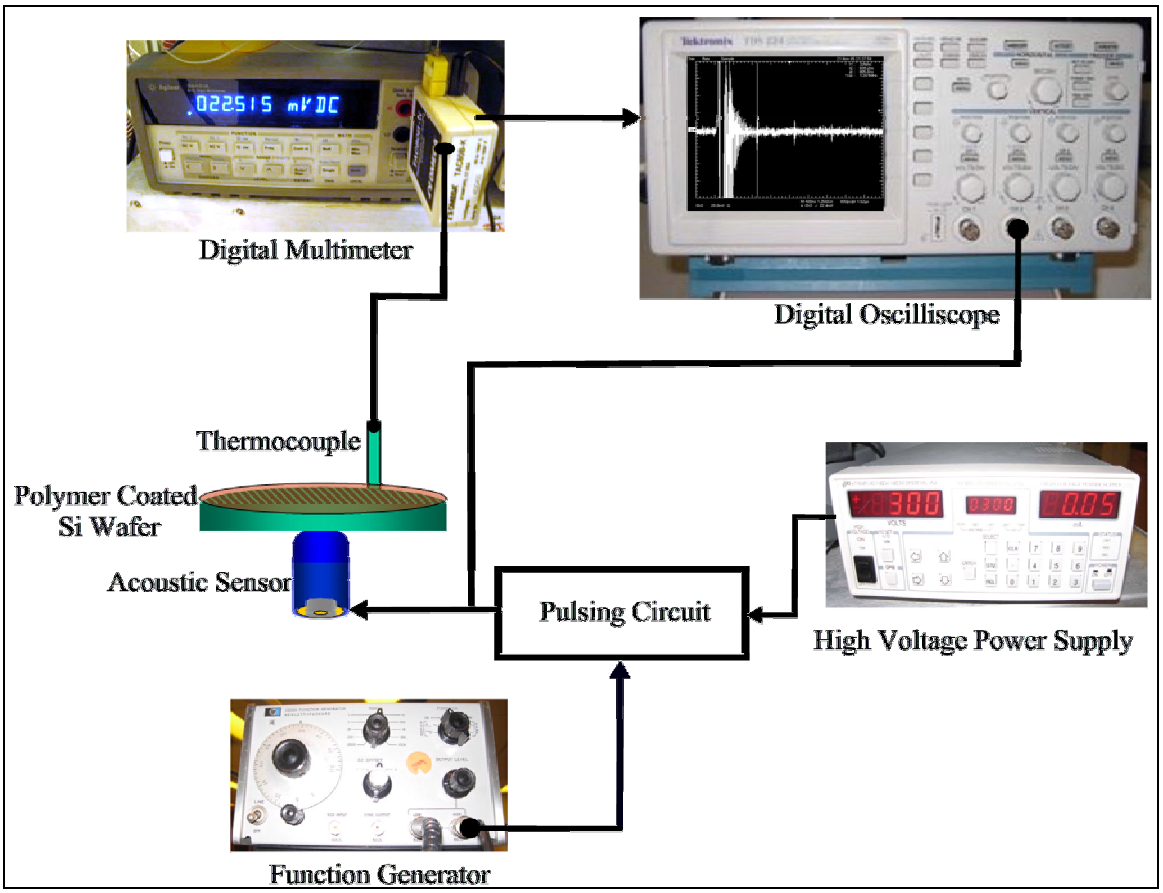

Figure 24 – ATS calibration schematic

The expected time-of-flight is calculated by dividing the buffer rod length (4.7 mm) by the speed of sound in sapphire (11000 m/s) and multiplying that by a factor of two (for the two-way travel time). This comes out to 854.5 ns. Figure 25 is a typical oscilloscope reading with the initial pulse, followed by several returned pulses. The returned pulses are approximately 805 ns apart. Figure 26 an oscilloscope image of one of the returned pulses.

For the calibration process, a MATLAB program was written to find the returned pulses and measure the time-of-flight as the temperature changed. The program captures an averaged waveform from the oscilloscope. Returned pulses are identified by applying a moving window across the waveform and evaluating each sample in the window to a threshold. The first waveform value in a particular window that is greater (or less) than the

maxima (or min) threshold is classified as a returned pulse. After the first two pulses are found, the time-of-flight calculation is made by multiplying the number of samples between the first and second pulses by the sampling rate. The top plot in Figure 27 illustrates three returned pulses where the program has identified the first two pulses and has placed a small circle at the leading edge of the pulse and plotted the pulses a different color than the waveform.

The top portion of Figure 28 represents a temperature profile, where the temperature is ramped to approximately 225 °C, then lowered to approximately 190 °C, where it was held for several time steps and allowed to cool to room temperature at that time. The bottom portion of Figure 28 plots time-of-flight measurements of the returned pulses. The time-of-flight measurements agree throughout the temperature range. Figure 29 illustrates a 4^{th} degree polynomial fit of the time-of-flight data plotted with 95% prediction bounds.

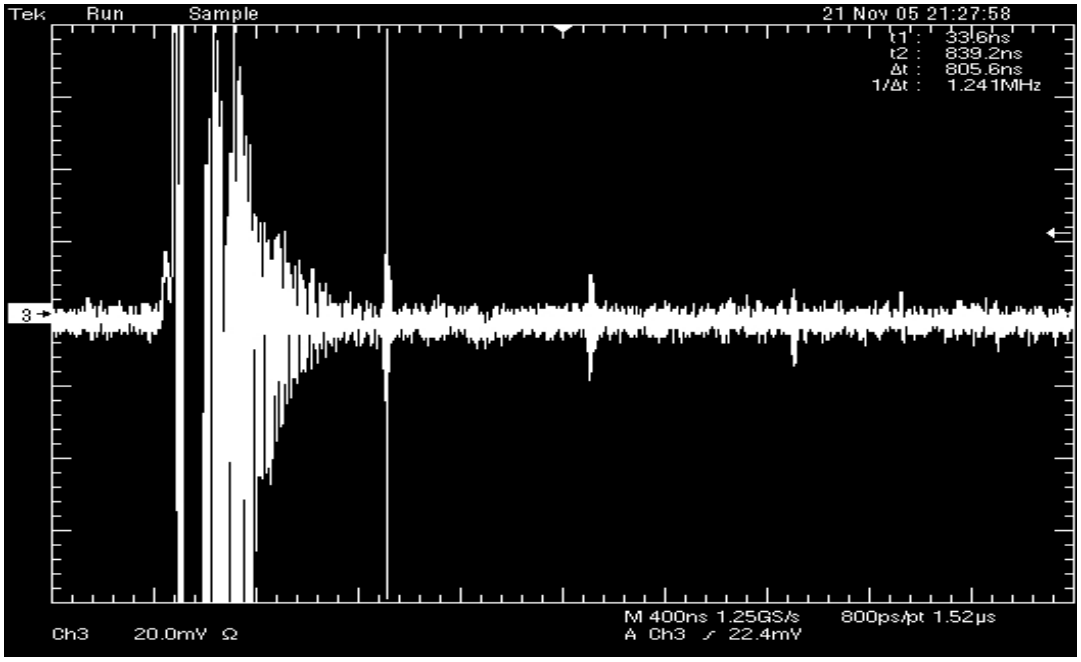

Figure 25 – Oscilloscope measurement showing initial pulse and several returned pulses

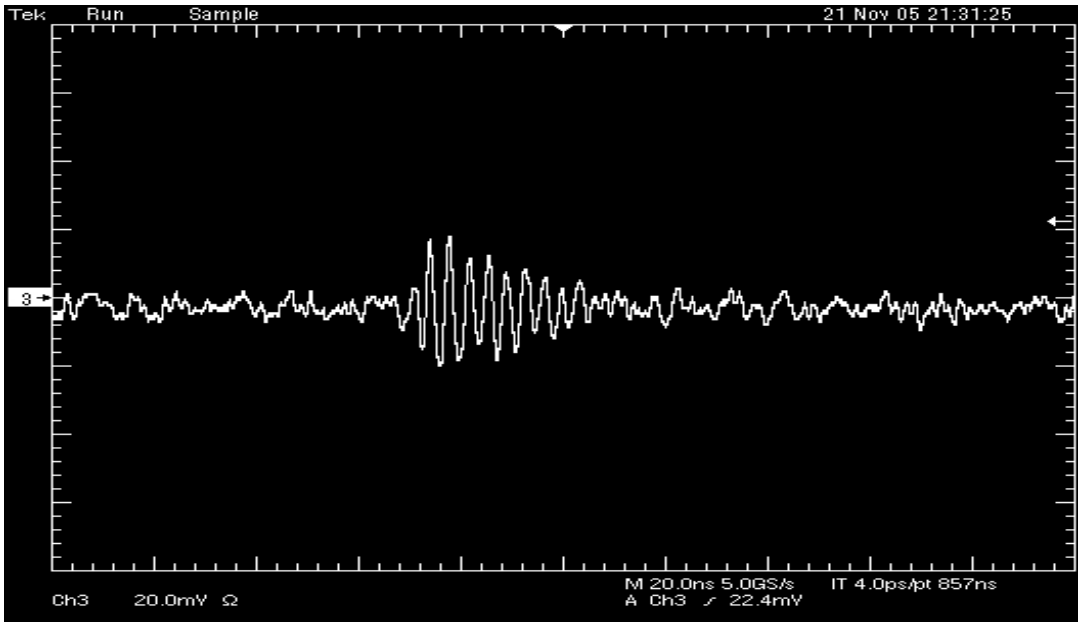

Figure 26 – Oscilloscope measurement showing one of the returned pulses

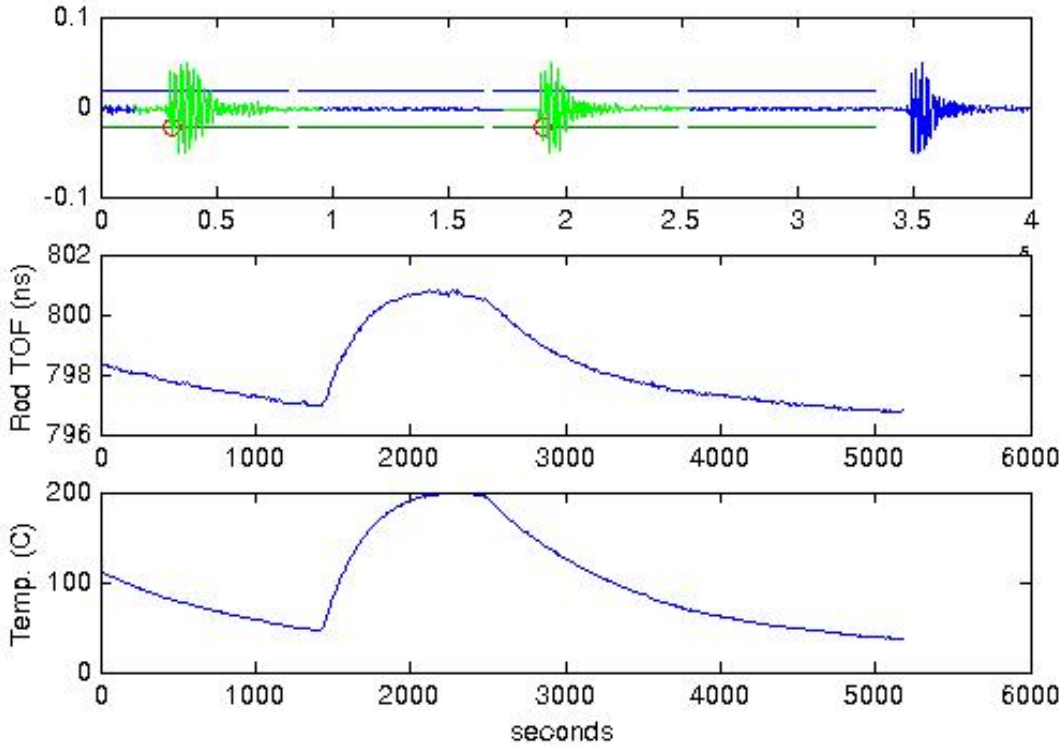

Figure 27 – ATS with temperature ramped to 200 °C and held there for approximately five minutes

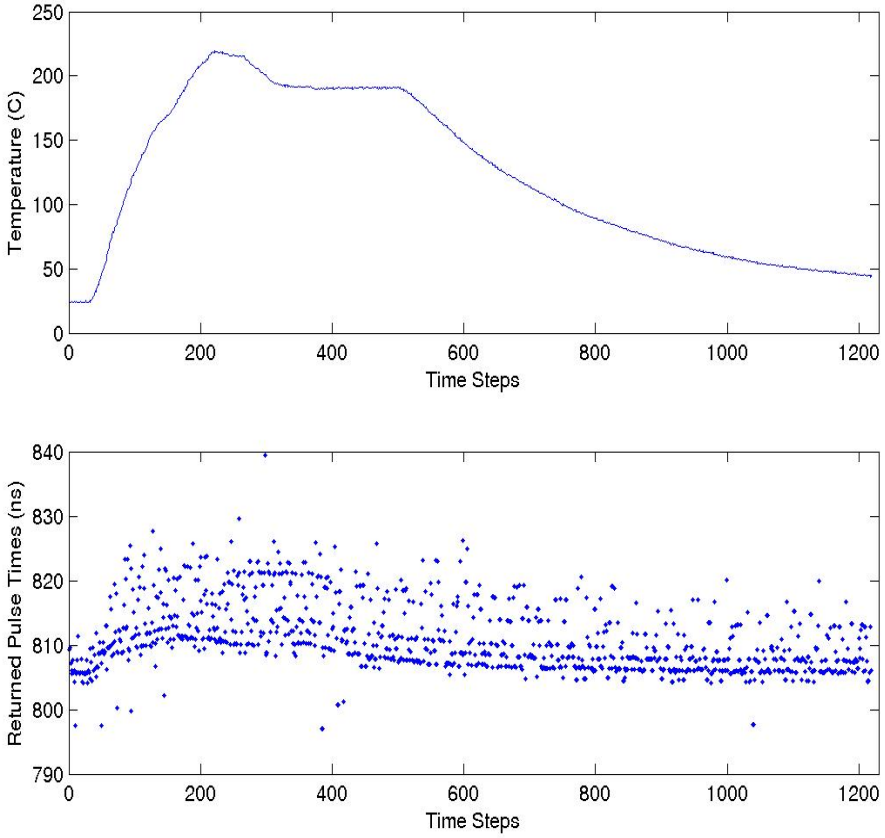

Figure 28 – ATS calibration data: (top) Temperature profile (bottom) time of flight data from ATS sensor during temperature calibration

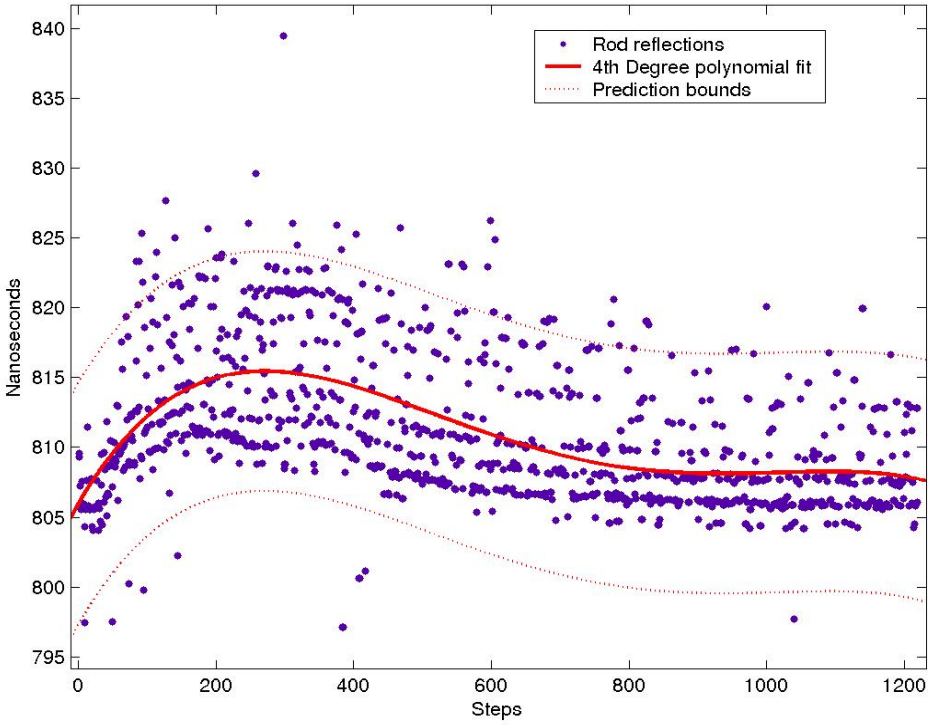

Figure 29 – Time-of-flight data fit to a 4th degree polynomial with 95% prediction bounds

Figure 30 illustrates the ATS measuring temperature that is ramped at a rate of 10 degrees per minute to 350 °C and held there for approximately 80 minutes. At several points during the measurement, there are spikes in the time-of-flight data, which correspond to the algorithm not being able to capture one of the leading edges of the subsequent returned pulse. However, Figure 27 illustrates an approximately linear relationship of the time-of-flight of the returned pulses and the temperature.

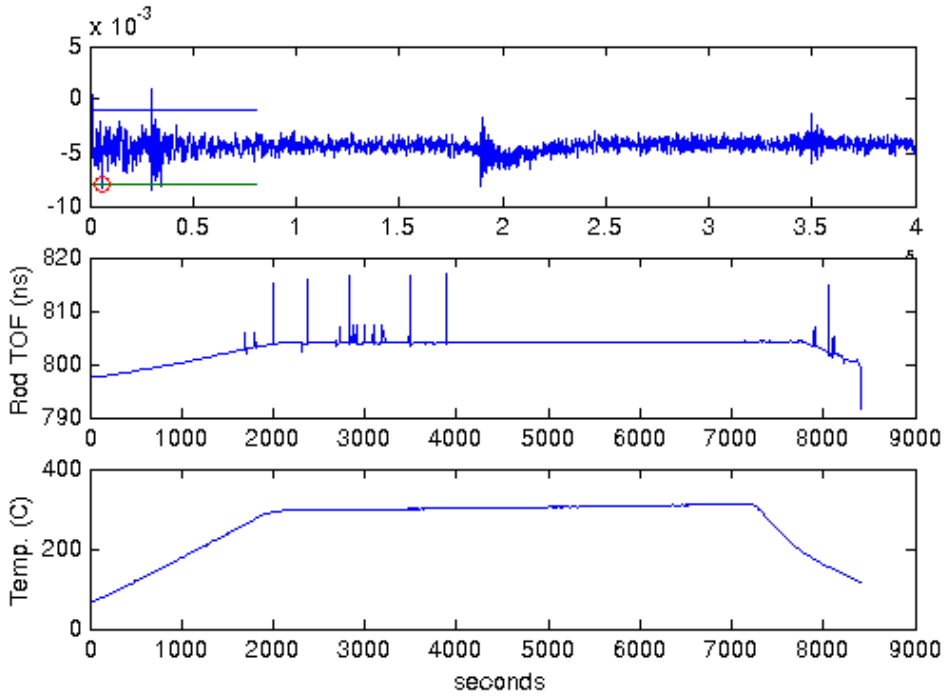

Figure 30 – ATS with temperature ramped to 350 degrees Celsius and held there for approximately 80 minutes

6.3 ATS Implementation in VFM

To implement the acoustic temperature sensor in the microwave oven, the sensor had to be housed in a holder. The sensor holder was developed such that it was the same size as the quartz rod and plate that were already being used in the VFM. The ATS was set in the holder such that the sensor protruded less than a half a millimeter out of the holder. In this way, when a wafer is placed on top of the holder, it stays in contact with the sensor.

Wire bonding was attempted to attach the sensor fabricated on the buffer rod to the connector on the sensor holder. However, the bond between the gold wire and the top contact on the buffer rod was not strong enough (when a bond was actually made) and did not stay attached during subsequent processing. After examination of the surface of the top contact, it was found that the surface was very rough. In addition, the clamps on the wire

bonder were not designed for circular devices, which meant that the buffer rod was not properly clamped down during bonding that could have caused the device to move during the ultrasonic phase of the bonding process. Because of this bonding issue with the transducer fabricated on to the buffer rod, the actual acoustic device that was implemented in the VFM furnace was fabricated on the double-sided polished sapphire wafer that was used for the XRD measurements with a top contact deposited on it. This acoustic sensor was mounted on to a sensor holder as described above. The sensor holder was placed inside the microwave chamber, and a polymer-coated wafer was placed on top of the sensor/sensor holder (see Figure 31).

(a) **(b)**

Figure 31 – (a) The ATS in the sensor holder next to the quartz plate and (b) illustrates a polymer-coated silicon wafer on top of the ATS in the sensor holder

A graphical user interface (GUI) was developed in MATLAB to monitor the time-of-flight from the returned pulses and to monitor the thermocouple that was attached to a polymer-coated wafer inside the VFM furnace. Figure 32 illustrates the GUI with the temperature being ramped from room temperature to 95 °C. This figure shows that the

profile of the returned pulses has a strong correspondence to the temperature profile from the thermocouple that was attached to the polymer-coated wafer.

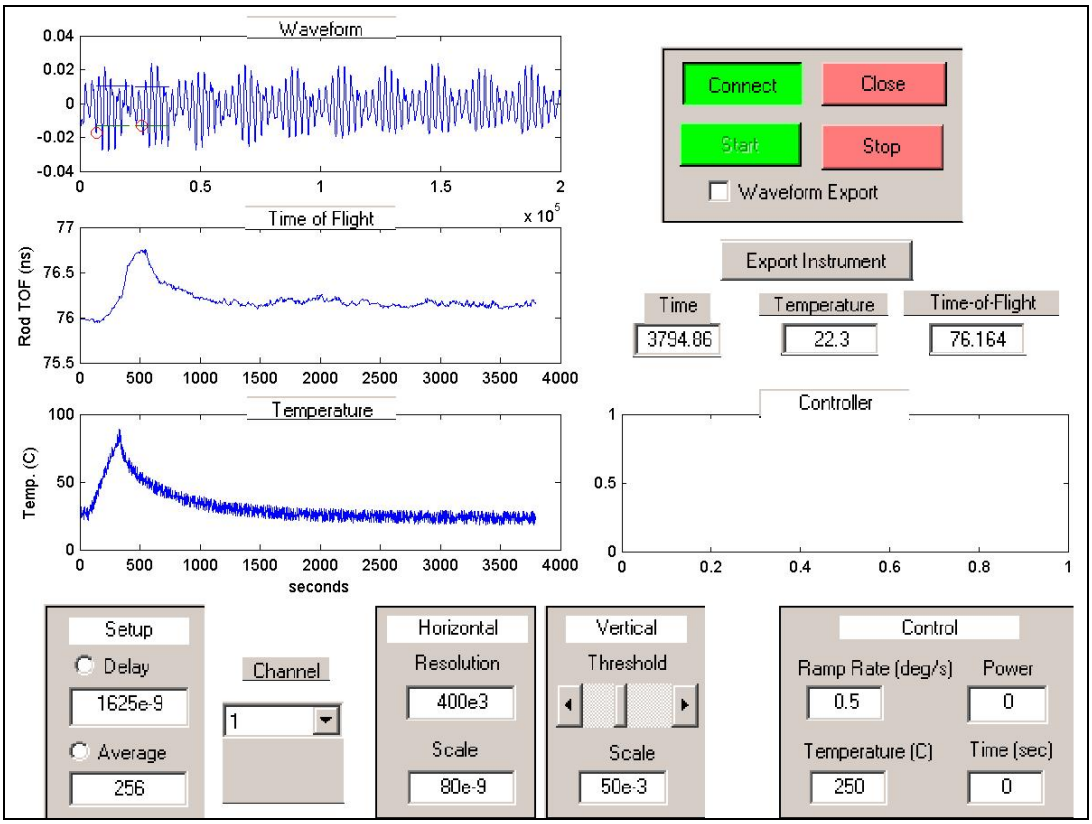

Figure 32 – Graphical user interface used to monitor in-situ the returned pulses and the thermocouple readings of a polymer-coated wafer inside the VFM chamber

6.4 Summary

In this chapter, the acoustic temperature sensor was modeled, tested, and evaluated. It was implemented in the VFM furnace. A GUI was developed in MATLAB to monitor the temperature of the thermocouple attached to the polymer-coated wafer and the returned pulses from the ATS *in-situ* in the VFM chamber. The next chapter will discuss the

development and implementation of the neural controller that will be used to control the VFM furnace.

CHAPTER 7

NEURAL NETWORK CONTROL

7.1 Introduction

The development of a control system involves many tasks, including modeling, designing of a control law, implementing the controller, and validating the system. Based on the capability of neural networks to model nonlinear processes and their capability to accurately approximate inverse relationships of complex functions, a neural network indirect adaptive control scheme [43, 51, 54, 121] was developed for VFM curing of polymer dielectrics. This chapter discusses the development of this indirect adaptive neural controller for VFM processing.

7.2 Adaptive Control

Åström and Wittenmark [122] define an adaptive controller as a controller with adjustable parameters and a mechanism for adjusting these parameters. An adaptive controller has a special structure, which can be thought of has having two loops: a normal feedback loop with the plant and the controller and a parameter adjustment loop [122]. The parameter adjustment loop is usually slower than the normal feedback loop. Because of the parameter adjustments, an adaptive controller is a nonlinear controller.

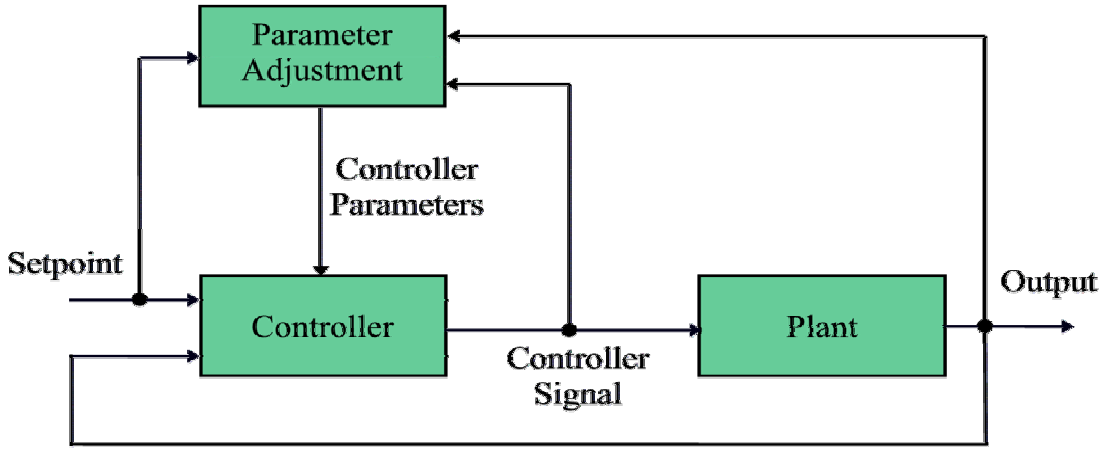

Figure 33 – Adaptive control schematic

The plant controller has adjustable parameters (see Figure 33). If the plant and its environment are known, it is assumed that there exists a design procedure that makes it possible to determine a controller that satisfies some design criteria. The adaptive control problem is to find a method of adjusting the controller when the characteristics of the plant and its environment are unknown and changing [122]. There are two types of adaptive control: direct and indirect. In direct adaptive control, the controller parameters are changed directly without determining the characteristics of the plant and its disturbances. In indirect adaptive control, the plant model and (possibly) the disturbances are first determined, and the controller parameters are designed on the basis of this information [122].

Adaptive methodologies consist of two tasks [43]: identification and control. Identification consists of measuring and identifying the forward dynamics of a plant in order to represent system behavior. System identification is necessary for plants where parameters are unknown or changing over time. This can be performed online or offline.

Offline implementations use a finite set of input/output data, and online implementations require continuous or frequent monitoring of input/output data. Adaptive systems use the online method.

Control, the second portion of an adaptive scheme, involves deriving a representation of the inverse characteristics of a system. An inverse model of the plant can be used as a controller to take a target value as input and produce the control signal that becomes the input to the plant. A controller should generate appropriate signals to cause the output of a plant to reach a desire target. This can be accomplished by adjusting the controller parameters to compensate for changes in the plant dynamics or by generating an optimal control signal directly from the plant's transfer function or state equations. Adjusting the controller parameters has the advantage of increased reliability because the system can operate even when adaptation fails [62]. The controller implemented in this research is based on the controller parameter modification method.

7.3 Neural Network Indirect adaptive control

Based on the system identification and control approach mentioned in the previous subsection, it is possible to develop a neural network adaptive controller for the VFM system. This method consists of a neural network controller and a neural network system identification model. Both of these neural networks can be trained offline and adaptation can continue online to adjust to changing system dynamics [62].

7.3.1 *Neural Network Plant Identification*

Neural network system identification is equivalent to the neural network modeling discussed in Chapter 4. However, for control, the training of the neural network model continues in real time as the process runs. Actual inputs are provided to the plant and the

neural network model simultaneously, with the error measure used with the back-propagation algorithm to update the model [62] (see Figure 34).

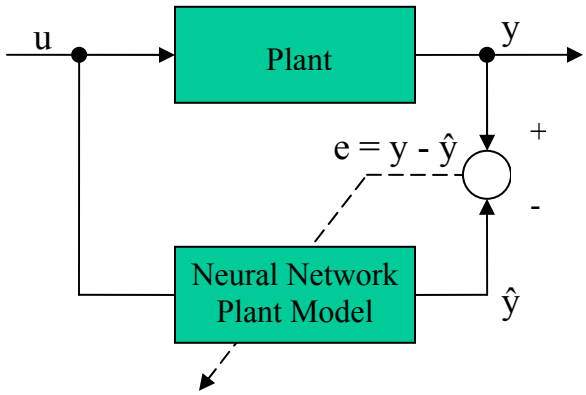

Figure 34 – Neural network plant identification

7.3.2 *Neural Network Controller Identification*

There are two supervised learning approaches that may be used to train a neural network inverse plant model (i.e., a model given the current state that produces a control signal (or proper input to the plant) that causes the plant to produce a desired state). There is the direct inverse modeling approach, which is illustrated in Figure 35, and the distal supervised learning approach that was developed by Jordan and Rumelhart [123] illustrated in Figure 36. The direct modeling technique uses the output of the plant as the input of the inverse network model, and its output is the estimated control signal. The error that is used for updating the weights is actual control signal (u) minus the output of the inverse model ($\hat{u}$). Thus, the goal of this training method is to match the output of the inverse model with the input of the plant.

The direct inverse modeling approach has two major drawbacks [123]. First, if the inputs and outputs have many-to-one mappings, this algorithm may not be able to find an inverse. For example, during the training of the plant, if multiple inputs to the plant produce the same output, then there is a many-to-one mapping. During the inverse modeling if the inverse model is given an input the maps back to multiple targets, then the network would produce output that is an average of the corresponding outputs. However, this averaged value may be outside of the solution space.

The second drawback of the direct inverse modeling approach is that it is not goal directed. Since the inverse model only samples the outputs from the plant, there is no direct way to find a particular control signal that produces the appropriate target output [62]. To find particular solutions, the algorithm must sample a sufficiently large range of inputs and interpolate to find the solution.

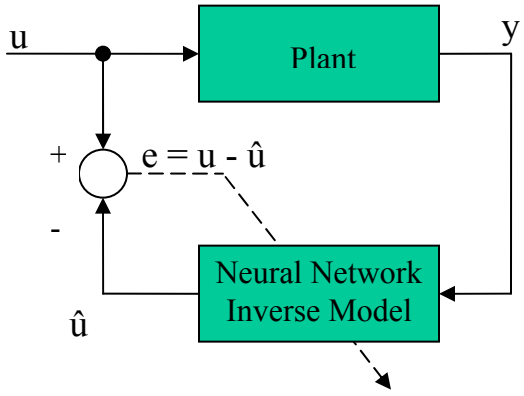

Figure 35 – Neural network direct inverse modeling

The second supervised learning approach, the distal learning method, is an indirect training method illustrated in Figure 36. It consists of placing an inverse model in series

with a plant model and using the error between the desired state and the current state of the plant to train the inverse model. The plant model is held constant while the error of the composite system is used for updating the weights of the inverse model. Any supervised training algorithm may be used. In this research, the back-propagation algorithm was selected.

The distal learning method is goal-directed. It attempts to minimize the error between the desired state and the output of the plant model, as opposed to the error between the control signal and the control estimate. Also, it does not suffer from the many-to-one mapping that plagues the direct modeling technique because it will find a particular inverse mapping. However, without the particular structure of a many-to-one mapping, there is no one to predict which of the possible inverses model the system will find.

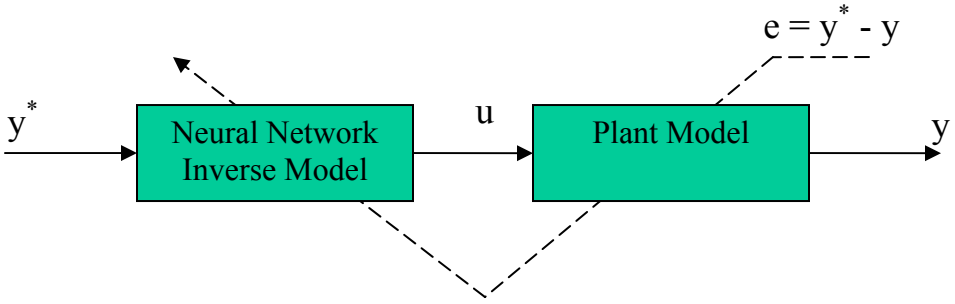

Figure 36 – Distal supervised learning where the weights of the inverse model are adapted while the weights of the plant model are held constant

7.4 Neural Network Control Simulation

7.4.1 *Plant Modeling*

As stated earlier, the first step to developing a neural controller is to develop a forward model of the plant. This was performed using the same techniques as outlined in

Chapter 3. A 2^n factorial experiment was performed to capture the actual power commands that the VFM system uses to apply temperature to the system. After completing the experiment, the data collected was used to train the plant model. The inputs to the plant model were power, ramp rate, hold time, hold temperature, center frequency, sweep rate, and target temperature. The output of the plant model was the estimated of the temperature. Figure 37 illustrates the output of the plant model and the error between output and the actual temperature of the VFM furnace when all of the input data from the experiment has been concatenated into a single training vector.

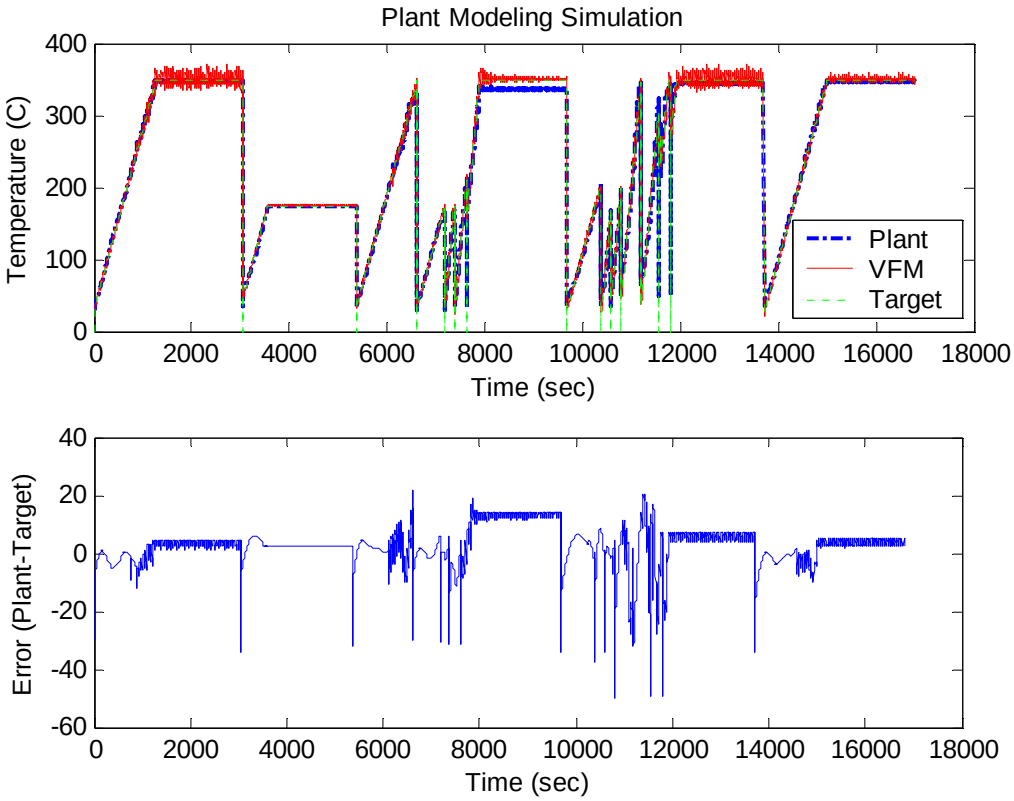

Figure 37 – Forward plant modeling simulation

7.4.2 *Inverse Plant modeling using Distal Learning*

Using the distal learning technique, the inverse model of the plant was trained. However, the algorithm was modified because the control signal for this research is only the power signal, and the other input parameters of the plant (ramp rate, center frequency, etc.) were not being generated by the inverse model. Figure 38 is a schematic of the modified distal learning approach. The bottom plot in Figure 39 is a plot of the output of the inverse neural network model utilizing this modified distal learning approach.

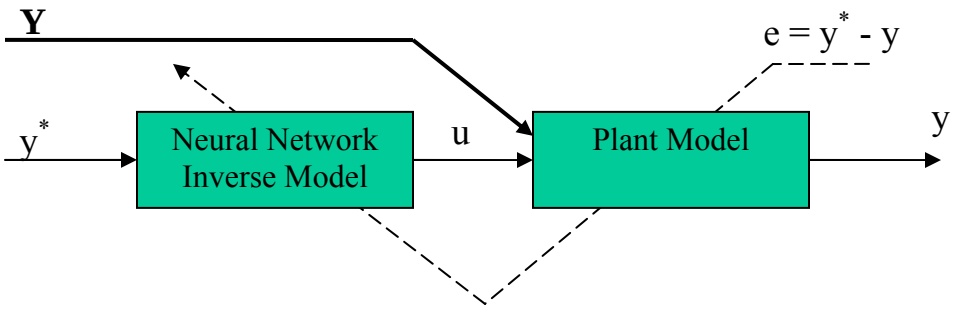

Figure 38 – Distal learning approach with additional input parameters to the plant model

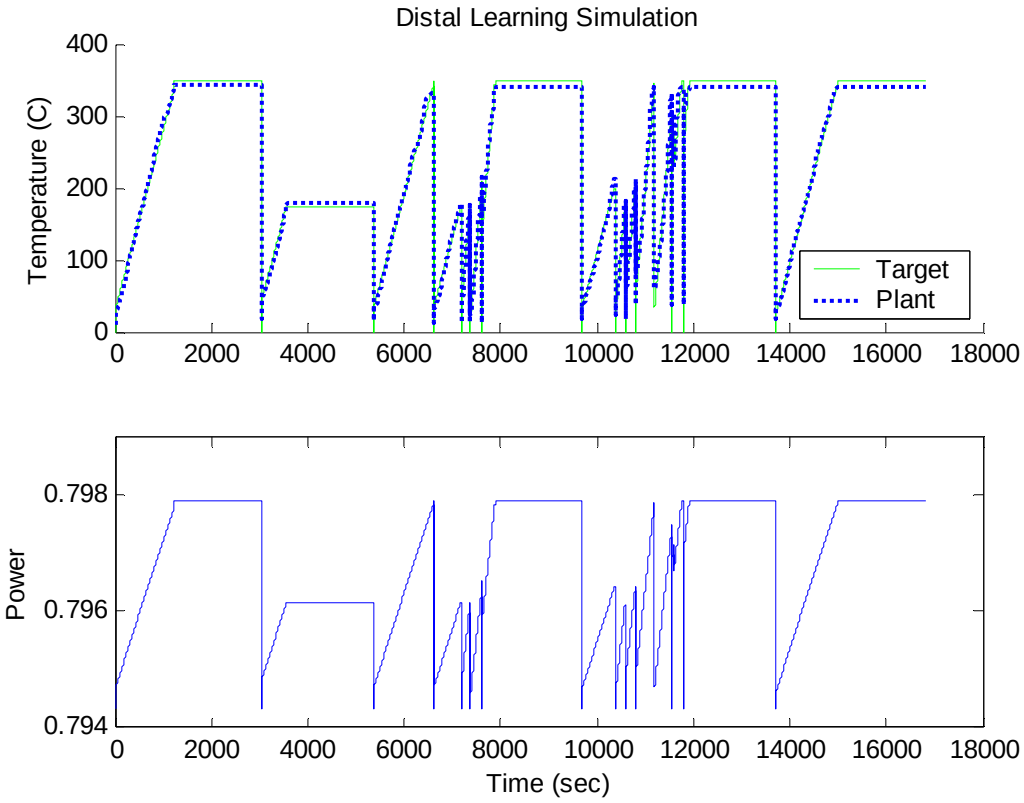

Figure 39 – Plot of the output of the distal learning simulation for the inverse plant model

7.4.3 *Indirect Adaptive Controller Simulation*

Figure 40 illustrates the control strategy [43]. The system consisted of a neural controller, a plant emulator, and the plant model. To simulate the control scheme, the plant, the plant emulator, and neural controller were implemented as back-propagation neural networks. The plant and the plant emulator was trained offline using experimental data. During the training of the controller using the modified distal learning approach, the weights of the plant model were held constant while the weights of the plant emulator were allowed to adapt. The neural controller was trained using feedback from the plant model and the plant emulator. This configuration updated the controller parameters adaptively

while the neural controller adjusted the plant's inputs to optimally match the output of the plant to the control set-point. The top plot of Figure 41 illustrates the temperature profile for the simulation of the plant, the plant emulator, and the targeted temperature. Again, the additional parameter (center frequency, ramp rate, hold time, etc.) are provided to both the plant model and the plant emulator. The bottom plot of Figure 41 illustrates the control signal going into the plant of this simulation.

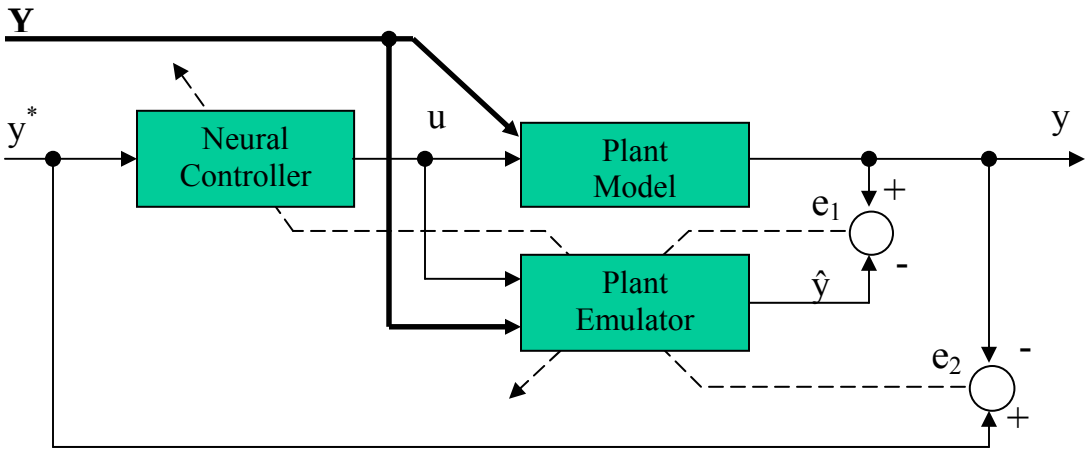

Figure 40 – Indirect adaptive control scheme

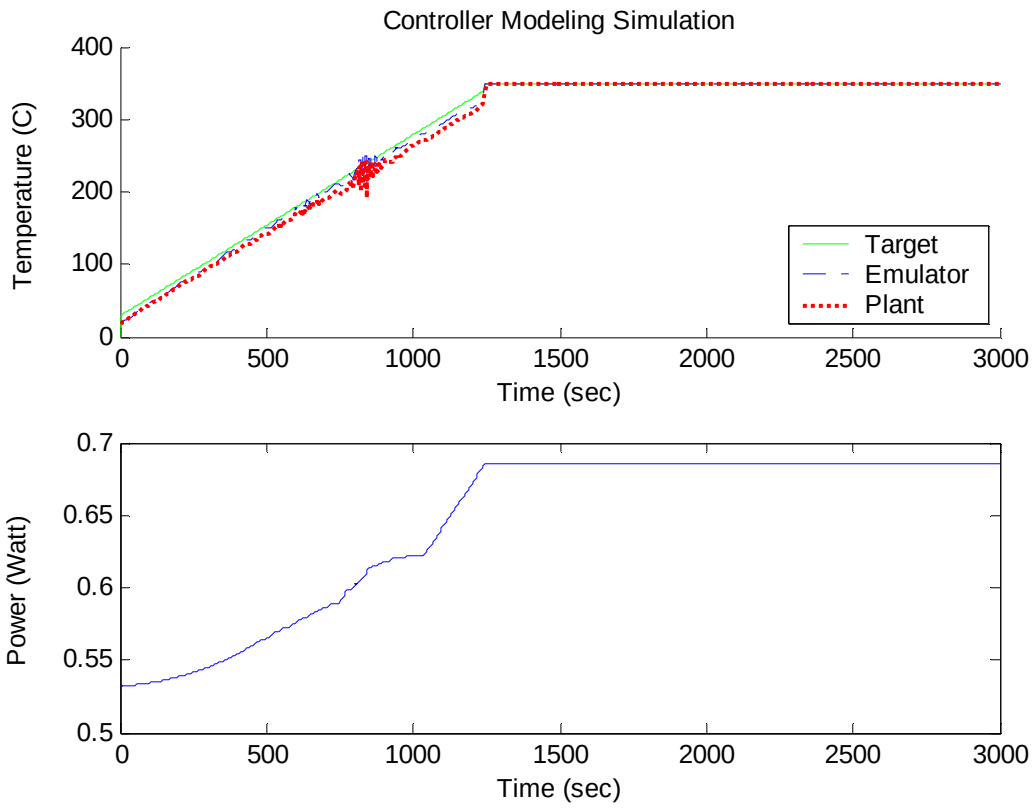

Figure 41 – Controller simulation results: (top plot) temperature profile of plant, plant emulator and target, (bottom plot) recommended power output of neural controller

7.5 Control System Implementation

In collaboration with Lambda Technologies, a simple, yet robust solution was proposed for integration of the ATS and control strategy with the MicroCure system. This solution consisted of a software change to the MicroCure system that allowed the computer-controlled oscilloscope to synchronize with the program running on the MicroCure controller and to send new constant output power commands. The host was responsible for controlling power to accomplish process control and for turning off the power when the process was complete.

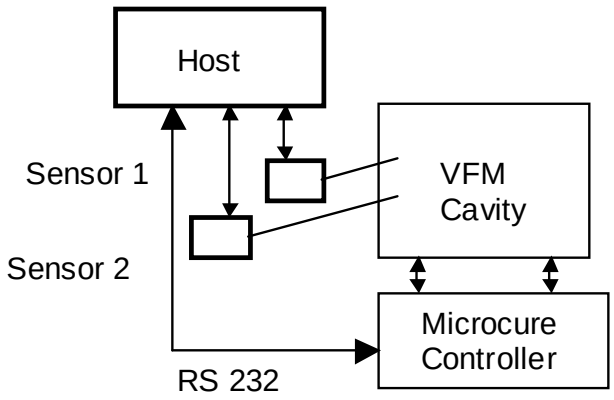

Figure 42 – MicroCure software implementation (Courtesy of Lambda Technologies)

Figure 42 is a block diagram of the proposed software solution. The MircoCure™ software was modified such that the ATS was able to monitor the temperature over a RS 232 serial communication link that was connected between the MicroCure controller and the digital oscilloscope. The external computer, which was apart of the digital oscilloscope, implemented the neural control scheme and transmitted new power setting information to the MicroCure controller. Presently, the only drawbacks are the limited control update rate of approximately 2 Hz maximum and the fact that the power control only changes in steps of 20 Watts.

Lambda Technologies provided the specifications for the serial interface. The external computer can send simple text string commands to the MicroCure controller to either specify a new power output level or exit the remote operation mode. Text commands are acknowledged by text sent back from the MicroCure controller, enabling the host to confirm and synchronize with the command processing on the MicroCure.

7.5.1 *VFM Processing with Indirect Adaptive Neural Network Controller*

The modified indirect adaptive controller was implemented to control the temperature and heating rate of a polymer-coated silicon wafer being cured inside the VFM furnace (see Figure 43). The controller consisted of the controller (inverse model), and the plant emulator. This time that plant was the actual VFM system. Since the output of the neural network was from 0-1, a scale factor had to be found to scale the control signal (power) coming from the network. This scale factor varies depending on the trained neural network model. In Figure 44, the temperature profiles of the plant (VFM), the plant emulator, and the target temperature are plotted (top) along with the scaled control signal from the network (Target) and the actual power produced by the VFM system.

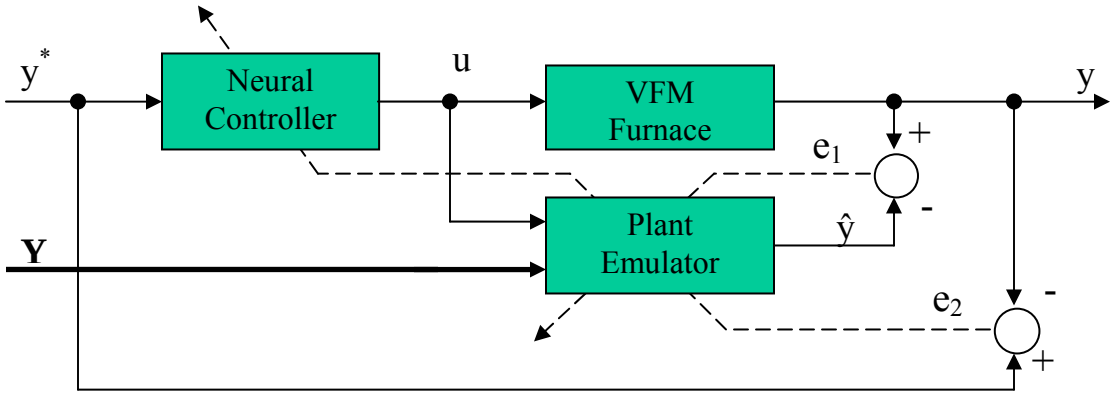

Figure 43 – Schematic of modified indirect adaptive control algorithm for VFM processing

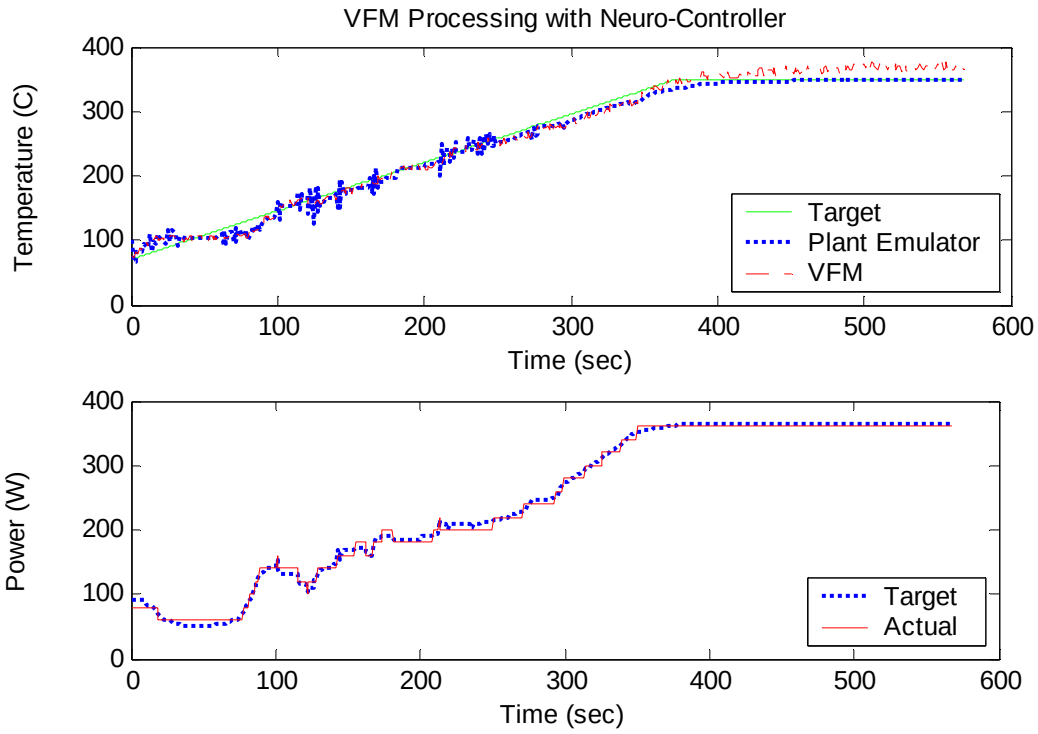

Figure 44 – VFM processing using the modified indirect adaptive control algorithm

7.5.2 *VFM Processing with Neural Network Controller and ATS monitoring*

The ATS discussed in the previous chapter was used to provide temperature measurements of a polymer-coated silicon wafer. The acoustic temperature sensor measured the bulk temperature of the wafer. The control inputs were the current temperature of the polymer measured by the ATS and target temperature. The output was the correct power setting for the MicroCure. The graphical user interface that was mentioned in the previous chapter was modified to display the target temperature, target power setting and actual power setting (see Figure 45).

At this point there are a few issues associated with using the ATS for monitoring the temperature while controlling the VFM with the modified IAC scheme. First, the time

it takes for the computer to calculate the time-of-flight estimate for the temperature measurement may be two long for the controller to properly regulate the temperature. One approach to counter this effect would be to reduce the number of waveforms averaged when taking a reading from the oscilloscope. The second approach would be to optimize both the ATS and controller algorithms by using less "FOR" loops while utilizing more vector multiplication, which can save processing time in a script language such as MATLAB. Additionally, the MATLAB script code could be complied in a different language such as C/C++ to further increase the speed of the program.

Second, during the IAC implementation, it was noted that the controller could be more effective if the power quantization levels of the VFM system were less than 20 Watts. For example, if the controller requested a power of 29 Watts, the power that would be executed by the VFM system would be 20 Watts, or if the system requested 31 Watts, the power delivered would be 40 watts. This quantization limitation along with the time that it takes to calculate the time-of-flight/temperature measurement could be a serious constraint to the current system. To address this problem, a power system with a higher power resolution would be required and/or an optimization of the algorithm, as discussed earlier, would be needed.

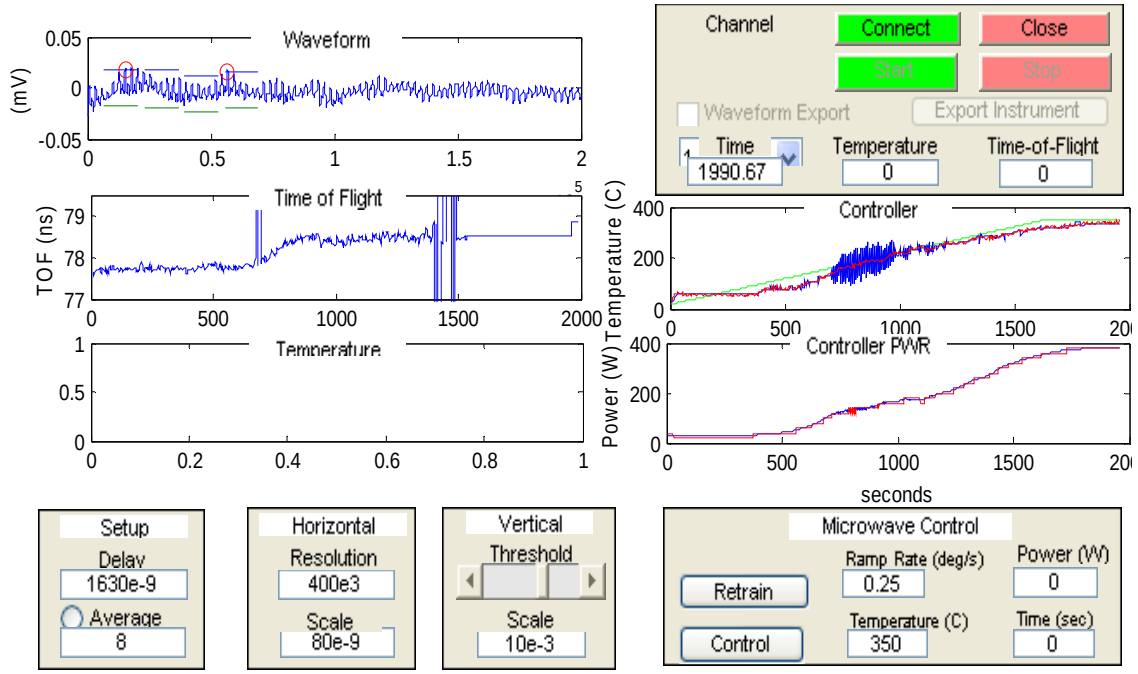

Figure 45 – Graphical user interface for in-situ monitoring of ATS and neural controller regulating the temperature inside the VFM

7.6 Summary

The indirect adaptive control technique was used to control the temperature during curing of a polymer on a silicon wafer in the VFM furnace. The ATS discussed in the previous chapter was also used as the temperature monitoring device. The next chapter will provide a summary of this research and will discuss possible future directions.

CHAPTER 8

CONCLUSTIONS AND FUTURE WORK

8.1 Contributions of the Research

In this thesis, neural networks were used to model VFM curing of polymer dielectrics. Utilizing the neural network models, genetic algorithms were used to optimize cure recipes for VFM processing. An acoustic sensor was developed to monitor and an indirect adaptive neural network scheme was developed to control the temperature of a polymer-coated silicon wafer *in-situ* in the VFM furnace. This chapter discusses the contributions of this research for VFM curing of polymer dielectrics and recommends possible extensions and future work.

8.1.1 *Neural Network Modeling and Genetic Optimization*

Several statically designed experiments were performed to verify that VFM curing results in comparable material properties to conventionally cured films. These experiments were performed on samples of the polymer benzocyclobutene (BCB) and the polyimide PI 2611 cured on silicon wafers. Curing was performed in the Lambda Technologies MircoCure™ 2100 system, as well as a conventional thermal furnace. All samples were heated to an appropriate temperature and held at temperature for a specific amount of time for both processing methods. After the BCB samples cooled, through-plane and in-plane indices of refraction were measured via ellipsometry. After the PI 2611 samples cooled, the indices of refraction were measured using a Metricon prism coupler. The percent

imidization was measured using attenuated total reflection Fourier transform infrared (ATR-FTIR) spectroscopy.

Neural networks were then trained using the data from the designed experiments to model the variation of the responses as a function of the process conditions. The back-propagation algorithm was utilized to train the neural networks. The network inputs were temperature and time-at-temperature. The outputs for cured BCB were the in-plane and through-plane indices of refraction. The indices of refraction were then used as metrics to determine the extent of cure of the BCB. The output variables of the cured polyimide were the in-plane and through-plane indices of refraction, the birefringence, and percent of imidization. To validate the neural network models, the root-mean-square (RMS) error was used as a performance metric. For the BCB models, RMS errors on the order of 1e-2 were achieved when comparing the outputs of the neural network models with test data. For the PI 2611 samples, the models yielded RMS errors are on the order of 5e-2 for the birefringence, and the in-plane and through-plane indices of refraction. The RMS error for the percent of imidization was on the order of 13.53.

The neural network models were then used for process optimization via genetic algorithms. Using this approach, the appropriate input conditions to achieve desirable film properties were determined. The optimal recipe indicated that an in-plane refractive index of 1.828, a through-plane refractive index of 1.637, a birefringence of 0.190, and a percent imidization of 95.6 could be achieved by using a ramp rate of 19 °C/minute, temperature of 294 °C, and a hold time of 23 minutes. These results suggest that using a VFM to cure polyimide can produce similar properties in less time and at lower temperatures than a conventional cure.

8.1.2 *Acoustic Temperature Sensor Monitoring*

To improve process monitoring for the VFM system, an acoustic temperature sensor was developed by depositing a ZnO transducer onto a sapphire buffer rod or sapphire wafer. To ensure that the ZnO is piezoelectrically active, the thin film must be c-planed oriented. This can be determined by XRD measurements.

The acoustic temperature sensor operates on the principle that the velocity of an acoustic wave in silicon is a function of temperature. Thus, an estimate of the temperature of a silicon wafer can be determined by measuring the time it takes for an acoustic wave to travel through silicon. For this research, the time-of-flight of a longitudinal wave is measured by generating a high voltage pulse, which produces the acoustic wave in the transducer. The acoustic wave travels through the sapphire into the silicon wafer and reflects off of either the silicon/air interface (or polymer/air interface if the silicon is coated with a polymer) and returns back to the transducer which then converts the mechanical signal back to an electrical signal, where it is read on an oscilloscope.

To calibrate the temperature, a MATLAB program was developed to capture the waveform from the oscilloscope and find the returned pulses within the waveform and by doing so measure, the time-of-flight as the temperature changed. The program captured averaged waveforms from the oscilloscope, and the returned pulses were identified by applying a moving window across the waveform and evaluating each sample in the window to a threshold. The first waveform value in a particular window that was greater (or less) than the maxima (or min) threshold was classified as a returned pulse. After the first two pulses were found, the time-of-flight calculation was made by multiplying the number of samples between the first and second pulses by the sampling rate. Some of the

data had an approximately linear relationship to the time-of-flight of the returned pulses and the temperature. The expected time-of-flight for the buffer rod was calculated by dividing the length of the rod (4.7 mm) by the speed of sound in sapphire (11000 m/s) and multiplying that by a factor of two (for the two-way travel time), which was 854.5 ns. The actual returned pulses were approximately 805 ns apart. Experimental data was taken with the acoustic buffer rod measuring the time-of-flight of silicon wafers with temperature profiles ramped to as high as 350 °C and held constant for as long as 80 minutes. For lower temperature and shorter runs, the time-of-flight data was approximately linear with the temperature as measured with a thermocouple. However, for the longer runs at higher temperature, there were spikes in the time-of-flight data. This corresponded to the algorithm being unable to capture one or more of the leading edges of the returned pulses.

A sensor holder was developed to house the acoustic sensor for use in the VFM furnace. This acoustic sensor consisted of the transducer deposited on a sapphire wafer. Once the sensor was mounted in the holder and placed inside the VFM furnace, MATLAB with a GUI was used to monitor both the time-of-flight of the returned pulses and a thermocouple that was attached to a polymer-coated wafer. The time-of-flight data had a strong correspondence to the temperature profile from the thermocouple that was attached to the polymer-coated wafer.

8.1.3 *Neuro-control*

Based on the capability of neural networks to model nonlinear processes and their capability to accurately approximate inverse relationships of complex functions, a neural network indirect adaptive control scheme was developed for VFM curing of polymer

dielectrics. This adaptive control scheme was used along with the ATS to monitor and control the temperature during curing of a polymer on a silicon wafer in the VFM furnace.

The control scheme consisted of a neural controller, a plant emulator, and a plant model. To simulate the control scheme, a forward model of the plant was developed using a neural network that was trained using experimental data. The controller was trained using a modified distal learning approach. For this simulation, the weights of the plant model were held constant while the weights of the plant emulator were allowed to adapt along with the weights of the controller. This configuration updated the controller parameters adaptively while the neural controller adjusted the plant's inputs to optimally match the output of the plant to the control set-point.

To implement the control scheme on the VFM, the MicroCure software needed to be modified so that an external controller could access the system. In collaboration with Lambda Technologies, a robust solution was implemented for the integration of the control strategy with the MicroCure system. This solution consisted of a software change to the MicroCure system that allowed the computer-controlled oscilloscope to synchronize with the program running on the MicroCure controller and to send new constant output power commands. The host was responsible for controlling power to accomplish process control and for turning off the power when the process was complete.

The modified indirect adaptive controller was implemented to control the temperature and heating rate of a polymer-coated silicon wafer being cured inside the VFM furnace. For implementation, the controller and the plant emulator were neural networks, but the forward plant model was replaced with the actual VFM furnace. Experimental

results illustrated that the control system was able send the appropriate power commands to the MicroCure software to regulate the temperature set point.

The last step in the process was to use the acoustic temperature sensor along with the control scheme, to effectively monitor and control curing of a polymer dielectric in the VFM system. The results illustrated that this was possible, but additional optimization of the control scheme and temperature measuring algorithms are needed to be able to properly control the system.

8.2 Recommendations and Future Work

At this point, there are a few remaining issues associated with using the ATS for monitoring the temperature while controlling the VFM with the modified IAC scheme. First, the time it takes for the computer to calculate the time-of-flight estimate for the temperature measurement may be too long for the controller to properly regulate the temperature. One approach to counter this effect would be to reduce the number of waveforms averaged when taking a reading from the oscilloscope. The second approach would be to optimize both the ATS and controller algorithms by using less "FOR" loops while utilizing more vector multiplication, which can save processing time in a script language such as MATLAB. Additionally, the MATLAB script code could be complied in a different language such as C/C++ to further increase the speed of the program.

Second, during the IAC implementation, it was noted that the controller could be more effective if the power quantization levels of the VFM system were less than 20 Watts. For example, if the controller requested a power of 29 Watts, the power that would be executed by the VFM system would be 20 Watts, or if the system requested 31 Watts, the power delivered would be 40 watts. This quantization limitation along with the time that it

takes to calculate the time-of-flight/temperature measurement could be a serious constraint to the current system. To address this problem, a power system with a higher power resolution would be required and/or an optimization of the algorithm would be needed.

To implement the scheme in a production VFM system, a redesign of the sensor holder may be needed. Currently the sensor holder is made of aluminum, but developing a sensor holder using a non-metal such as quartz may be beneficial. The insulation of the wire that was used to contact the sensor in the VFM was burned during one of the runs. Thus, the insulation should be inert to microwave radiation. A potentially better approach would be to have the sensor mounted such that the wire contacts the transducer outside of the chamber, where no wires would be needed inside the chamber.

As improvements to the control scheme, more experiments would are needed to better characterize the system and thus develop a more robust plant emulator for the controller. In addition, having the capability to control more parameter than just the power setting could increase the controller's capability to maintain temperature set points.

To further improve the monitoring capabilities of the VFM furnace, other sensors should be investigated. Some of the following sensors should be explored for *in-situ* monitoring of VFM curing: Fourier transform infrared spectroscopy (FTIR), dual wavelength IR pyrometer, and ellipsometer. In addition to equipping the VFM furnace with these new sensors, an investigation could be performed to test other intelligent control strategies such as neuro-fuzzy control. Both algorithms for computing the temperature estimate and performing control should be optimized further.

In general, there is more information contained in the returned pulses from a transducer than just the time-of-flight information. There is the amplitude of the returned

pulse, which can be used to determine the reflection coefficient. Obtaining the reflection coefficient as well as determining phase change of a returned pulse was used by Morton [79] to characterize the glass transition temperature of a polymer during pre-bake and post-bake. In addition, Ban et .al. [124] used three signal processing techniques to extract information out of an acoustic signal transmitted through PVD targets during sputtering. Thus, further investigation can be conducted to see if this information, in addition to using a network analyzer to measure the phase of returned pulses, could be useful for VFM processing.

REFERENCES

[1] "International Technology Roadmap for Semiconductors: Interconnect," 2005.

[2] J.-W. Kang, B. R. Kim, G.-G. Kang, M.-S. Moon, B.-M. Choi, and M.-J. Ko, "New Hybrid Low-K Dielectric Materials Prepared by Vinylsilane Polymerization," in *Material Research Society: Symposium Proceedings*, 2004, pp. 25-30.

[3] J. J. Senkevich, C. Jezewski, D. Lu, W. A. Lanford, G.-C. Wang, and T.-M. Lu, "Molecular Caulk: A Pore Sealing Technology for Ultra-low-k Dielectrics," in *Material Research Society: Symposium Proceedings*, San Francisco, CA, 2004.

[4] D. S. Soane and Z. Martynenko, *Polymers in Microelectronics: Fundamentals and Applications*. Amsterdam: Elsevier, 1989.

[5] T. Wang and J. Liu, "A Review of Microwave Curing of Polymeric Materials," *Journal of Electronics Manufacturing,* vol. 10, pp. 181-189, 2000.

[6] R. V. Tanikella, "Variable frequency microwave processing of materials for microelectronic applications," in *Chemical Engineering*. vol. PhD Atlanta, GA: Georgia Institute of Technology, 2003.

[7] K. D. Farnsworth, R. Manepalli, S. Bidstrup-Allen, and P. Kohl, "Variable Frequency Microwave Curing of 3,3',4,4-Biphenyltetracarboxylic Acid Dianhydride/P-Phenylenediamine (BPDA/PPD)," *International Journal of Microelectronic Packaging,* vol. 23, pp. 162-171, 2000.

[8] K. D. Farnsworth, R. N. Manepalli, S. A. Bidstrup-Allen, and P. Kohl, "Variable Frequency Microwave Curing of Photosensitive Polyimides," *IEEE Transactions on Components and Packaging Technologies,* vol. 24, pp. 474-480, 2001.

[9] M. Bramanti, E. A. Salerno, A. Tonazzini, S. Pasini, and A. Gray, "An acoustic pyrometer system for tomographic thermal imaging in power plant boilers," *IEEE Transactions on Instrumentation and Measurement,* vol. 45, pp. 159 - 167, February 1996.

[10] G. T. Herb and C. Fendrock, "Ultrasonic Thermometer System." vol. US 6,517,240 B1, U. S. Patent, Ed. United States: DuraMetrics, Inc., Sudbury, MA, 2003.

[11] J. Jacob, L. Chia, and F. Boey, "Comparative Study of Methyl Methacrylate Cure by Microwave Radiation Versus Thermal Energy," *Polymer Testing,* pp. 343-354, 1995.

[12] S. Zhou and M. C. Hawley, "A study of microwave reaction rate enhancement effect in adhesive bonding of polymers and composites," *Composite Structures,* vol. 61, pp. 303-309, September 2003.

[13] A. D. Surrett, R. J. Lauf, F. L. Paulauskas, and A. C. Johnson, "Polymer Curing Using Variable Frequency Microwave Processing," in *Materials Research Society Symposium Proceedings*, 1994, pp. 691-696.

[14] D. Lewis, S. J. LaMaire, and T. Nunes, "Microwave Processing of Polyimide Thin Films," in *Materials Research Society Symposium Proceedings*, 1994, pp. 681-689.

[15] R. V. Tanikella, S. A. Bidstrup-Allen, and P. A. Kohl, "Variable Frequency Microwave Curing of Benzocyclobutene," *Journal of Applied Polymer Science,* vol. 83, pp. 3055-3067, 2002.

[16] B. Geisler, B. Adams, and I. Ahmad, "Advanced Process Finds Optoelectronic Applications," *Advanced Packaging,* April 2002.

[17] M. Sadiku, *Elements of Electromagnetics*. Fort Worth, Texas: Saunders College Publishing, 1989.

[18] J. Mijovic and J. Wijaya, "Review of Polymers and Composites by Microwave Energy," *Polymer Composites,* vol. 11, June 1990.

[19] Lambda, "System and apparatus for reducing arcing and localized heating during microwave processing ", L. T. Corp, Ed., 1998.

[20] R. V. Tanikella, S. A. Bidstrup-Allen, and P. Kohl, "Novel Low-Temperature Processing of Polymer Dielectrics on Organic Substrates by Variable Frequency Microwave Processing," in *IEEE 8th International Symposium on Advanced Packaging Materials*, 2002, pp. 254-259.

[21] S. Allen, *Dielectric Techniques: Principles and Practice* vol. 1, 1998.

[22] J. Mijovic, A. Fishbain, and J. Wijaya, "Mechanistic Modeling of Epoxy-Amine Kinetics. II: Comparison of Kinetics in Thermal and Microwave Fields," *Macromolecules,* vol. 25, pp. 986-989, 1992.

[23] D. Rogers, E. Marand, D. Hill, and G. George, "Anomalies between Microwave and Thermal Cure Kinetics of Epoxy-amine resin systems," *High Performance Polymers,* vol. 11, pp. 27-39, 1999.

[24] D. Rogers, M. Bialkowski, and D. Hill, "Kinetic Study of Epoxy-Amine Microwave Cure Reactions. Part I: Design and Operation of a Single-mode Resonant Microwave Cavity," *High Performance Polymers,* vol. 10, pp. 341-351, 1998.

[25] E. Marand and e. al., "Comparison of Reaction Mechanisms of Epoxy Resins Undergoing Thermal and Microwave Cure from in Situ Measurements of Microwave Dielectric Properties and Infrared Spectroscopy," *Macromolecules,* vol. 25 pp. 2243-2252, 1992.

[26] D. Acierno and e. al., "Thermal and Dielectric Properties of Thermal and Microwave Cured Thermoset Polymers," *Material Research Innovation,* vol. 2, pp. 28-32, 1998.

[27] T. Sung, "Variable Frequency Microwave Curing of Polymer Dielectrics on Metallized Organic Substrates," in *Chemical Engineering*. vol. MS Atlanta, GA: Georgia Institute of Technology, 2003.

[28] T. Wang, Y. Fu, M. Becker, and J. Liu, "Microwave Cure of Metal-Filled Electrically Conductive Adhesive," in *Electronic Components and Technology Conference*, 2001.

[29] G. Glinski and B. Bailey, "Microwave Cure of Conductive Adhesive for Flip-chip & Microsystems Applications," in *IEEE, 2002 Inter Soc. Conf. on Thermal Phenomena*, 2002, pp. 848-853.

[30] G. S. May, "Manufacturing ICs the Neural Way," *IEEE Spectrum,* pp. 47-51, September 1994.

[31] G. S. May, "Application of neural networks in semiconductor manufacturing processes," in *Fuzzy Logic and Neural Network Handbook,*, C. H. Chen, Ed. New York: ASME Press, 1996.

[32] B. Kim and G. S. May, "Reactive Ion Etch Modeling Using Neural Networks and Simulated Annealing," *IEEE Transactions on Semiconductor Manufacturing,* vol. 19, pp. 3-8, 1996.

[33] S. Hong and G. S. May, "Neural Network Based Time Series Modeling of Optical Emission Spectroscopy Data for Fault Detection in Reactive Ion Etching," in

Proceedings of the SPIE Conference on Advance Microelectronic Manufacturing Santa Clara, CA, 2003.

[34] R. Pratap, S. Pinel, D. Staiculescu, J. Laskar, and G. S. May, "A Neural Network Model for Sensitivity Analysis of Circuit Parameters for Flip Chip Interconnects," in *Proceedings of the Electronic Components and Technology Conference* San Diego, CA, 2003, pp. 1619-1625.

[35] C. D. Himmel and G. S. May, "Advantages of Plasma Etch Modeling Using Neural Networks Over Statistical Techniques," *IEEE Transaction on Semiconductor Manufacturing,* vol. 6, pp. 103-111, May 1993.

[36] C. Davis, R. V. Tanikella, P. Kohl, and G. May, "Neural Network Modeling of Variable Frequency Microwave Curing," in *Proceedings of the Electronic Components and Technology Conference*, 2002, p. 931–935.

[37] C. Davis, R. Tanikella, T. Sung, P. Kohl, and G. May, "Optimization of Variable Frequency Microwave Curing using Neural Networks and Genetic Algorithms," in *53rd Proceeding of Electronic Component and Technical Conference* New Orleans, 2003, pp. 1718-1723.

[38] T. Thongvigitmanee and G. May, "Optimization of Nanocomposite Integral Capacitor Fabrication Using Neural Networks and Genetic Algorithms," in *Electronics Manufacturing Technology Symposium. IEMT 2002. 27th Annual IEEE/SEMI International*, 2002, pp. 123-129.

[39] S. Han, L. Cai, G. S. May, and A. Rohatgi, *Optimizing the Growth of PECVD Silicon Nitride Films for Solar Cell Applications Using Neural Networks and Genetic Algorithms* vol. 6. New York: ASME Press, 1996.

[40] S. S. Han, "Modeling and Optimization of Plasma Enhanced Chemical Vapor Deposition using Neural Networks and Genetic Algorithms," in *Electrical and Computer Engineering*. vol. PhD Atlanta, GA: Georgia Institute of Technology, 1996.

[41] S. S. Han and G. May, "Recipe Synthesis for PECVD SiO2 Films Using Neural Networks and Genetic Algorithms," in *Proceedings of the Electronic Components and Technology Conference*, 1996, pp. 855-860.

[42] T. S. Kim and G. May, "Intelligent Control of Via Formation Process in MCM-L/D Substrate Using Neural Networks," in *1999 International Symposium on Advance Packaging Materials*, 1999, pp. 106-112.

[43] D. Stokes and G. S. May, "Real-Time Control of Reactive Ion Etching Using Neural Networks," *IEEE Transaction on Semiconductor Manufacturing,* vol. 13, pp. 469-480 November 2000.

[44] H.-F. Guo and C. J. Spanos, "Real Time Statistical Process Control for Plasma Etching," *IEEE/SEMI Int'l Semiconductor Science Symposium,* pp. 113-118, 1991.

[45] Mathworks, "http://www.mathworks.com/products/neuralnet/," (Last accessed: October 2006).

[46] L. Fausett, *Fundamentals of Neural Networks: Architectures, Algorithms, and Applications*: Prentice-Hall, Inc., 1994.

[47] D. Goldberg, *Genetic Algorithms in Search, Optimization, and Machine Learning*. Reading, MA: Addison-Wesley, 1989.

[48] J. F. Frenzel, "Genetic Algorithms: A New Breed of Optimization," *IEEE Potentials,* vol. 12, pp. 21-24, 1993.

[49] K. S. Narendra and K. Parthasarathy, "Identification and Control of Dynamical Systems Using Neural Networks," *IEEE Transactions on Neural Networks,* vol. 1, pp. 4-27, March 1990.

[50] K. Hornik, M. Stinchcombe, and H. White, "Multilayer Feedforward Networks are Universal Approximators," *Neural Networks,* vol. 2, pp. 359-366, 1989.

[51] M. Khalid and S. Omatu, "A Neural Network Controller for a Temperature Control System," *IEEE Control Systems Magazine,* vol. 12, pp. 58-64, June 1992.

[52] K.-I. Funahashi, "On the approximate realization of continuous mappings by neural networks," *Neural Networks,* vol. 2, p. 183, 1989.

[53] A. G. Barto, R. S. Sutton, and C. W. Anderson, "Neuronlike Adaptive Elements That Can Solve Difficult Learning Control Problems," *IEEE Transactions on Systems, Man, and Cybernetics,* vol. SMC-13, pp. 834-846, Sept./Oct. 1983.

[54] D. Psaltis, A. Sideris, and A. A. Yamamura, "A multilayered neural network controller," *IEEE Control Systems Magazine,* vol. 8, pp. 17-21, April 1988.

[55] M. S. Saerens, A. , "A neural controller," *First IEE International Conference on Artificial Neural Networks,* pp. 211-215, October 1989.

[56] M. S. Saerens, A. , "Neural controller based on back-propagation algorithm," *IEE Proceedings Radar and Signal Processing,* vol. 138, pp. 55-62, 1991.

[57] J. Tanomaru and S. Omatu, "Process control by on-line trained neural controllers," *IEEE Transactions on Industrial Electronics,* vol. 39, p. 511, 1992.

[58] S. Stitt and Y. F. Zheng, "Distal learning applied to biped robots," in *Proceedings of Robotics and Automation*, 1994, p. 137.

[59] T. Yamada, "Remarks on neural network controller for an inverse dynamics of many-to-one plant," in *1995 International IEEE/IAS Conference on Industrial Automation and Control: Emerging Technologies,* 1995, pp. 314 - 319.

[60] F. Rufus, "Intelligent approaches to mode transition control." vol. PhD: Georgia Institute of Technology, 2000.

[61] T. S. Kim, D. Stokes, and G. S. May, "Real-Time Feedback Control of Reactive Ion Etching Using Neural Networks," *1996 IEEE International Conference on Neural Networks* pp. 2039-2043, 06/03/1996 - 06/06/1996 1996.

[62] D. Stokes, "Real-Time Monitoring and Control of Reactive Ion Etching Using Neural Networks," in *Electrical and Computer Engineering*. vol. PhD Atlanta, GA: Georgia Institute of Technology, 2000, p. 194.

[63] D. Stokes and G. S. May, "Indirect adaptive control of reactive ion etching using neural," *IEEE Transactions on Robotics and Automation,* vol. 17, pp. 650 - 657 October 2001.

[64] Y. Pei and G. S. May, "Neural Network Based Adaptive Tracking Controller for a Reactive Ion Etching System," in *Proceedings of the American Controls Conference* Arlington, VA 2001.

[65] Werbos, "Neural Networks for Control: An Overview," *Proceedings of the Twelfth Annual International Conference of the IEEE Engineering in Medicine and Biology Society,* vol. 12, pp. 1796-1797, 1990.

[66] M. Khalid, S. Omatu, and R. Yusof, "Temperature Regulation With Neural Networks and Alternative Control Schemes," in *1994 IEEE World Congress on Computational Intelligence, and1994 IEEE International Conference on Neural Networks* vol. 4 Orlando, FL USA 1994, pp. 2599 - 2604

[67] C. D. Himmel, T. S. Kim, A. Krauss, E. W. Kamen, and G. S. May, "Real-Time Predictive Control of Semiconductor Manufacturing Processes Using Neural

Networks," in *Proceeding of the American Control Conference* Seattle, Washington, 1995.

[68] H. R. Berenji and P. Khedkar, "Learning and Tuning Fuzzy Logic Controllers Through Reinforcements," *IEEE Transactions on Neural Networks,* vol. 3, pp. 724-740, 1992.

[69] L. J. Lin, "Reinforcement Learning, Planning and Teaching," *Machine Learning,* vol. 8, pp. 293-321, 1992.

[70] H. R. Berenji, "Fuzzy Q-Learning: A New approach for Fuzzy Dynamic Programming," *Proceedings of IEEE 3rd International Conference on Fuzzy Systems,* pp. 486-491, 1994.

[71] L. P. Kaelbling, M. L. Littman, and A. W. Moore, "Reinforment Learning: A Survey," *Journal of Artificial Intelligence Research,* vol. 4, pp. 237-285, 1996.

[72] R. S. Sutton and A. G. Barto, *Introduction to Reinforcement Learning*. Cambridge, MA: MIT Press/Bradford Books, 1988.

[73] V. Gullapalli, J. A. Franklin, and H. Benbrahim, "Acquiring Robot Skills via Reinforcement Learning," in *IEEE Control Systems Magazine*, 1994, pp. 13-24.

[74] J. A. Franklin, "Qualitative Reinforcement Learning Control," in *Proceeding of the 31st Conference on Decision and Control*, 1992.

[75] G. Tesauro, "Practical Issues in Temporal Difference Learning," *Machine Learning,* vol. 8, pp. 257-277, 1992.

[76] C.-T. Lin, C.-F. Juang, and C.-P. Li, "Temperature Control with a Neural Fuzzy Interface," *IEEE Transactions on Systems, Man, and Cybernetics--Part C: Applications and Reviews,* vol. 29, pp. 440-451, 1999.

[77] C.-F. Juang and J.-S. Chen, "A Recurrent Neural Fuzzy Network Controller for a Temperature Control System," *IEEE International Conference on Fuzzy Systems,* pp. 408-412, 2003.

[78] Y. J. Lee, B. T. Khuri-Yakub, and K. Saraswat, "Temperature Measurement in Rapid Thermal Processing Using the Acoustic Temperature Sensor," *IEEE Transactions on Semiconductor Manufacturing,* vol. 9, August 1996.

[79] S. Morton, F. Degertekin, and B. T. Khuri-Yakub, "Ultrasonic Sensor for Photoresist Process Monitoring," *IEEE Transactions on Semiconductor Manufacturing,* vol. 12, 1999.

[80] J. Lu, K. Wakai, S. Takahashi, and S. Shimizu, "Acoustic computer tomographic pyrometry for two-dimensional measurement of gases taking into account the effect of refraction of sound wave paths," *Measurement Science and Technology,* vol. 11, pp. 692-697, June 2000.

[81] R. H. Stones and P. J. Webb, "The application of acoustic pyrometry to gas temperature measurement and mapping," *IEE Colloquium on Ultrasound in the Process Industry,* pp. 9/1-2 September 23 1993.

[82] F. L. Degertekin, J. Pei, B. V. Honein, B. T. Khuri-Yakub, and K. C. Saraswat, "Thin film effects in ultrasonic wafer thermometry," in *Proceedings of the 1994 IEEE Ultrasonics Symposium*. vol. 3 Cannes 1994, pp. 1337-1341.

[83] F. L. Degertekin, J. Pei, Y. J. Lee, B. T. Khuri-Yakub, and K. C. Saraswat, "In-situ ultrasonic thermometry of semiconductor wafers," in *Proceedings of the 1993 IEEE Ultrasonics Symposium*. vol. 1 Baltimore, MD 1993, pp. 375-377.

[84] J. Pei, F. L. Degertekin, B. V. Honein, B. T. Khuri-Yakub, and K. C. Saraswat, "In situ thin film thickness measurement using ultrasonics waves," in *Proceedings of the 1994 IEEE Ultrasonics Symposium*, 1994, pp. 1237-1240.

[85] Y. J. Lee, C. H. Chou, B. T. Khuri-Yakub, and K. C. Saraswat, "Non-invasive process temperature monitoring using laser-acoustic techniques," in *1990 Symposium on VLSI Technology*, 1990, p. 105.

[86] S. L. Morton, F. L. Degertekin, and B. T. Khuri-Yakub, "Ultrasonic cure monitoring of photoresist during pre-exposure bake process," in *Proceedings of the1997 IEEE Ultrasonics Symposium*, 1997, pp. 837-840.

[87] C. E. Wold, J. D. Sternhagen, R. D. Mileham, K. D. Mitzner, and D. W. Galipeau, "Temperature measurement using surface skimming bulk waves," in *Proceedings of the1999 IEEE Ultrasonics Symposium*, Caesars Tahoe, NV USA 1999, pp. 441 - 444

[88] J. D. Sternhagen, C. E. Wold, W. A. Kempf, M. Karlgaard, K. D. Mitzner, R. D. Mileham, and D. W. Galipeau, "A novel integrated acoustic gas and temperature sensor," *IEEE Sensors Journal,* vol. 2, p. 301, 2002.

[89] I. Dow Chemical Company, "BCB Technical Data Sheets," Midland, MI, 48642.

[90] F. G. Bobel, A. Wowchak, P. P. Chow, J. Van Hove, and L. A. Chow, "Real Time Process Monitoring with Multiwave-Length Pyrometer Interferometry (PI)," in *Materials Research Society, Symposium Proceedings*. vol. 324, O. J. Glembocki, Ed. Boston, Massachusetts, 1994, pp. 105-110.

[91] P. J. Timans, "Emissivity of silicon at elevated temperatures," *Journal of Applied Physics,* vol. 74, pp. 6353-6365, 1993.

[92] Dow, "Cure and Oxidation Measurements for Cyclotene Advanced Electronics and Resins," Dow Chemical Company 1997.

[93] F. Yang, W. A. McGahan, C. E. Mohler, and L. M. Booms, "Using Optical Metrology to Monitor Low-k Dielectric Thin Films," *Micro,* pp. 31-38, May 2000.

[94] H. D. MicroSystems, "http://www.hdmicrosystems.com/tech/process.html," (Last accessed: April 2007).

[95] R. J. Pratap, D. Staiculescu, S. Pinel, J. Laskar, and G. S. May, "Modeling and Sensitivity Analysis of Circuit Parameters for Flip-Chip Interconnects Using Neural Networks," *IEEE Transactions on Advanced Packaging,* vol. 28, pp. 71-78, February 2005.

[96] M. K. Ghosh and K. L. Mittal, *Polyimides: Fundamentals and Applications*. New York, New York: Marcel Dekker, Inc., 1996.

[97] H. J. McSkimin, "Measurement of elastic constants at low temperatures by means of ultrasonic waves - data for silicon and germanium single crystals, and for fused silica," *Journal of Applied Physics,* vol. 24, pp. 988-997, August 1953.

[98] T. M. Reeder and D. K. Winslow, "Characteristics of Microwave Acoustic Transducers for Volume Wave Excitation," *IEEE Transactions on Microwave Theory and Techniques,* vol. 17, pp. 927-941, 1969.

[99] B. T. Khuri-Yakub, G. S. Kino, and P. Galle, "Studies of the Optimum Conditions for Growth of RF-Sputtered ZnO Films," *Journal of Applied Physics,* vol. 46, pp. 3266-3272, August 1978 1975.

[100] M. J. Vellekoop, A. Venema, C. C. G. Visser, and P. M. Sarro, " Processing and Passivation of Zinc Oxide Films in Silicon Applications," *American Ceramic Society Bulletin,* vol. 69, pp. 1503-1505, 1990.

[101] F. S. Hickernell, "ZnO Processing for Bulk- and Surface-Wave Devices," in *1980 Ultrasonic Symposium*, 1980, pp. 785-794.

[102] Y. Kim, W. D. Hunt, F. S. Hickernell, R. J. Higgins, and C.-K. Jen, "ZnO Films on {001}-Cut <100>-Propagating GaAs Substrates for Surface Acoustic Wave Device Applications," *IEEE Transactions on Ultrasonics, Ferroelectrics and Frequency Control,* vol. 42, pp. 351-361, 1995.

[103] S. W. Wenzel and R. M. White, "Flexural Plate-Wave Gravimetric Chemical Sensor," *Sensors and Actuators A: Physical,* vol. 22, pp. 700-703, 1990.

[104] S. L. Pinkett, "Techniques to facilitate the fabrication of ZnO-based thin film bulk acoustic wave devices," in *Electrical and Computer Engineering*. vol. Ph. D. Atlanta, GA: Georgia Institute of Technology, 2003.

[105] V. Ristic, *Principles of Acoustic Devices*. New York: John Wiley & Sons, Inc., 1983.

[106] J. B. Lee, S. H. Kwak, and H. J. Kim, "Effects of surface roughness of substrates on the c-axis preferred orientation of ZnO films deposited by r.f. magnetron sputtering " *Thin Solid Films* vol. 423, pp. 262-266 2003.

[107] B. T. Khuri-Yakub, J. G. Smits, and T. Barbee, "Reactive Magnetron Sputtering of ZnO," *Journal of Applied Physics,* vol. 52, pp. 4772-4774, July 1981.

[108] N. J. Ianno, L. McConville, N. Shaikh, S. Pittaland, and P. G. Snyder, "Microstructural evolution and preferred orientation change of radio-frequency-magnetron sputtered ZnO thin films," *Journal of Vacuum Science Technology: A,* vol. 14, pp. 1943-1948, May/June 1996.

[109] J. C. Zesch, B. Hadimioglu, B. T. Khuri-Yakub, M. Lim, R. Lujan, and J. Ho, "Deposition of Highly Oriented Low-Stressed ZnO Films," in *1991 Ultrasonic Symposium*, 1991, pp. 445-447.

[110] A. Cimpoiasu, N. M. v. d. Pers, T. H. d. Keyser, A. Venema, and M. J. Vellekoop, "Stress Control of Piezoelectric ZnO films on Silicon Substrates," *Smart Material Structures,* vol. 5, pp. 744-750, 1996.

[111] Y. Chen, N. T. Tuan, Y. Segawa, H.-j. Ko, S.-k. Hong, and T. Yao, "Stimulated emission and optical gain in ZnO epilayers grown by plasma-assisted molecular-beam epitaxy with buffers," *Applied Physics Letters,* vol. 78, pp. 1469-1471, 2001.

[112] H. Sheng, N. W. Emanetoglu, S. Muthukumar, B. V. Yakshinskiy, S. Feng, and Y. Lu, "Ta/Au Ohmic Contacts to n-Type ZnO," *Journal of Electronic Materials,* vol. 32, pp. 935-938, 2003.

[113] B. J. Jin, S. Im, and S. Y. Lee, "Violet and UV luminescence emitted from ZnO thin films grown on sapphire by pulsed laser deposition " *Thin Solid Films,* vol. 366, pp. 107-110, 2000.

[114] T. Shibata, K. Unno, E. Makino, and S. Shimada, "Characterization of Sputtered ZnO Thin Film as Sensor and Actuator for Diamond AFM Probe," *Sensors and Actuators A: Physical,* vol. 102, pp. 106-113, 2002.

[115] M. J. Vellekoop, C. C. G. Visser, P. M. Sarro, and A. Venema, "Compatibility of Zinc Oxide with Silicon IC Processing," *Sensors and Actuators A: Physical,* pp. 1027-1030, 1990.

[116] J. Rosenbaum, *Bulk Acoustic Wave Theory and Devices*. Norwood, MA: Artech House, 1988.

[117] X. Zhu, "Micromachined Self-Focusing Acoustic Wave Transducers," in *Electrical Engineering*. vol. Master of Science: University of Hawaii, 1997, p. 79.

[118] R. Krimholtz, D. A. Leedom, and G. L. Matthaei, "New Equivalent Circuits for Elementary Piezoelectric Transducers," *Electronic Letters,* vol. 6, pp. 398-399, June 25, 1970 1970.

[119] S. Sherrit, S. P. Leary, B. P. Dolgin, and Y. Bar-Cohen, "Comparison of the Mason and KLM Equivalent Circuits for Piezoelectric Resonators in the Thickness Mode," in *IEEE Ultrasonics Symposium*, 1999.

[120] S. L. Morton, "Ultrasonic Sensor for Photoresist Process Monitoring," in *Electrical Engineering*. vol. Ph. D. Palo Alto, CA: Stanford University, 1999.

[121] D. H. Nguyen and B. Widrow, "Neural networks for self-learning control systems," *IEEE Control Systems Magazine,* vol. 10, pp. 18-23, April 1990.

[122] K. J. Åström and B. Wittenmark, *Adaptive Control*, Second ed. Readings, Massachusetts: Addison-Wesley Publishing Company, Inc., 1995.

[123] M. I. Jordan and D. E. Rumelhart, "Forward Models: Supervised Learning with a Distal Teacher," *Cognitive Science,* vol. 16, pp. 307-354, 1992.

[124] L. Ban, A. K. Ziarani, and C. Cetinkaya, "Acoustic Monitoring of Nonuniformly Eroded PVD Targets," *IEEE Transactions on Semiconductor Manufacturing,* vol. 19, pp. 425-431, 2006.